

Wildfire Risk Prediction: A Review

Zhengsen Xu^a, Jonathan Li^{a,b}, Sibo Cheng^c, Xue Rui^d, Yu Zhao^e, Linlin Xu^b

^aDepartment of Geography of Environmental Management, University of Waterloo, 100 University Avenue, Waterloo, N2L3G1, Ontario, Canada

^bDepartment of Systems Design Engineering, University of Waterloo, 100 University Avenue, Waterloo, N2L3G1, Ontario, Canada

^cCEREA, Ecole des Ponts and EDF R&D, Ile-de-France, France

^dSchool of Emergency Management, Nanjing University of Information Science and Technology, 219 Ningliu Road, Nanjing, 210044, China

^eDivision of Geoinformatics, KTH Royal Institute of Technology, Brinellvägen 8, Stockholm 100 44, Demark

Abstract

Wildfires significantly impact global ecosystems, wildlife, and human populations, destroying plant communities, habitats, and settlements. They also contribute to increased emissions of pollutants such as carbon dioxide, nitrogen oxides, and methane. Thus, accurate wildfire risk prediction is essential for reducing emissions, mitigating pollution, and protecting biodiversity and human health. However, predicting wildfire risk is a complex challenge that involves defining risk, integrating multi-source data, selecting appropriate algorithms, ensuring algorithm interpretability, and calibrating predictions.

This paper addresses the entire wildfire risk prediction process. It first introduces the concept of wildfire risk and summarizes the geographic distribution of referenced studies. It then reviews commonly used factors in wildfire risk prediction, such as fuel, meteorological, and socio-economic data, along with associated sources and computational methods. Additionally, we explore the issue of feature collinearity in data, presenting approaches to evaluate collinearity and attribute feature importance, with an emphasis on addressing the black-box nature of machine learning models.

We further provide an overview of wildfire danger rating systems and traditional machine learning algorithms. Given the rapid advancement of deep learning and its increasing application in wildfire risk assessment, we identify a gap in the systematic review of these methods. To bridge this gap, we categorize and review deep learning algorithms into three groups: time series prediction, image segmentation and classification, and spatiotemporal prediction. We also discuss methods for converting model outputs into actionable probabilities. Finally, we offer insights and propose future directions for deep learning-based wildfire prediction.

Keywords: wildfire prediction, remote sensing, machine learning, review

1. Introduction

Wildfires occur in diverse environments such as forests, grasslands, farmlands, and peatlands, with significant impacts on global ecosystems, wildlife, human health, air quality, and carbon balance. They not only destroy plant communities, habitats, and human settlements but also contribute to elevated emissions of greenhouse gases and toxic pollutants like carbon dioxide, nitrogen oxides, methane, ozone, particulate matter, and mercury (Pelletier et al., 2023; Hua and Shao, 2017; McNorton and Di Giuseppe, 2024; Yang et al., 2022). For instance, the devastating 2019 Australian wildfires burned approximately 18.6 million hectares of land, destroyed over 5,900 structures, and caused the deaths of at least 34 people and 1 billion animals (Naderpour et al., 2020). In the coming decades, climate change is expected to shorten fire return intervals and increase the burned area in vulnerable regions (Parks and Abatzoglou, 2020; Holdrege et al., 2024). As a result, accurate wildfire risk prediction is essential for mitigating future impacts.

In response to these challenges, wildfire risk prediction has attracted growing attention from governments, academia, and industry. Current prediction models consider essential components such as defining the study area and timescale, data selection and processing, method selection, setting prediction objec-

tives, and evaluating model accuracy. However, a systematic review of these elements remains lacking. This paper addresses this gap by providing a comprehensive review of the data, workflows, and prediction methods used for wildfire risk assessment, while also outlining potential future research directions.

A major challenge in wildfire risk prediction lies in the lack of a clear and consistent definition of risk across studies. Based on the literature, this paper categorizes wildfire risk into four types: explicit definitions, implicit definitions, ignition risk, and burning risk. Wildfire ignition and spread result from complex interactions among various factors, including fuel conditions, climate, weather, socio-economic factors, terrain, hydrology, and historical wildfire data. This paper details the definitions, calculations, proxies, and frequency of use of these features, alongside an overview of publicly available spatial datasets for wildfire spread prediction.

A key concern in the design of prediction algorithms is evaluating feature collinearity and improving model interpretability. Including highly correlated features can degrade model performance and obscure feature importance, while model interpretability helps to clarify patterns of ignition and spread. This paper introduces techniques for assessing feature collinearity and enhancing the interpretability of machine learning models.

Another critical aspect of wildfire prediction is the choice

of algorithms. Methods range from wildfire danger rating systems and statistical models to traditional machine learning and deep learning approaches. While [Jain et al. \(2020\)](#) provides a comprehensive review of machine learning models, this paper focuses on deep learning, which has seen rapid adoption and is becoming a crucial tool for wildfire prediction. To address the lack of systematic reviews in this area, we categorize deep learning-based models into three task types: time series prediction, image segmentation and classification, and spatiotemporal prediction. This study reviews existing deep learning models in these categories, providing a structured overview of their applications.

Finally, with the ongoing advancements in satellite observation, integrated air-ground-space remote sensing technologies, and deep learning models, wildfire risk prediction using multi-source remote sensing presents significant opportunities and challenges. This paper concludes by discussing the current limitations in data and algorithms and highlighting potential future developments.

2. Wildfire risk definition

In the majority of published wildfire risk methodology studies, the concept of wildfire risk is not clearly defined, leading to instances of confusion regarding the interchangeable use of terms such as risk, hazard, and danger. Consequently, this paper initiates by presenting a precise definition of wildfire risk. [Miller and Ager \(2012\)](#), based on the Society for Risk Analysis's definition of risk, proposed a comprehensive fire risk framework (Fig. 1), which divides wildfire risk into three components: likelihood, intensity, and effects. This framework emphasizes the impact of wildfires on human activities and the environment rather than solely considering the probability of occurrence. For instance, low-intensity and low-impact wildfires might not significantly affect areas of concern, meaning that a high likelihood of wildfire occurrence does not necessarily equate to high wildfire risk.

Additionally, their study distinguishes between commonly used terms in wildfire risk research, such as risk, hazard, exposure, threats, vulnerability, and fire danger. It is important to note that most of the studies summarized in this paper focus more on the threats posed by wildfires to human life and property rather than solely on environmental and ecological impacts. Therefore, these studies are often conducted in areas with high social value density. Based on the aforementioned definitions, wildfire risk can be approximately equated to wildfire likelihood.

When summarizing related work, we focus only on studies concerning wildfire risk and danger, excluding those on hazard, exposure, and threats. The former primarily describes the outlook for fire occurrence over a certain period, while the latter tends to evaluate the hazard of wildfires (Fig. 1). Consequently, if we consider only the likelihood of fire occurrence without considering its potential harm, the definition of wildfire risk can be simplified to the probability of a wildfire igniting or spreading at a specific location and time ([Deeming, 1972](#)). Many researchers in the past have described risk as the likelihood of

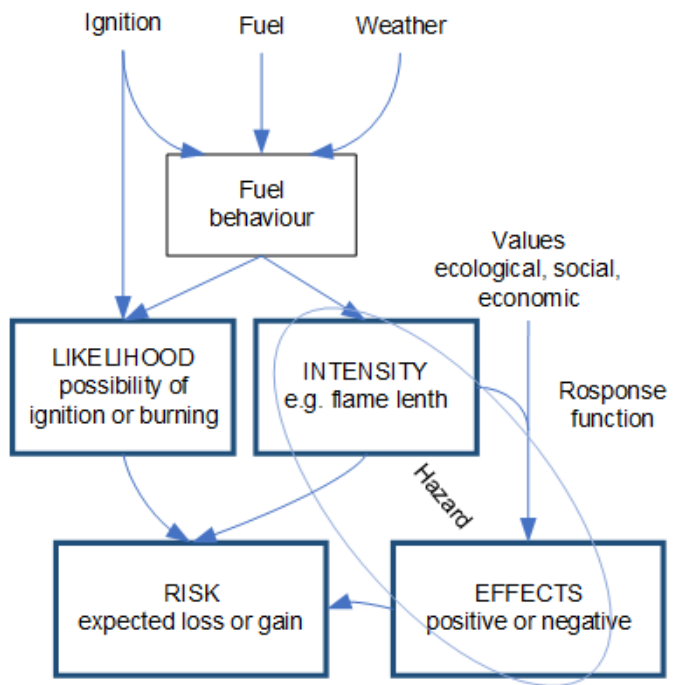


Figure 1: The generalized wildfire risk framework proposed by [Miller and Ager \(2012\)](#)

wildfire occurrence, which also aligns with the wildfire framework established by the European Commission ([Depicker et al., 2020](#)).

More specifically, these studies often treat wildfire risk assessment as a conditional probability, where wildfire risk is defined as the probability of a wildfire igniting or spreading under the influence of factors such as fuel, terrain, and weather conditions. In this context, wildfire risk equates to wildfire probability ([Yang et al., 2004](#)). In addition, some definitions emphasize the role of causal agents and their frequency in influencing wildfire risk ([Hardy, 2005](#)). In this definition, the importance of "causal agents" is highlighted—without these agents, the existing hazard would have zero potential to cause harm. Causal probability refers to the conditions that trigger wildfires, such as lightning or human activities [Deeming \(1972\)](#).

Based on these definitions, the specific form of wildfire risk varies across studies. This paper categorizes wildfire risk definitions into four types based on the algorithms used and the research objectives: explicit definitions, implicit definitions, wildfire ignition risk, and wildfire burning risk. On one hand, definitions are categorized according to whether they explicitly represent various wildfire influencing factors and the contributions of historical wildfire records. These categories include definitions based on historical observed wildfire occurrence data, influencing factors, and simulation data, as well as data-driven machine learning implicit definitions. On the other hand, wildfire prediction research is generally divided into studies on wildfire ignition risk and wildfire burning risk. Wildfire ignition risk is typically estimated using ignition data, while wildfire burning risk refers to the risk of a fire encountering a particular place. Although this risk partly depends on ignition,

it is also influenced by subsequent wildfire spread and fire suppression efforts and is generally derived from historical burn data or simulation methods (Miller and Ager, 2012).

2.1. Explicit definition methods

This section focuses on explicit definition methods, which include directly using historical observation data to define wildfire risk, defining wildfire risk based on the weights of influencing factors, and combining these factors to simulate wildfire distribution and define risk through simulation results. It is worth noting that this subsection does not cover the details of the simulation algorithms, but rather how to convert simulation results into wildfire risk.

Firstly, the simplest and most direct method in wildfire risk estimation is using historical fire occurrences to predict future risk. For example, Rubí and Gondim (2023) classified regions where one or more fires occurred within an hour as "high risk," while other areas were classified as "low risk." Preisler et al. (2004) selected all fire voxels within a past time (t) and spatial range and sampled a π percentage of non-fire voxels using the scheme proposed by Brillinger et al. (2003). The occurrence of fire can then be characterized using conditional probability, which can be constrained within the $[0, 1]$ interval using a sigmoid function.

$$p(n) = \sum_{t=0}^T \frac{y_{t,n}}{T}, \forall n \in [N] \quad (1)$$

where $y_{t,n}$ is the wildfire occurrence at a specific time t and location (grid cell) n 0, 1; N is the duration of the wildfire season. Similarly, Umunnakwe et al. (2022) estimated the spatiotemporal ignition probability using a similar function.

$$m_{g,j} \approx \frac{n_{g,j}}{N} \quad (2)$$

where $m_{g,j}$ represents the fire ignition probability in grid cell g during period j ; $n_{g,j}$ and N are the total number of wildfires and the total number of considered periods, respectively. They also introduced Monte Carlo techniques to interpolate grid cells. Xu et al. (2023) modeled wildfire risk using a marked spatiotemporal Hawkes process, with the conditional intensity function before location k and time t .

$$\lambda(t, k, m|\mathcal{H}_t) = \lim_{\Delta t, \Delta u \rightarrow 0} \frac{\mathbb{E}[\mathbb{N}(|t, t + \Delta t) \times B(k, \Delta k) \times B(m, \Delta m))|\mathcal{H}_t]}{\Delta \times B(k, \Delta k) \times B(m, \Delta m)} \quad (3)$$

where $B(a, r)$ is a sphere with center a and radius r , and \mathbb{N} is the counting measure. Lall and Mathibela (2016) assessed wildfire risk in Cape Town, South Africa, by defining daily risk ratings based on the average number of wildfires per day and their corresponding standard deviation over seven years. Specifically, fire occurrences below the average were rated as 1 or lower, those between the average and one standard deviation above were rated as 2 or moderate, those between one and two standard deviations above were rated as 3 or higher, and occurrences more than two standard deviations above the average were rated as 4 or extreme. An ANN model was then

established using temperature, humidity, wind speed, and precipitation as inputs to predict wildfire risk.

The above models based on historical data do not consider the conditions for wildfire ignition or spread, thus having poor robustness and generalization ability. Moreover, due to the infrequent occurrence of wildfires over long time scales and large areas, there is a severe class imbalance between the occurrence and non-occurrence of wildfires in space and time. Therefore, the risk assessment results of these models are greatly influenced by data sampling. Consequently, some studies have begun to incorporate or solely use factors such as fuel, terrain, weather conditions, and wildfire triggers as proxies to estimate ignition risk. For example, Castro et al. (2003) used shrub moisture content, specifically live fuel moisture, as a proxy variable for wildfire risk in Spain. More complexly, Sadashivuni et al. (2013) defined wildfire risk as the interaction between human activity and fuel distribution. Specifically, they integrated population and fuel layers through additive operations as input variables for a gravity model in a spatial interaction model. The prediction results were then classified into five levels. Similarly, Gentilucci et al. (2024) categorized wildfire influencing factors and input them into a weight of evidence model, categorizing wildfire risk into low and high levels through regression of various influencing factor weights. Oliveira et al. (2021a); Bergonse et al. (2021) conducted comprehensive classifications of land use, land cover, slope, elevation, and aspect. They then calculated the likelihood ratio for each category and determined fire susceptibility by summing the weight values of different categories. This process can be mathematically represented as follows:

$$\begin{cases} Lr_i = \frac{S_i/S}{N_i/N}, \\ Lr_j = \sum_{i=0}^n X_{ij} Lr_i \end{cases} \quad (4)$$

where Lr_i represents the likelihood ratio of the variable corresponding to category i ; S_i and S represent the number of burning pixels associated with category i and the total number of burning pixels; N_i and N represent the number of pixels belonging to category i and the total number of pixels in the study area; the total likelihood ratio Lr_j of each grid cell j is obtained by summing the Lr_i values of all n variables. Similarly, South Africa's official wildfire danger rating system, the Lowveld model (Meikle and Heine, 1987; Lall and Mathibela, 2016), defines wildfire risk using the burn index (BI), wind correction factor (WCF), and rain correction factor (RCF), where BI is a function of temperature and relative humidity:

$$\begin{cases} BI = ((T - 35) - (\frac{35-T}{30})) + ((100 - RH) \times 0.37) + 30 \\ FDI = (BI + WCF) \times RCF \end{cases} \quad (5)$$

Srivastava et al. (2014) differed from the aforementioned studies by simultaneously considering both causal and anti-causal factors through an expert knowledge system to quantify the likelihood of forest fires.

Simulation methods based on the above influencing factors are also commonly used in wildfire risk modeling. For instance, Ager et al. (2010) utilized the minimum travel time

(MTT) fire spread algorithm, calculating the burn probability of each pixel through the burn frequency in 10,000 simulations. The simulation results defined wildfire risk as burn probability. Similarly, [Salis et al. \(2021\)](#) used MTT but calculated burn probability through a combination of different simulation results rather than frequency. [Ujjwal et al. \(2022\)](#) used the Spark model and parameters such as temperature, relative humidity, wind speed, and wind direction to model wildfire risk in Tasmania, Australia, defining risk categories as low or high based on the spread area of wildfires at different locations. Another typical example of a simulation method is the Monte Carlo algorithm. For example, [Adhikari et al. \(2021\)](#) defined wildfire risk through the overlap of multiple Monte Carlo algorithm predictions. Specifically, they predicted wildfire boundaries within 30 hours of ignition under various random weather and fuel moisture conditions using the Monte Carlo algorithm. The spatial overlap of all Monte Carlo predictions then generated risk levels.

Wildfire ignition and spread are highly random and exhibit a strong nonlinear relationship with various factors. Data-driven machine learning methods are often used in wildfire risk prediction research due to their ability to fit nonlinear functions effectively with large-scale data. However, these methods cannot explicitly express the influence of various factors on the final wildfire risk. Specifically, commonly used machine learning-based wildfire risk probabilities use binary historical wildfire event datasets as labels, with multiple features as input parameters, defining the binary output or probability output as wildfire risk.

For example, [Yahia et al. \(2023\)](#) used the normalized binary burn ratio as a proxy for wildfire risk probability. This probability, along with proxy variables such as temperature, vegetation dryness, vertical drought index, differential water index, and indices derived from the optical trapezoid model, were used to train a Gaussian naive Bayes classifier. [Malik et al. \(2021\)](#) similarly used historical binary wildfire occurrence records to train an ensemble model combining Adaboost and two random forest models to predict wildfire risk probability. [Qiao et al. \(2024\)](#) constructed a Transformer-based deep learning wildfire risk prediction model, using the output of an MLP as the predicted risk probability. Similarly, [Ghorbanzadeh et al. \(2019\)](#) used MODIS historical wildfire records to train a multilayer perceptron model, with the logistic function output of the model representing wildfire susceptibility. [Jiang et al. \(2024b\)](#) also used MODIS historical wildfire events as true values but created a balanced dataset by selecting non-fire areas in a 1:1 ratio to fire points and used a deep learning model to predict risk probability maps. [Botequim et al. \(2013\)](#) used annual wildfire occurrence records as the dependent variable to regress a logistic function and plotted wildfire occurrence probability. They then used a sigmoid function to describe the relationship between the independent and dependent variables:

$$y = \frac{1}{1 + e^{-(\beta_0 + \beta_1 x_1 + \dots + \beta_n x_n)}} \quad (6)$$

where x_i and y represent the i -th independent variable and historical wildfire occurrence records, respectively. After calculat-

ing the regression coefficients β_i , the logistic model uses the independent variables to output a continuous wildfire occurrence probability between 0 and 1.

It is important to note that the wildfire risk defined by the aforementioned machine learning models is essentially a pseudo-probability rather than a true probability density ([Pelletier et al., 2023](#)). For example, the predicted pseudo-probability in XGBoost is the inverse log transformation of the sum of terminal leaf weights; in SVM, it is estimated by calculating the distance to the classification decision boundary and using these distances for probability estimation; in Random Forest, it is the average of the voting results from multiple decision trees; and in Multilayer Perceptron (MLP), Long Short-Term Memory (LSTM), and Convolutional Neural Network (CNN), it is typically the probability estimate from the final layer activation function. Furthermore, compared to explicit definitions, these models do not provide specific impacts of various features on wildfire occurrence and strongly depend on the construction of the label sample set and the choice of model.

Specifically, different preprocessing methods for historical wildfire data, as well as model selection and performance, can greatly influence the predicted probability values. For instance, when using wildfire influencing factors and historical records at time t as model inputs and selecting historical records at time $t + 1$ as labels to train the model, the model, if performing well, will predict high probabilities for positive regions at time $t + 1$, such as greater than 0.8. However, wildfire risk probabilities are usually low; for example, [Ager et al. \(2014a\)](#) and [Preisler et al. \(2004\)](#) used millesimal probabilities in their wildfire risk assessments for the Mediterranean region and the United States, respectively. Therefore, it is necessary to perform post-processing on the probability predictions, such as establishing a link between explicit and implicit definitions.

2.2. Wildfire ignition risk

Wildfire ignition refers to the first occurrence of a fire event during a wildfire. According to [Badia-Perpinyà and Pallares-Barberà \(2006\)](#), to combat forest fires most effectively, the importance of assessing wildfire ignition risk should be emphasized. Similarly, [Catry et al. \(2009\)](#) highlighted that it is not sufficient to consider only factors influencing wildfire spread and suppression difficulty, such as fuel, weather, and terrain. They cited the definitions provided by the Food and Agriculture Organization and the Glossary of Wildland Fire Terminology, which define wildfire risk as fire ignition risk, meaning "the chance of a fire starting as determined by the presence and activity of any causative agent." Furthermore, estimating wildfire ignition risk is crucial for wildfire management, as it guides decisions related to fuel treatment and the allocation of suppression resources. Generally, wildfire ignition risk can be modeled using historical ignition data ([Miller and Ager, 2012](#)) and used to generate broader or spatially continuous ignition risk maps. Therefore, the following section will focus on how various studies have identified or defined ignition points and converted these records into probability values or modeled dependent variables.

In the study of wildfire ignition risk in Central Spain, [Romero-Calcerrada et al. \(2008\)](#) utilized wildfire records provided by the Sección de Defensa Contra Incendios Forestales of the Madrid regional government. These records included the coordinates of ignition points, land cover of the burned area, and the time of the fire. The researchers then defined the probability of wildfire ignition during the fire season as a prior probability and calculated the posterior probability based on this prior probability. Finally, they generated predicted wildfire risk levels by comparing the ratio of prior to posterior probabilities.

In the study by [Catry et al. \(2009\)](#), they first cleaned and corrected a dataset of 137,204 ignition points selected from the official wildfire dataset provided by Portuguese Forest Services, ultimately retaining 127,409 fire ignition locations. To construct a balanced dataset, they randomly selected a number of non-ignition points across the country, 1.5 times the number of fire ignition locations. The ignition and non-ignition points were then encoded as binary variables, forming the final dependent variable dataset for fire ignition. The researchers used frequency analysis and the natural breaks method to convert the historical fire locations dataset into observed and expected frequencies, which were used to train a logistic regression model. In this model, the expected frequency of fire ignition was calculated proportionally to the land area of each observed frequency interval. The output of the logistic regression model was classified into six risk levels. Similarly, [Ager et al. \(2014b\)](#), in their study of wildfire ignition and burning risk in Sardinia, Italy, and Corsica, France, defined the dependent variable of their regression model as the frequency of wildfire ignition on a daily basis, using wildfire ignition area as a condition for burning risk. It is noteworthy that ignition points in Corsica were assumed to be the centroids of burned areas. [Braun et al. \(2010\)](#) used forest inventory data from Ontario's Ministry of Natural Resources to identify wildfire ignition areas and employed generalized additive models, coordinate offsets, and cubic spline interpolation to generate spatially continuous wildfire ignition probability maps, i.e., risk maps.

In the study of wildfires in Belgium, [Depicker et al. \(2020\)](#) defined the probability of wildfire occurrence in a given area as the average probability of ignition within a calendar year:

$$P(I|C_i) = \frac{P(I)P(C_i|I)}{P(C_i)} \quad (7)$$

where $P(C_i)$ and $P(C_i|I)$ represent the ratio of the area of ignition unit C_i to the total study area and the ratio of the number of ignitions to the total study area, respectively, while P_i denotes the ratio of the number of ignitions to the number of units over a one-year span. To mitigate the issue of class imbalance, smaller areas were merged into larger ones:

$$P_A = 1 - \prod_{i=1}^n (1 - P(I|C_i))^{N_i} \quad (8)$$

where n and N_i represent the number of environments within a larger area A and the number of grid cells within environment i , respectively. In the study of wildfire ignition risk in Galicia, Spain, [Calviño-Cancela et al. \(2017\)](#) analyzed the differences between historical ignition points obtained from the

Spanish Forest Fire Statistics and an equal number of randomly selected locations, examining the relationships between wildfire occurrences and factors such as the wildland-urban interface (WUI), land use/land cover (LULC), and elevation. Similarly, [Ying et al. \(2021\)](#), in their analysis of wildfire ignition causes in Yunnan Province, China, used historical records from the Yunnan Forestry Bureau for the period 2003-2015. These records, like those in previous studies, included information on the date, location, size, and cause of each ignition. In total, 5,145 ignition events were recorded, and approximately 1.5 times as many non-ignition points were randomly selected. The relationship between wildfire risk and influencing factors was modeled based on the presence or absence of ignition, rather than frequency.

It is important to note that the studies mentioned above utilized ground-based wildfire databases rather than the more commonly used MODIS or VIIRS fire/hotspot data in wildfire risk assessment research. This may be due to the relatively low spatiotemporal resolution of these data, making it difficult to detect ignition points with very low intensity and duration. [Benali et al. \(2016\)](#) compared the consistency of wildfire field records in Portugal, Greece, Alaska, California, and southeastern Australia with MODIS active fire products (MCD14ML). They proposed a clustering algorithm to calculate the ignition and end dates of a wildfire in the MCD14ML product and used the Nash-Sutcliffe Model Efficiency Index to estimate the consistency between satellite-estimated fire dates and ground records. The study found that satellite data could not estimate the start and end dates of most fires smaller than 500 ha. Similarly, [Coskuner \(2022\)](#) compared the performance of MODIS and S-NPP VIIRS active fire or hotspot detection products, i.e., MCD14ML V6 and VNP14IMG, in detecting wildfires across five different land cover types in Turkey and compared these detections with records from Turkey's ground-based wildfire database. The authors found that both MODIS and VIIRS had very low detection capabilities for small fires (<1 ha) ($<3.5\%$). They also cited studies by [Fusco et al. \(2019\)](#) and [Ying et al. \(2019\)](#), showing that MODIS fire products had high omission rates in the United States and China. Specifically, [Fusco et al. \(2019\)](#) reported detection rates for MODIS products in the United States ranging from 3.5% to 23.4%, with detection rates increasing with fire size. Similarly, [Ying et al. \(2019\)](#) found that in Yunnan Province, China, only 11.10% of 5,145 ground-recorded wildfire events were detected by MODIS fire products, with most omissions attributed to the small size of the fires. These analyses suggest that the commonly used MODIS and VIIRS fire and hotspot products are not suitable for estimating ignition locations and events, nor for corresponding ignition risk estimation.

In contrast to wildfire ignition risk, wildfire burning risk is more broadly defined as the risk of a fire encountering a particular location, influenced by both ignition and spread. Therefore, most studies do not distinguish between ignition and spread when defining wildfire burning risk but consider both simultaneously. In general, there are two methods for defining wildfire burning risk: using historical burn data through explicit or implicit methods, or defining it based on simulation or spread



Figure 2: The spatial distribution of included research.

models (Finney, 1998, 2002; Scheller et al., 2007; Miller et al., 2008; Tolhurst et al., 2008; Tymstra et al., 2010; Chen et al., 2024d). These methods have been discussed in the previous sections of this chapter, so they will not be repeated here. It is important to note that in choosing between these two methods, (Miller and Ager, 2012) suggests that for smaller fire extents (e.g., 1-10 hectares), ignition risk assessment can accurately reflect the likelihood of fire occurrence. However, for larger fire extents (e.g., 20-50 km), it is necessary to consider using burning risk to represent wildfire risk.

3. Research area distribution

This paper counts 138 recent wildfire risk prediction works in various regions around the world. Fig. 2 illustrates the geographic distribution and quantity of wildfire prediction research globally. The figure indicates that North America and Asia are the most concentrated regions for wildfire prediction studies. The United States has the highest number of studies, totaling 71, followed by China and Australia, each with 18 studies. Additionally, Canada, Iran, and India exhibit considerable research activity, with 11, 14, and 6 studies, respectively.

In Europe, the research is primarily concentrated in Western and Southern Europe. Spain, France, Greece, and Portugal have a notable number of studies, with 8, 5, 7, and 9 studies, respectively. Other countries such as Italy, Sweden, Serbia, and Turkey also have a smaller number of studies. Research on the African continent is relatively sparse, with South Africa, Algeria, Morocco, and Senegal each having one study. Similarly, South America has a limited number of studies, with Brazil and Chile each contributing one study. In Oceania, aside from Australia, no other countries have been recorded as having studies.

Furthermore, there are several studies categorized as global, totaling 18, and studies focused on the Mediterranean basin, totaling 6. These global and regional studies highlight the complexity and diversity of wildfire prediction across different climate zones and ecosystems.

Given the geographic distribution and quantity of research, future studies could focus on expanding research regions, promoting cross-regional studies, and enhancing data sharing and model validation. Specifically, although North America and Asia have concentrated research efforts, other regions such as Africa, South America, and parts of Europe have significantly fewer studies. Future research should aim to strengthen wildfire prediction studies in these underrepresented regions to address the geographic distribution gaps and emphasize the climate justice issue (Jones et al., 2024). Additionally, global and Mediterranean basin studies suggest that cross-regional research is crucial for understanding wildfire behavior under different ecosystems and climatic conditions. Enhancing international collaboration to conduct more comprehensive cross-regional studies can provide more robust prediction models and methods. Finally, many current studies rely on region-specific datasets, limiting the generalizability and applicability of the models. Future efforts should focus on promoting data sharing and openness, establishing unified data platforms, and conducting model validation across different regions to improve the reliability and applicability of prediction models.

4. Data

Essentially, wildfires are uncontrolled processes involving the continuous combustion of organic matter in landscapes (Duff et al., 2017). The ignition and burning processes of wildfires are influenced by factors such as fuel conditions, meteo-

rological and climatic conditions, human interventions, topographical and hydrological characteristics, and historical wildfire occurrences (Fuller, 1991). Therefore, in this section, the data used in wildfire risk prediction are categorized into these types, and their components, definitions, and estimation or proxy methods are introduced.

4.1. Fuel Conditions

Duff et al. (2017) suggests that wildfire is a function of the characteristics of the fuel that sustains it. Compared to other factors influencing the ignition and spread of wildfires, such as meteorological conditions, climate, topography, and hydrology, fuel is relatively straightforward to control (Chuvieco et al., 2012). Some studies even posit that fuel is the only element in the landscape that can be altered to influence fire behavior (Thompson et al., 2013; Fernandes and Botelho, 2003). These studies highlight the importance of assessing fuel conditions in wildfire risk evaluations. Fuel refers to any combustible material; in the context of wildfire studies, this includes the combustible organic matter contained in both live and dead vegetation (McLauchlan et al., 2020; Leite et al., 2024). The influence of fuel conditions on wildfire potential, behavior, duration, and emissions is typically described using four variables: Fuel Moisture Content (FMC), fuel load, fuel type (fuel model), and fuel continuity. These parameters directly impact the likelihood of fire occurrence, its intensity, and its rate of spread.

4.1.1. Fuel moisture content

Fuel Moisture Content (FMC) is defined as the ratio of the weight of water to the dry weight of the sample (Eq. 9) (Mbow et al., 2004; Chuvieco et al., 1999). FMC can be categorized into two types: Live Fuel Moisture Content (LFMC) and Dead Fuel Moisture Content (DFMC). It regulates the combustibility of the fuel (Yebra et al., 2013b) and is a significant factor influencing the spread rate of wildfires and the emissions produced during a fire (Fernandes et al., 2008; May et al., 2019).

$$FMC = \frac{\text{Weight of water in sample}}{\text{Dry weight of the sample}} \times 100\% \quad (9)$$

In FMC, LFMC is influenced by various plant ecophysiological characteristics, adaptations, and environmental factors affecting transpiration, such as soil moisture and ambient humidity (Castro et al., 2003). In contrast, dead fuel differs from live fuel in that it cannot actively regulate its moisture content through water uptake via roots or water loss through stomatal transpiration. Instead, its moisture content is determined by fuel size, meteorological and microclimate conditions (Nolan et al., 2016), and the biochemical composition of the fuel (Viney, 1991a). These factors are generally determined through experiments or empirical data (Viney, 1991b; Ager et al., 2010). Dead fuel absorbs or loses moisture in response to environmental conditions and eventually reaches equilibrium with the surrounding atmosphere, known as Equilibrium Moisture Content (EMC). The time required to reach EMC is primarily determined by the size of the fuel (Catchpole et al., 2001). Fuel size can be classified into fine fuels, such as small twigs and leaves

(1-hour fine fuels), coarser branches and small trunks (10-hour and 100-hour coarse fuels), large trunks and coarse branches (1000-hour fuels), dead grasses and forbs, as well as surface litter and fallen leaves. In some cases, soil is also considered a type of dead fuel, and its moisture content is measured (Rothermel et al., 1986). The moisture content of dead fuel, which is more influenced by environmental and weather factors, plays a decisive role in fire ignition and rapid spread at the beginning of the fire season, whereas the moisture content of live fuel has a greater impact on the persistence and extent of fire spread.

a) Dead Fuel Moisture Content

DFMC is a crucial input in nearly all wildfire risk assessment models (Matthews, 2013). For example, estimates of DFMC are integral to current operational fire prediction systems, including the Fire Weather Index (FWI) and the National Fire Danger Rating System (NFDRS) in the United States (Vitolo et al., 2020). Estimating DFMC involves calculating EMC based on factors like temperature, relative humidity, and fuel response time, combined with precipitation data and drying algorithms (Nieto et al., 2010). DFMC estimation methods can generally be divided into four categories: measurements at meteorological stations, field sampling, estimates based on meteorological data, and indirect retrieval using multi-source remote sensing data.

DFMC can be measured using standard wooden dowels installed 10-12 inches above the ground at meteorological stations (Rakhmatulina et al., 2021). However, due to the sparse network of DFMC measurement stations and the limited accuracy, it is challenging to cover large areas even with interpolation of atmospheric parameters. Similarly, field sampling of DFMC is highly accurate and provides data and theoretical support for physical process models and empirical modeling. However, field measurements of fuel properties like DFMC require consideration of terrain, vegetation type, ecosystem structure, climate type, and soil type, making it time-consuming, costly, and limited in scope (Duff et al., 2017). Therefore, studies combining field measurement data with station or numerical weather prediction and meteorological reanalysis data to develop empirical and mechanistic models for estimating FMC are more common (Matthews, 2013). Physical process models primarily consider energy and water balance equations, with the Nelson Dead Fuel Moisture Model, proposed by Nelson Jr (2000), being the most widely used for DFMC estimation. This model predicts DFMC by calculating heat conduction and moisture transfer between a wooden cylinder, the surrounding atmosphere, and external conditions, using hourly input data on temperature, humidity, radiation, and precipitation.

Additionally, McNorton and Di Giuseppe (2024) designed a new method for estimating DFMC by grouping fuels and simplifying the Nelson model. Other models used for DFMC estimation include bulk litter layer models, Byram's diffusion equation-based models, and complete process-based models (Matthews, 2013). Empirical methods for estimating DFMC rely on observed relationships between measured DFMC and factors such as air temperature, relative humidity, wind speed, soil moisture content, and vapor pressure deficit. These data-driven methods include statistical techniques (Ferguson et al.,

2002; Ray et al., 2010; Cawson et al., 2020; Rakhmatulina et al., 2021), but their primary limitation is that they are entirely data-driven, making it difficult to explain the relationship between driving factors like temperature, heat and water vapor fluxes, radiation, and precipitation, and DFMC. Consequently, some studies have started to combine data-driven approaches with physical process models (Fan and He, 2021; Fan et al., 2024).

Apart from the meteorological data-based FMC estimation methods mentioned above, indices such as the Cellulose Absorption Index (CAI), the Lignocellulose Absorption Index (LCAI), the Normalized Difference Tillage Index (NDTI), the Normalized Difference Vegetation Index (NDVI), and the Shortwave Infrared Normalized Difference Residue Index (SINDRI) have been shown to correlate with DFMC (ZORM-PAS et al., 2017; Zacharakis and Tsirhrintzis, 2023b). This forms the theoretical basis for DFMC estimation using remote sensing. However, research on DFMC estimation using multi-source remote sensing data is still limited (McCandless et al., 2020).

b) Live Fuel Moisture Content

In early studies, the live fuel moisture content (LFMC) was measured similarly to the dead fuel moisture content (DFMC) through field sampling and weighing methods, with interpolation or inversion used to estimate the entire study area (Bianchi and Defossé, 2015). While this method is highly accurate locally, it is time-consuming, labor-intensive, and not scalable to landscape, regional, or global levels (Yebra et al., 2013a). Like DFMC, LFMC can be estimated on a large scale in near real-time using meteorological parameters. This is because plant water regulation is influenced by environmental factors such as precipitation, soil moisture, and evapotranspiration (Bowyer and Danson, 2004). For example, the NFDRS used by the US Forest Service calculates LFMC using empirical formulas based on precipitation, temperature, and relative humidity (Bradshaw et al., 1984). Moreover, Castro et al. (2003) modeled the live fine fuel moisture content (LFFMC) of *Cistus* spp. in the Catalonia region of Spain using factors such as temperature, soil water availability, and atmospheric water content. Similarly, Ruffault et al. (2018) compared six drought indices' ability to estimate LFMC across six different Mediterranean shrubs in southern France, finding that drought indices were effective only at stand scale, with indices simulating long-term drought dynamics (DC, RWC, and KBDI) providing better LFMC predictions. Viegas et al. (2001) used DC, BUI, and DMC from the FWI to estimate LFFMC in various plant species in central Portugal and Catalonia. Furthermore, Vinodkumar et al. (2021) successfully predicted LFMC across Australia using the lag relationship between soil moisture changes and vegetation moisture responses combined with regression analysis and physical models.

Meteorological data can also be combined with other datasets to estimate LFMC. For instance, Miller et al. (2023) proposed a method using a multimodal Multi-tempCNN model that incorporates multitemporal meteorological data, MODIS MCD43A4 BRDF-Adjusted Reflectance data, and climate zone, topography, and location information. This method enables large-scale LFMC estimation at medium resolution (500 m) over periods

longer than two weeks. Similarly, McNorton and Di Giuseppe (2024) integrated soil moisture data and leaf area index (LAI) to estimate LFMC, validating the estimates using MODIS data. In the western United States, Wang and Quan (2023) used meteorological indicators, soil moisture data, and vegetation indices to estimate LFMC, finding that inversion accuracy varied with vegetation cover type.

The advantage of meteorological parameter-based LFMC estimation methods is the ability to generate near real-time LFMC estimates or predictions using data from weather stations, meteorological satellites, or numerical weather forecasting (Capps et al., 2021). However, LFMC is more challenging to estimate using meteorological parameters compared to DFMC. This is because plants actively regulate their water content through absorption and transpiration, with significant differences in physiological characteristics between plant species and a greater influence from phenological conditions and medium-term meteorological conditions (Pellizzaro et al., 2007; Ruffault et al., 2018; Jolly and Johnson, 2018).

Therefore, compared to LFMC estimation methods based on meteorological data or drought indices, most studies prefer using multi-source remote sensing data to estimate LFMC (Rao et al., 2020a; Capps et al., 2021; Quan et al., 2021a; Rodriguez-Jimenez et al., 2023). Remote sensing technology, as a low-cost means of large-scale, long-term dynamic Earth observation, also enables near real-time, high-resolution LFMC estimation in highly heterogeneous real-world scenarios (Quan et al., 2021b; Zhu et al., 2021; Verbesselt et al., 2002). The exponential growth of Earth observation missions (Ustin and Middleton, 2021) has provided new opportunities for LFMC estimation (Leite et al., 2024). Studies on LFMC estimation using multi-source satellite remote sensing primarily utilize multispectral reflectance data, thermal infrared data, and active and passive microwave data, combined with data-driven empirical or machine learning models, radiative transfer-based physical models, or hybrid models that integrate physical constraints with data-driven approaches (Yebra et al., 2013a; McNorton and Di Giuseppe, 2024).

The theoretical basis for LFMC inversion methods using multispectral reflectance data lies in the presence of water absorption bands in the near-infrared (750-1100 nm) and short-wave infrared (1100-2500 nm) spectral regions. Plant stress due to drought leads to changes in chlorophyll concentration and leaf internal structure, allowing the relationship between vegetation spectral reflectance (i.e., spectral characteristics) and LFMC to be established (Knippling, 1970; Kriedemann and Barrs, 1983; Bowyer and Danson, 2004; Yebra et al., 2013a; Sow et al., 2013; Zacharakis and Tsirhrintzis, 2023b; Leite et al., 2024). Thus, LFMC can be inverted by simulating the relationship between spectral characteristics under different water content levels and observed spectral characteristics (Hao and Qu, 2007; Yebra et al., 2008, 2013a; Marino et al., 2020; Quan et al., 2021a). While this physical method is generally more robust, it is also more complex in terms of parameterization (Yebra et al., 2013a). Alternatively, empirical methods based on spectral reflectance or spectral indices, including the normalized difference vegetation index (NDVI), enhanced vegetation

index (EVI), soil-adjusted vegetation index (SAVI), normalized difference infrared index (NDII), water index (WI), normalized difference water index (NDWI), visible atmospheric resistance index (VARI), Leaf Water Content Index (LWCI) (Hunt Jr et al., 1987), Global Vegetation Moisture Index (GVMI), and Short-wave Infrared Water Stress Index (SIWSI) (Fensholt and Sandholt, 2003), are simpler and only require fitting the relationship between in situ LFMC measurements and spectral reflectance characteristics. These methods can perform as well as or better than physical models at local scales and across specific vegetation types (Cunill Camprubi et al., 2022).

For example, Chuvieco et al. (2002) compared the ability of shortwave infrared bands, NDVI, NDII, LWCI, the wetness and greenness components of the Tasseled Cap transformation, and spectral derivatives to model LFMC in Mediterranean grasslands and shrubs. They found that shortwave infrared bands and indices using these bands performed better due to the high correlation between shortwave infrared and LFMC, attributed to water absorption in leaves. Near-infrared and red bands also showed good correlation with LFMC, particularly for herbaceous plants, where drought stress led to changes in chlorophyll content and structure. The study recommended further use of thermal bands and meteorological data to improve modeling accuracy. Additionally, Myoung et al. (2018) used Pearson correlation analysis to compare the correlations between 16-day NDVI and EVI products (MOD13Q1 and MYD13Q1) and NDWI, NDII, and VIARI calculated from MOD09A1 reflectance data and in situ LFMC measurements from the National Fuel Moisture Database. The study ultimately selected EVI and introduced daily minimum temperature data to establish an empirical model for estimating LFMC in southern California. This choice was because EVI effectively captured changes in chlorophyll concentration related to water content, showing better response than other vegetation indices and shortwave infrared bands under water stress, particularly for Mediterranean vegetation. Introducing temperature data improved the model's ability to capture excessive water loss during extreme heat, correcting overestimates of minimum LFMC. Similarly, García et al. (2020) found that EVI performed better than other ratio vegetation indices, such as NDII, NDVI, and VARI, for LFMC modeling in Eastern California and Oregon.

Marino et al. (2020) used NDVI, NDII, GVMI, NDWI, EVI, SAVI, VARI, and VI_{green} from MCD43A4 and MOD09GA products, as well as the same indices calculated from Sentinel-2 data, to estimate the LFMC of Mediterranean shrubs. The main difference between MOD09GA and MCD43A4 and the MOD13Q1 and MYD13Q1 products used by Myoung et al. (2018) is that the former are daily data, which do not smooth out short-term LFMC changes. This feature is more conducive to capturing abnormal LFMC values under extreme conditions and to estimating LFMC for shrubs and grasslands that are more sensitive to short-term environmental changes. Similar to Myoung et al. (2018), Marino et al. (2020) also found that using vegetation indices to estimate LFMC tends to overestimate lower LFMC values. However, Marino et al. (2020) found that VARI had the highest accuracy in LFMC modeling compared to other vegetation indices. Combining VARI with NDVI can

further improve the accuracy of the model. This is because VARI and NDVI are based on visible (blue, green, red) and near-infrared reflectance data, which are suitable for measuring changes in greenness and LAI related to leaf drying and can indirectly reflect leaf water content. Similarly, Stow et al. (2006); Peterson et al. (2008); Caccamo et al. (2011) found that VARI performed better than other vegetation indices or reflectance bands in estimating LFMC for shrubs in Southern California, Mediterranean climate regions, and southeastern Australia. Although these studies did not show that any particular vegetation index is the best choice in all scenarios, they emphasized the importance of chlorophyll (or greenness) response to water stress.

Water availability is a key parameter for plant transpiration. Therefore, changes in LFMC affect not only reflectance spectral bands but also canopy temperature (ST). When plants dry out, transpiration and latent heat transfer decrease, which in turn increases sensible heat (Kozlowski et al., 1990; Yebra et al., 2013a). As a result, introducing thermal infrared bands (2500-14000 nm) into LFMC estimation can improve model performance under certain conditions. It is worth noting that in most studies, land surface temperature (LST) is used as a proxy for ST. Chuvieco et al. (2004) used NDVI and ST data from the AVHRR sensor to estimate LFMC for grasslands and shrubs in Cabañeros National Park, central Spain, based on a linear regression model. The study found that NDVI and ST were positively and negatively correlated with LFMC, respectively, and that the introduction of ST significantly improved the model's performance. Cunill Camprubi et al. (2022) combined MODIS spectral bands, vegetation indices, land surface temperature, and day of the year as predictors, using a random forest algorithm to estimate LFMC in the Mediterranean basin wildlands. They found that the combination of LST and day of the year had the highest importance, and that when the temperature exceeded 20°C, LST was negatively correlated with LFMC. However, in LFMC estimation experiments based on MODIS LST products, LST did not show a significant advantage over other factors. For example, Sow et al. (2013) compared the performance of the NDVI-to-LST ratio and GVMI, WI, NDWI, NDII, and MSI in estimating LFMC and equivalent water thickness (EWT) in three study areas in Senegal, finding that the NDVI-to-LST ratio had no significant advantage in correlating with LFMC and EWT compared to other vegetation indices. It is worth noting that this study did not compare the performance of using NDVI alone to model LFMC or EWT. (McCandless et al., 2020) used machine learning methods to model LFMC across the continental United States using MODIS reflectance data, meteorological data, and terrain data. The random forest method was used to evaluate the importance of various predictors, finding that the importance of LST was only 6

Although spectral features can model canopy LFMC, they are more sensitive to dry matter such as canopy structure, resulting in lower robustness (Rao et al., 2020b). Additionally, these spectral features couple dry matter and water content information, so when both change due to water stress, there can be issues with estimating LFMC using vegetation indices and other spectral features (Danson and Bowyer, 2004; Yebra et al.,

2013b). Moreover, spectral features are affected by lighting conditions and clouds or rain, making it difficult to provide full-time or near-real-time large-scale, long-term series LFMC mapping (Rao et al., 2020b). Compared to spectral reflectance, microwave remote sensing is more capable of penetrating clouds and is more sensitive to water content (Rao et al., 2020b). For example, active microwave sensors are sensitive to vegetation structure or dielectric properties (including vegetation moisture) through backscatter signals, and their penetration capability can be used to model soil moisture, thus monitoring vegetation water stress (Dorigo et al., 2017). Passive microwave sensors can also be used to estimate LFMC through soil moisture time lags or vegetation optical depth (VOD) (Lu and Wei, 2021a; Forkel et al., 2023). Commonly used microwave sensors primarily operate in the P-band (≈ 70 cm), L-band (≈ 23 cm), C-band and X-band (≈ 3 cm), and Ku-band ($\approx 1.6\text{--}2.5$ cm). Among them, the backscatter signal of P and L bands is primarily coupled with backscatter from the soil and lower canopy, while the backscatter signal of C, X, and Ku bands mainly comes from the interaction between microwave radiation and the upper canopy.

Tanase et al. (2015) used vertical-vertical (VV), vertical-horizontal (VH), horizontal-vertical (HV), and horizontal-horizontal (HH) polarization L-band radar backscatter signals to model the relationship between backscatter intensity, polarization decomposition signals, radar vegetation index (RVI) (Kim et al., 2012), and canopy height with LFMC and EWT. Experiments in Australian forests demonstrated that the modeling capability of L-band radar data was superior to spectral reflectance data. The penetration of L-band data enables modeling of the lower canopy and surface fine fuel moisture content. However, when the forest is high and dense, and both lower canopy and soil moisture are low, there will be a large error in estimating LFMC for the lower canopy. Wang et al. (2019) explored the performance of C-band Sentinel-1A (5.4 GHz) VV and VH polarization data in estimating LFMC in Texas forests. The model coupled an empirical bare soil backscatter model with the Water Cloud Model (WCM) (De Roo et al., 2001) to establish an LFMC lookup table, directly estimating LFMC, and compared this LFMC with results obtained from Landsat 8 OLI spectral reflectance data using the empirical partial least squares (PLSR) method and measured LFMC data. The experiment showed that the accuracy of LFMC inversion based on Sentinel-1A data was higher than that based on Landsat 8 OLI data and that it could reproduce the temporal variation trend of LFMC. Lu and Wei (2021b) used multi-source microwave soil moisture products ECV_SM and SMAP L-band Level 4 surface and root zone soil moisture data, using a robust linear regression model with a time lag to assess LFMC across the continental United States. The study showed that LFMC was most correlated with soil moisture conditions 60 days before LFMC sampling in most regions.

Considering the influence of soil moisture content and canopy dry matter on radar backscatter, reflectance, or emission signal intensity, some studies have integrated SAR and multispectral reflectance data, along with vegetation cover, canopy height, and soil moisture data, to estimate LFMC. For instance,

Jia et al. (2019) employed soil moisture data obtained from the SMAP L-band radiometer, combined with VARI calculated from MODIS MCD43A4 reflectance data, growing degree days (GDD), and precipitation, to estimate LFMC in Southern California using a regression model. This study found that using cumulative soil moisture data combined with cumulative growing degree days yielded better performance in LFMC estimation compared to using MODIS VARI combined with cumulative growing degree days. The superior performance is attributed to a more accurate representation of the water cycle processes between vegetation and soil.

Rao et al. (2020b) designed a knowledge-assisted neural network to estimate LFMC in the western United States, utilizing Sentinel-1 VV and VH polarized SAR backscatter data, Landsat-8 red, green, blue, near-infrared (NIR), and shortwave infrared (SWIR) optical reflectance data, along with NDVI, NDWI, and near-infrared spectral indices derived from the reflectance data. To separate the contributions of vegetation and soil moisture to the backscatter signal, the study proposed a knowledge-based method and a data-driven approach. The former method leverages the differential sensitivity of VV and VH polarizations to soil and vegetation moisture, using the difference between VV and VH polarizations to separate the contributions of soil and vegetation to backscatter intensity. The latter approach involves training the deep learning model to learn the separation of vegetation moisture and soil moisture contributions by incorporating soil type as an input. The study also established a ratio of backscatter signals to spectral reflectance, utilizing the high water sensitivity of backscatter signals and the high spectral reflectance of dry matter, alongside the aforementioned vegetation indices to separate the contributions of dry matter and water content to LFMC estimation.

Similarly, Xie et al. (2022a) employed Sentinel-1 data along with MODIS MCD43A4 nadir BRDF-adjusted reflectance (NBAR) data, original band reflectance data from Landsat-8 OLI (red, green, blue, NIR, and SWIR channels), and vegetation indices such as NDVI, NIRV, and NDWI. The study used canopy height and land cover type as auxiliary data to estimate LFMC in the western United States. These data were interpolated to unify spatial and temporal resolutions before being input into an integrated model, where LFMC was predicted through end-to-end training.

Furthermore, Forkel et al. (2023) achieved global LFMC estimation by combining Ku-band, X-band, and C-band VOD data derived from passive microwave technology with MODIS LAI, AVHRR vegetation cover data, LULC, and meteorological and topographical data. This study demonstrated that the combination of Ku-VOD and LAI as predictors significantly improved LFMC estimation performance. Conversely, Chaparro et al. (2024) conducted LFMC inversion experiments in the western United States, showing that when a model effectively separates vegetation structure and dry matter information, the accuracy of LFMC estimation based on VOD is independent of canopy height, land cover type, and radar backscatter signals.

While the aforementioned LFMC estimates based on multispectral and microwave remote sensing data have achieved satisfactory accuracy, it is noteworthy that some studies sug-

gest that the inclusion of microwave data does not necessarily enhance LFMC inversion accuracy. For example, [Tanase et al. \(2022\)](#) explored the estimation of LFMC in Mediterranean vegetation using C-band Sentinel-1 and Sentinel-2 multispectral data combined with canopy height, vegetation cover, and topographical data. The study found that incorporating radar data did not improve model performance and thus only recommended its use in areas with significant cloud cover.

Research has also been conducted on the effectiveness of different data sources for LFMC estimation. For instance, [Fan et al. \(2018\)](#) compared the performance of LFMC estimation in southern France using ECV_SM, root zone soil moisture from ECV_SM, microwave polarization difference index (MPDI) calculated from C, X, Ku, K, and Ka band passive microwave data at 6.9, 10.7, 18.7, 23.8, and 36.5 GHz, VOD derived from AMSR-E C and X band data, and vegetation indices such as NDVI, SAVI, VARI, NDWI, NDII, and GVMI calculated from MODIS data. The MPDI and VOD were averaged over 15 days prior to in-situ measurements. The study found that the optical vegetation indices VARI and SAVI outperformed the microwave-derived indices and other optical indices. Among the microwave indices, X-band VOD showed the highest consistency with in-situ measured LFMC.

4.1.2. Fuel load

Another crucial variable in fuel conditions is fuel load, which refers to the total biomass per unit area and provides a baseline for the available biomass in wildfires ([McNorton and Di Giuseppe, 2024](#)). Fuel load influences the severity and spread of fires ([García-Llamas et al., 2019; Alonso-Rego et al., 2020; McNorton and Di Giuseppe, 2024](#)). It can be categorized into live fuel load and dead fuel load, or further divided by size into fine fuel load—such as grass, small shrubs, twigs, and leaves—and coarse fuel load, including trunks and logs ([Gould et al., 2011](#)). Moreover, the definition of fuel load varies slightly across different studies. For instance, [Lee et al. \(2022\)](#) defines fuel load as the amount of fuel in the upper parts of trees, specifically canopy fuel load, while [McNorton and Di Giuseppe \(2024\)](#) defines the above-ground component of fuel load as above-ground biomass. Notably, there is an emphasis on dead fine fuel because it is the primary carrier of fire ignition and spread ([Cruz et al., 2003; Elia et al., 2020; D'Este et al., 2021](#)), while canopy fuel load is highlighted because crown fires typically consume fine fuel, resulting in more intense and faster-spreading fires ([Arellano-Pérez et al., 2018; Walker et al., 2020; de Groot et al., 2022](#)).

The methods for estimating fuel load are similar to those for estimating FMC, including direct sampling and the use of physical models or multispectral and microwave remote sensing data. Direct measurement involves collecting field samples, weighing, drying them, and then estimating biomass in the area, which is considered the most accurate assessment method and can provide a data foundation for physical or empirical model evaluations. First, fuel load estimation methods based on ground-measured data combined with vegetation or forest growth models can predict or estimate fuel load by forecasting future vegetation growth, forest structure, and more. For ex-

ample, [Lee et al. \(2022\)](#) used a Weibull function and mortality model based on forest inventory data to predict the fuel load of Korean red pine (*Pinus densiflora*) for the next 20 years in Korea. Meanwhile, [Nolan et al. \(2022\)](#) modeled above-ground biomass in the shrub layer of eucalyptus forests in southeastern Australia using allometric equations, considering it as fuel load. Furthermore, [Li and He \(2022\)](#) developed a semi-empirical fuel load estimation model for the Krycklan region in northwestern Sweden by combining L-band ALOS PALSAR and Landsat 7 ETM+ reflectance data, along with NDII, NDVI, NDTI, and RVI vegetation indices, using vegetation cover and land cover type as auxiliary data. The study used the Water Cloud Model (WCM) to simulate forest scattering and corrected the influence of vegetation cover on the simulated scattering signal using reflectance data.

While ground sampling offers high accuracy, it is inefficient and costly. In contrast, remote sensing technology provides an efficient and comprehensive method for assessing fuel load. For example, [Saatchi et al. \(2007\)](#) used airborne SAR data and a semi-empirical algorithm to estimate the distribution of forest biomass and canopy fuel load in Yellowstone National Park. Additionally, [Duff et al. \(2012\)](#) developed a biophysical model to explore the feasibility of using satellite-based NDVI to estimate forest fuel load in southeastern Australia. [Li et al. \(2020\)](#) estimated changes in live fuel load in shrubs and grasslands in the Owyhee Basin, southern Idaho, using MODIS NPP products combined with the Biome-BGC model, and calculated changes in dead fuel load based on the estimates. The study found that even with the same productivity, the fuel load of shrubs was higher than that of grasslands.

In addition to fuel load estimation using physical or semi-empirical models based on remote sensing data, empirical model-based methods are simpler and more commonly used. For instance, [Arellano-Pérez et al. \(2018\)](#) used the random forest method and Sentinel-2 multispectral and vegetation index data to estimate the canopy fuel load of *Pinus radiata* and *Pinus pinaster* stands in northwestern Spain. However, due to the low penetration capability of optical sensors, the accuracy of canopy fuel load estimation in this study was limited. Furthermore, [Li et al. \(2021a\)](#) compared the effectiveness of L-band SAR (ALOS-PALSAR) and Landsat 7 ETM+ in estimating fuel load in coniferous mixed forests and found that L-band SAR outperformed optical data in all three fuel load types, with estimation accuracy further improved when both were integrated. [Li et al. \(2022b\)](#) used a data-driven random forest model to correlate long-term spatiotemporal characteristics derived from Landsat 8 OLI and Sentinel-1 data with field-measured fuel load, estimating the fine fuel load (FFL) of pine forests in some areas of Sichuan Province, China. The study found that combining SAR and multispectral data improved FFL estimation accuracy, and temporal features were more important than spatial features.

The comparison between optical and SAR sensor-based fuel load estimation accuracy highlights the importance of canopy structure information in remote sensing-based fuel load estimation. Compared to the fuel load assessment methods based on optical or SAR imagery mentioned earlier, airborne LiDAR provides more detailed information about vegetation's three-

dimensional structure (Aragoneses et al., 2024). Therefore, airborne and satellite-based LiDAR sensors can more directly and accurately estimate fuel load at different scales. For instance, Skowronski et al. (2011) used a LiDAR system to estimate canopy fuel load in pine-dominated forests in New Jersey, USA, predicting crown bulk density and canopy fuel weight. Chen et al. (2017) effectively estimated ground fuel load in Western Australia's Jarrah forests by combining LiDAR data with previous year fire data, canopy density, elevation, and fuel types. Bright et al. (2017) compared the performance of airborne LiDAR and Landsat time-series data in estimating forest canopy and surface fuel load in a study area in Grand County, Colorado, USA, finding that Landsat provided limited improvement in fuel load estimation. Labenski et al. (2023) further combined Sentinel-2 multispectral data with airborne LiDAR data to extract forest structure and composition information for two forest areas in southwestern Germany, using a random forest model to predict and map surface fuel load. In another study, D'Este et al. (2021) incorporated Sentinel-1 SAR data into a fuel load estimation model based on Sentinel-2 multispectral data and airborne LiDAR data for southeastern Italy, estimating dead fine fuel load. The study found that compared to NDVI and C-band SAR data, LiDAR variables had a stronger capacity to estimate dead fine fuel load. The study also found that woody vegetation contributed more to fuel load, consistent with the findings of Li et al. (2020).

In addition, the more recent NASA Global Ecosystem Dynamics Investigation (GEDI) full-waveform LiDAR sensor has been widely used for large-scale above-ground biomass estimation and vegetation canopy structure analysis (Myroniuk et al., 2023; Liang et al., 2023; Aragoneses et al., 2024; Guerra-Hernández et al., 2024), aiding wildfire simulation, assessment of wildfire impacts on vegetation, and understanding wildfire severity. However, only a few studies have directly used GEDI LiDAR data to estimate fuel load. For example, Leite et al. (2022) used unmanned aerial vehicle (UAV) simulations and GEDI data to study the ability to stratify fuel load in grasslands, savannas, and forests within tropical savannas in Brazil. However, the study found that GEDI performed poorly in estimating fuel load for ground and low-lying vegetation, and was significantly affected by terrain.

Finally, it is worth noting that due to the similarity in definitions, particularly the emphasis on crown fires, some studies have used above-ground biomass as a proxy for fuel load (Eames et al., 2021; Vega et al., 2022). Additionally, other studies have used different proxies for fuel load. For instance, Su et al. (2021) used fractional vegetation cover (FVC) as a proxy for fuel load in a study on wildfire drivers in tropical rainforests in southern China. FVC represents the percentage of an area covered by green vegetation within a statistical region. In practical applications, the MODIS NDVI product is commonly used as a proxy for FVC. Helman et al. (2015) analyzed time-series NDVI data from MODIS to distinguish between woody and herbaceous vegetation in Mediterranean forest regions, using long-term mean woody NDVI and its trends as a proxy for fire fuel. In actual wildfire risk prediction, using proxies instead of directly estimating fuel load is more common because it is

simpler and avoids cumulative errors.

4.1.3. Fuel types

Another method to describe fuel properties, aside from fuel moisture code and fuel load, is by categorizing fuels into homogeneous groups that exhibit similar characteristics under specified burning conditions. These groups are defined as "fuel types" or "fuel models" (Arroyo et al., 2008). The description of fuel types is generally complex, taking into account various fuel characteristics such as vegetation type, canopy height, canopy base height, canopy bulk density, vegetation cover ratio, horizontal and vertical continuity, fuel load, fuel moisture, and biomass (Chuvieco et al., 2003; Pettinari and Chuvieco, 2020; Aragoneses and Chuvieco, 2021). In recent years, various standardized fuel classification systems have been proposed in different regions (Fig.1), including the NFDRS (Cohen, 1985), Northern Forest Fire Laboratory (NFFL) (Albini, 1976; Burgan, 1984), Fuel Characteristics Classification System (FCCS) (Sandberg et al., 2001; Ottmar et al., 2007), McArthur fuel types (McArthur, 1966, 1967), Canadian Fire Behaviour Prediction (FBP) (Group et al., 1992), and Prometheus (Riaño et al., 2002). These systems are either fire rating systems or fuel classification systems defined by wildfire simulation methods, or simplified versions of such systems (Arroyo et al., 2008).

Table 1: Comparison of Fuel Classification Systems (Arroyo et al., 2008)

Fuel classification system	Number of fuel types	Country of application
NFDRS fuel types	20	USA
NFFL fuel types	13 ^a	USA
FCCS	216 ^b	USA
McArthur fuel types	3	Australia
FBP fuel types	16	Canada
Prometheus fuel types	7	Europe ^c

^a Option of developing custom fuel types.

^b New fuelbeds added periodically.

^c Mediterranean countries.

Similar to the assessment methods for fuel load and fuel moisture, fuel type mapping can also be conducted through field sampling and remote sensing techniques, including the use of optical, microwave, and LiDAR sensors (García et al., 2012; Pettinari and Chuvieco, 2020; Aragoneses and Chuvieco, 2021). This generally involves the classification of vegetation types and the retrieval of vegetation structure and biochemical parameters such as canopy, followed by the classification of fuel types using expert knowledge or experimental data (Chuvieco et al., 2020). At large scales, such as global or continental levels, fuel type maps are usually created by combining satellite imagery with land use types and the aforementioned fuel classification systems (Pettinari et al., 2013; Pettinari and Chuvieco, 2016; Aragoneses and Chuvieco, 2021).

In addition to detailed classification of fuel types, many wildfire risk assessment studies based on multi-source remote sensing data employ simpler, but coarser, land use type maps as proxies for fuel types to analyze the impact of different land cover types or human activities on wildfire risk. For instance, Jaafari et al. (2019) used logistic regression to analyze the impact of various explanatory variables, including topography, el-

elevation, TWI, meteorological factors, and land use, on wildfire risk in the Zagros ecoregion of western Iran. They found that the most important variable was land use type, with dry farmland and forests being the most susceptible to wildfires. Additionally, the type and continuity of vegetation determined the likelihood of large fires. Similarly, [Ager et al. \(2014b\)](#) analyzed wildfire occurrence and size on the islands of Sardinia, Italy, and Corsica, France, finding that early in the fire season, the probability of large fires was ten times higher in agricultural lands in southern Sardinia compared to forest and shrubland land use types near roads. However, by the end of the fire season, the latter land use types exhibited a higher probability of fires. Conversely, [Calviño-Cancela et al. \(2016\)](#) analyzed the wildfire risk in the wildland-urban interface (WUI) and LULC in northern Spain, finding that primary forests and agricultural areas had the lowest fire risk. Similarly, [Donovan et al. \(2020\)](#) assessed wildfire risk in the Great Plains ecoregion of the United States, considering five land use types: grasslands, woody vegetation, croplands, pastures and hayfields, and developed areas. Their study found that woody vegetation and grasslands were most prone to wildfires and large fires, while other land use types had lower risks. Among them, croplands had the lowest probability of large fires, and as the percentage of crop cover increased, the likelihood of large fires decreased.

It is noteworthy that various vegetation state description parameters are generally used in studies evaluating their effectiveness in wildfire risk modeling but are rarely directly utilized in wildfire risk assessment models. Commonly used wildfire risk assessment models often directly employ raw multispectral or microwave data or indices derived from these data. This could be due to several reasons:

Firstly, evaluating fuel state is complex, often requiring multiple sensors, and the models built for this purpose tend to have poor generalization ability, making them suitable only for specific regions. Additionally, the availability of sensors is a limiting factor for the application of certain fuel state description parameters. For example, estimating vertical canopy structure typically requires LiDAR data. However, satellite-based LiDAR canopy structure is limited by spatiotemporal resolution, and airborne LiDAR has limited coverage and high costs.

Moreover, most wildfire risk assessment studies require long time series data, which, due to cost constraints, are often based on low-cost and readily available data such as multispectral or microwave satellite data. These data, due to limitations in spatiotemporal resolution and canopy penetration, often struggle to accurately retrieve various descriptive parameters. The descriptive parameters obtained from inaccurate data inversions may lead to error accumulation, which can further impact prediction accuracy.

Lastly, data-driven algorithms are becoming increasingly popular, and these algorithms can either rely on or bypass manual feature engineering, allowing them to directly learn the necessary abstractions from features or raw data.

4.1.4. Fuel continuity

Since fire lines spread both horizontally and vertically, fuel continuity is generally considered in terms of both vertical

and horizontal directions. Vertical canopy continuity primarily refers to the vertical structure of fuels, also known as ladder fuels. These are composed of low-lying shrubs, seedlings, upper canopy trees, and intermediate understory vegetation. In areas where vertical fuels are present, this structure can cause low-intensity surface fires to escalate into severe crown fires ([Agee and Skinner, 2005](#); [Menning and Stephens, 2007](#)). There has been significant research on ladder fuels, including methods for precise field measurements of fuel structure ([Kilgore and Sando, 1975](#); [Pye et al., 2003](#)) and approaches combining field measurements with expert knowledge ([Menning and Stephens, 2007](#)). However, due to the complexity of field measurement, the more common proxy for vertical fuel continuity is the estimation of canopy base height (CBH) ([Scott, 2001](#)).

CBH is defined as the height above which there is sufficient canopy fuel per unit volume to support vertical fire spread into the canopy ([Scott, 2001](#)). It has widespread application in various wildfire behavior models ([Hall and Burke, 2006](#)). CBH can be estimated using allometric equations based on species, diameter at breast height (DBH), and tree height, or it can be retrieved from remote sensing data. However, due to the limitations of passive optical remote sensing signals and synthetic aperture radar (SAR) in penetrating the canopy, studies using multi-angle observations or bidirectional reflectance distribution function (BRDF) retrievals to obtain three-dimensional vegetation structure information are rare in wildfire prediction ([Pisek et al., 2015](#); [Canisius and Chen, 2007](#)). More commonly, LiDAR is used to estimate CBH at the individual tree or local scale ([Andersen et al., 2005](#); [Luo et al., 2018](#); [Wang et al., 2022](#)). Some studies suggest that while the definition of CBH is clear, its practical application is complicated by the lack of a clear fuel threshold per unit volume and the potential neglect of fine fuels, which can lead to errors in modeling canopy fire risk ([Cruz et al., 2004](#); [Kramer et al., 2014](#)). As a result, a quick and simple method to estimate ladder fuels is by estimating the coverage area or coverage rate of low-lying fuels as a representation of ladder fuel ([Clark et al., 2009](#); [Wing et al., 2012](#)).

In addition to vertical continuity, horizontal fuel continuity is also crucial. However, there are various definitions of horizontal continuity. For example, [Frandsen et al. \(1979\)](#) defines horizontal continuity as the degree of variation in the physical characteristics of fuels within a given area, with an emphasis on the impact of fuel type. Conversely, a more commonly used definition in describing horizontal continuity focuses on the spacing between fuels ([Ritter et al., 2023](#)). Tree spacing significantly affects the intensity and scale of wildfires ([Kim et al., 2016](#)). For instance, [Qadir et al. \(2021\)](#) showed in a study on wildfire risk prediction in Nepal that areas with high forest cover density have a higher risk of fires. In contrast, when there is canopy discontinuity, fire spread may slow down or even be extinguished ([Taneja et al., 2021](#)). For example, [Kim et al. \(2016\)](#) used the Fire Dynamics Simulator (WFDS) to model fire behavior in Korean pine (*Pinus densiflora*) and found that when the spacing between trees is 6 meters or more, most crown fires stop spreading within 100 meters. Therefore, fuel management techniques that fragment fuels can be used to suppress wildfires ([Srivastava et al., 2014](#); [Harrison et al., 2021](#)). Based on our

review, research on horizontal fuel continuity is less prevalent compared to vertical continuity, likely because many studies use proxies rather than directly assessing horizontal continuity. For instance, many crown fire spread models use canopy bulk density to describe horizontal fuel continuity (Wagner, 1993; Cruz et al., 2005). Additionally, proxies such as fraction vegetation cover, canopy cover, vegetation cover density, and various vegetation indices are also commonly used.

4.2. Weather and climate conditions

Weather and climate factors are major drivers of wildfire activity, influencing the occurrence, burned area, and fire behavior (Swetnam and Betancourt, 1990; Bessie and Johnson, 1995; Abatzoglou and Kolden, 2013). Firstly, weather conditions are central to almost all global fire danger risk systems. High temperatures, low relative humidity, insufficient precipitation, and strong winds have been proven to be key factors in the ignition of fires in the short term (Keane et al., 2001; Zacharakis and Tsihrintzis, 2023b), and they also affect fire size and spread (Abatzoglou and Kolden, 2011). On the other hand, climate conditions generally refer to the long-term average weather conditions of a region and their variations. Some studies specifically define these as the collective atmospheric conditions months or even years before the start of the fire season, emphasizing the use of prior climate conditions to convert fuel conditions into wildfire potential (Abatzoglou and Kolden, 2013). This approach enables predictions of large-scale fire risks over seasonal, annual, or even multi-decadal time scales.

4.2.1. Weather conditions

Short-term weather conditions focus primarily on predicting the impact of weather conditions over quarters, months, weeks, or days on fire risk. These include short-term temperature, wind, relative humidity, soil moisture, precipitation, and lightning, as well as corresponding indices like the Palmer Drought Severity Index (PDSI) and the Fire Weather Index (FWI). Temperature and various humidity conditions affect fuel conditions, such as evapotranspiration and moisture content, which in turn influence ambient humidity conditions and wildfire risk. Wind direction, wind speed, and other related metrics like Mean Wind Power Density (MWPD) and Mean Wind Speed (MWS) affect fire spread and intensity, making them commonly used parameters in wildfire prediction. Unlike other parameters, lightning can act as an ignition factor for wildfires.

Short-term weather parameters are widely used in wildfire risk prediction. For example, Tavakkoli Piralilou et al. (2022) used temperature, precipitation, MWPD, and MWS as parameters in their wildfire prediction model for the forested areas of Gilan Province, Iran. In another study conducted in Pakistan, Kanwal et al. (2023) utilized 16 meteorological parameters, including monthly average precipitation, evapotranspiration, wind speed, soil temperature, humidity, heat flux, albedo, average land surface temperature, soil moisture, actual evapotranspiration, moisture deficit, downward surface shortwave radiation, precipitation accumulation, minimum/maximum temperature, and vapor pressure. An assessment of their importance indicated that heat flux, evapotranspiration, and vapor

pressure were relatively more important compared to other meteorological parameters, although the differences in importance were not significant. Bergado et al. (2021) used seven meteorological factors in their wildfire prediction study for Victoria, Australia: daily maximum temperature, daily minimum relative humidity, daily total solar radiation, daily total precipitation, daily average wind speed, daily average wind direction, and lightning frequency. The lightning data was derived from an annual lightning climatology dataset that provided estimates of lightning density for each day of the year. Their study found that total precipitation, lightning density, and surface temperature consistently held high weight in all models. In contrast, Quan et al. (2023) used various meteorological variables from the ERA5 dataset, including precipitation, relative humidity, temperature, wind speed, and the Keetch-Byram Drought Index, to predict wildfire risk in parts of the western Tibetan Plateau in China. The study revealed that relative humidity was the most critical factor in the occurrence of forest and grassland fires in the region. Higher relative humidity leads to higher Dead Fuel Moisture Content (DFMC), thereby reducing the likelihood of ignition.

4.2.2. Climate conditions

Climate conditions mainly describe annual or multi-year meteorological parameters such as temperature, humidity, precipitation, and evaporation. Unlike meteorological conditions that influence short-term fuel status, climate conditions can control fuel types, distribution, life cycles, and more, thereby influencing fuel load and fuel continuity (Aldersley et al., 2011; Jaafari et al., 2017; Tavakkoli Piralilou et al., 2022). However, the distinction between climate and meteorological conditions lies in that climate variables are often the primary drivers of large-scale wildfire activity (Pollina et al., 2013; Jain et al., 2020). This is because fuel characteristics respond to climatic accumulation before the start of the fire season (Chen et al., 2016). Therefore, climate conditions are more suitable for predicting large-scale and long-term wildfires. Climate conditions can also explain strong seasonal variations in wildfire risk in certain regions (Martell et al., 1989), especially considering the intensification of climate change in recent years, which has raised concerns about its impact on the occurrence of large-scale wildfires over the long term (Prior and Eriksen, 2013; Jolly et al., 2015; Jain et al., 2024).

Specifically, Chen et al. (2016) used large-scale sea surface temperature anomalies to predict the severity of the fire season in South America on a seasonal time scale. Their study found that using a single ocean climate index could predict about 48% of the burned area globally for up to three months or longer before the peak burning month. In a study by Jaafari et al. (2019) in the Zagros ecoregion of western Iran, they used three climate conditions: annual temperature, rainfall, and wind effects. However, the results showed that only the annual temperature parameter was relatively important. Similarly, Naderpour et al. (2020) studied the northern beaches of New South Wales, Australia, using three climate factors: annual rainfall, annual humidity, and annual wind speed. Holdrege et al. (2024) studied the Great Basin sagebrush regions across 13 western

U.S. states and used three climate factors: annual mean temperature, annual precipitation, and the proportion of summer (June to August) precipitation to total annual precipitation. The study found that areas with low summer precipitation proportion, medium to high annual precipitation, and high temperatures had the highest wildfire probability. Similarly, [Aldersley et al. \(2011\)](#) used annual cumulative precipitation, annual lightning frequency, monthly precipitation frequency, monthly average temperature, and climate data from the British Atmospheric Data Centre (BADC) to study the drivers of monthly fire area on a global and regional scale. They found that climate factors such as high temperatures, moderate precipitation, and drought were the most important drivers globally. [Mansuy et al. \(2019\)](#) conducted a study across the U.S. and Canada and found that climate variables were the primary control factors for the burned area in most ecoregions, both inside and outside protected areas, surpassing landscape and anthropogenic factors. The climate data used in their study included annual average precipitation, annual average relative humidity, the Hargreaves climate moisture deficit (an annual measure of energy and moisture), and degree days below 18°C. [Abdollahi and Pradhan \(2023\)](#) conducted a wildfire prediction study in the Gippsland region of Victoria, Australia, and found that humidity, wind speed, and rainfall were the most influential factors in wildfire prediction. [Zhao and Liu \(2021\)](#) used data from over 600 meteorological stations in forest, grassland, and shrubland areas to calculate two drought indices, the Keetch-Byram Drought Index and the Standardized Precipitation Index. They then used global-scale PDSI data to mask these indices and assess long-term wildfire risk in China. The results showed that drought indices had a stronger correlation with seasonal and annual fire occurrences compared to climate indicators such as temperature and precipitation.

From the analysis above, it is evident that various forms of temperature, wind, humidity, and evaporation data are commonly used as meteorological or climate variables in wildfire prediction models. A few studies have combined both meteorological and climate factors to analyze their roles in the occurrence, spread, and scale of wildfires. For example, [Abatzoglou and Kolden \(2011\)](#) found in their study on the influence of weather and climate factors on the occurrence and scale of individual wildfires in Alaska that prior climate conditions had no significant effect on the final fire size, whereas post-ignition weather conditions, such as precipitation, had a greater impact over days to weeks. Thus, the authors suggest using short-term weather factors in wildfire risk assessment models and spread models. From another perspective, weather variables are more important than climate variables for small-scale and short-term wildfire risk and spread assessments.

4.3. Socio-economic factors

In the early stages of wildfire risk assessment, considerable attention was given to factors influencing wildfire spread and suppression difficulty ([McArthur, 1958, 1966; Hollis et al., 2024](#)). However, numerous studies have shown that the proportion of fires caused directly or indirectly by human activities surpasses those triggered by natural factors, such as lightning

([FAO, 2006](#)). Indirect human activities typically refer to the impact of human actions on climate change, which in turn influences wildfire risk. This effect can be modeled by analyzing the influence of climate on wildfire risk. Furthermore, the impact of indirect human activities on wildfire risk also includes changes in vegetation types, land use patterns, and landscape fragmentation, as well as alterations in fuel load and fuel continuity due to activities like grazing, planting, and harvesting ([Harris et al., 2023](#)). These changes can significantly affect local wildfire risk. Direct human activities, on the other hand, primarily involve ignition and suppression. The risk of wildfires caused by direct human ignition is particularly significant. For instance, from 1992 to 2012, 84% of wildfires in the United States were human-induced ([Balch et al., 2017](#)). Similarly, [Vilar et al. \(2016\)](#) found that 95% of wildfires in Mediterranean Europe between the 1980s and 2010s were caused by human activities. Notably, human factors not only increase the frequency of fires but also extend the fire season and lead to more random distributions of fire locations ([Balch et al., 2017](#)). This randomness introduces greater uncertainty into wildfire risk prediction, as wildfires may occur in areas with infrequent lightning or where lightning does not coincide with high temperatures, dryness, and strong winds ([Abatzoglou et al., 2016](#)).

Since [Chuvieco and Congalton \(1989\)](#) first introduced human activity variables into wildfire risk research by considering the proximity of road networks and areas with high human activity, such as recreational zones, an increasing number of studies have incorporated human activity variables into wildfire risk prediction models. These variables include the distance of various locations from nearby roads, power lines, villages, and cities, as well as road density, population density, and land use. The assumption underlying the inclusion of these variables is that wildfire frequency is negatively correlated with distance from human infrastructure and positively correlated with road density and population size ([Gilreath, 2006; Martínez et al., 2009](#)). In addition to these easily describable features, there are more complex factors influencing wildfire risk, such as the potential for urban development to increase fuel loads in rural areas, or the possibility that controlled burns for agricultural purposes in remote areas may increase the likelihood of uncontrolled wildfires ([Martínez et al., 2009](#)). Several studies have confirmed these assumptions. For example, [Jaafari et al. \(2019\)](#) found a strong correlation between high wildfire probability and road network density in the Zagros ecoregion of western Iran. [Ghorbanzadeh et al. \(2019\)](#), in their study of the forest areas in Amol County, Mazandaran Province, northern Iran, similarly found that human activities near major roads significantly influenced wildfire risk. The interaction between human settlements and vulnerable infrastructure in areas with high or moderate forest fire susceptibility leads to the emergence of high-risk zones on wildfire risk maps.

Therefore, most wildfire risk prediction studies consider the socio-economic factors mentioned above. For instance, [Sadasivuni et al. \(2013\)](#) generated a population interaction map based on forest resources and human settlement patterns and studied wildfire risk in Mississippi, southeastern United States. They found that areas with dense fuel and sparse populations

were most likely to experience wildfires. [Malik et al. \(2021\)](#) mapped wildfire risk in a densely vegetated area of approximately 63 km^2 between Monticello and Winters, California, using the location of power lines as a proxy for socio-economic factors, given that power lines can serve as ignition sources during high wind events. [Nami et al. \(2018\)](#) considered land use/land cover (LULC) and proximity to roads and settlements when mapping wildfire risk in the Hyrcanian ecoregion of northern Iran. They found that the probability of fire occurrence was highly dependent on human infrastructure and related activities. Additionally, the study revealed a positive correlation between fire occurrence and landscapes within 4,000 meters of human settlements, and a negative correlation for areas beyond 4 kilometers. [Rubí and Gondim \(2023\)](#) conducted a study in Brazil's Federal District, dividing the region into zones based on the coverage of different weather stations and calculating the distance from each zone's center to the nearest road and building as proxies for socio-economic factors. [Bergado et al. \(2021\)](#) carried out a wildfire prediction study in Victoria, Australia, and found that land cover categories (such as farmland, forests, mines, and quarries) and distance from power lines were relatively low in importance. In their wildfire risk assessment in Guangdong Province, China, [Jiang et al.](#) considered socio-economic factors such as gross domestic product (GDP), distance from roads, and population density. The results showed that, aside from meteorological factors, GDP was the most significant factor in wildfire risk. Similarly, [Jiang et al. \(2024b\)](#) in their wildfire risk assessment in Guangdong Province, China, also utilized GDP, distance to highways, and population density as socio-economic factors. However, their results indicated that the contribution of socio-economic factors to wildfire risk was not significant. Furthermore, in a study conducted in the western part of the Tibetan Plateau in China, [Quan et al. \(2023\)](#) found that although government reports indicated that the majority (about 95%) of wildfires in the region were caused by human activities, the importance of distance from roads and residential areas was relatively low compared to meteorological factors.

It is noteworthy that current research on the impact of human activities on wildfire risk primarily focuses on using the distribution density of population, roads, and other infrastructure, as well as the straight-line distance of different locations within the study area from infrastructure, as input features for models. However, the consideration of these distances is typically limited to simple linear measurements, without accounting for human accessibility. This limitation may reduce model performance in regions with rugged terrain. Additionally, current research on human factors mainly focuses on human-induced wildfires, with little consideration given to the mitigating effects of firefighting facilities, such as fire stations, firebreaks, and lookout towers.

4.4. Wildfire historical records

Wildfire historical records are indispensable in all studies and form the data foundation for wildfire risk assessment models. The sources and scales of wildfire historical records vary widely. For example, in Canada, many

provinces, cities, or forestry management agencies maintain their own wildfire historical records. Additionally, the Canadian Natural Resources Department maintains its wildfire information data system, such as the Canadian Wildfire Information System. Specifically, commonly used public global or regional scale wildfire historical records include the National Burned Area Composite dataset (NBAC), the Canadian National Fire Database (CNFDB), the National Institute for Space Research database (INPE), the Fire Planning and Analysis Fire Occurrence Database (FPA-FOD), the Global Fire Emissions Database (GFED), and FireCII. In regions without systematic wildfire records, most studies use satellite-derived thermal anomalies or wildfire products from MODIS, Suomi-National Polar-orbiting Partnership (S-NPP), National Oceanic and Atmospheric Administration (NOAA) VIIRS, GOES, AVHRR, Sentinel, Landsat, Himawari, FY-4, among others.

Specifically, [Pelletier et al. \(2023\)](#) used the NBAC dataset from the Canadian Forest Service for their study on the northern Canadian forest peatlands. [Liang et al. \(2019\)](#) utilized the CNFDB dataset for wildfire research in Alberta, Canada, which includes fire location (latitude and longitude points), ignition date, extinguishment date, burned area, and cause of fire provided by provincial, regional, and the Canadian Parks Service firefighting agencies. [Rubí and Gondim \(2023\)](#) employed the INPE database for their study in the Federal District of Brazil. The INPE fire database is primarily based on thermal anomaly data collected from satellites such as AQUA, TERRA, NOAA-15, 16, 17, 18, and 19, METEOSAT-02, and GOES-12. It covers the geographic location and timing of fires (latitude, longitude, and date/time) since the year 2000. [Wang et al. \(2021\)](#) used the FPA-FOD dataset to assess the drivers of wildfires in the continental United States, which includes discovery date, burned area, and geographical location (longitude and latitude) of wildfires from 1992 to 2020. The dataset intentionally excludes prescribed fires that escaped and required suppression response. Despite the possibility of missing data on smaller fires, the omission is tolerable for analytical purposes since the largest 5% of all fires account for the majority of the burned area. [Song and Wang \(2020\)](#) utilized the Global Fire Emissions Database version 4.1 (GFEDv4) for predicting global monthly wildfire risks throughout the year. This dataset covers monthly wildfire areas globally from 1997 to 2016, with a spatial resolution of $0.25^\circ \times 0.25^\circ$. It also includes daily burned area data globally from August 2000 to 2015. [Bakke et al. \(2023\)](#) employed the FireCCI dataset in their study in Fennoscandia, Finland, which provides global-scale pixel products at spatial resolutions of 250m or 300m, or gridded products at a resolution of 0.25×0.25 degrees, with a temporal resolution equal to or less than one month.

Satellite thermal anomaly products are commonly used in wildfire risk prediction studies, such as the MODIS MCD14 and MCD64A1 products ([Giglio et al., 2003, 2016](#)). The MCD14 series dataset has a spatial and temporal resolution of 1km and one day, respectively, offering a long time series (from 2006 to present) and providing near-real-time wildfire hotspot maps. The MCD64A1 dataset has a higher spatial resolution of 500m, although it does not offer near-real-time products. In

specific studies, Abdollahi and Pradhan (2023) used MODIS fire and thermal anomaly data in their wildfire prediction research in the Gippsland region of Victoria, Australia, along with the NPWS Fire History - Wildfire and Prescribed Burning dataset provided by the New South Wales Department of Climate Change, Energy, the Environment, and Water. Ghorbanzadeh et al. (2019) acquired polygon data for 34 wildfire areas through field surveys and assessed data for the forested regions of Amol County, Mazandaran Province, northern Iran using MODIS data. Jaafari et al. (2019) and Nami et al. (2018) also employed historical data, field surveys, and validated using MODIS hotspot products in their studies in the western Zagros ecoregion and the northern Hyrcanian ecoregion of Iran, respectively, to enhance the reliability of historical data. Kanwal et al. (2023) in their study in Pakistan used MODIS data from the Fire Information for Resource Management System (FIRMS) as wildfire historical data, setting a 60% confidence threshold to reduce false alarm errors.

Additionally, some studies argue that MODIS products may overlook fires that are smaller in scale or shorter in duration (Hantson et al., 2013; Benali et al., 2016; Fusco et al., 2019; Ying et al., 2019). Therefore, other satellite data are also used in conjunction with MODIS data or independently for fire hotspot detection or burned area mapping, and for generating historical datasets. For instance, the study by Zhang et al. (2021) used the GFED dataset, which utilizes the MODIS MCD64A1 dataset and VNPIMG14ML dataset (Schroeder et al., 2014; Hall et al., 2024), to mitigate errors of commission and omission in agricultural fire detection in the MODIS dataset. Moreover, some studies have begun to explore using other high temporal resolution data to build global or regional wildfire detection datasets, such as the Sea and Land Surface Temperature Radiometer (SLSTR) sensor on Sentinel-3A/B (Xu and Wooster, 2023).

4.5. Frequency of different data utilization

In the "Fuel Conditions" category, the Normalized Difference Vegetation Index (NDVI) is the most frequently utilized variable, with a frequency of 27, underscoring NDVI's critical role in assessing vegetation health and fuel availability. Other significant variables include Tree Species, which appears 8 times, and Leaf Area Index (LAI) and Vegetation Type, each with a frequency of 6. These variables are essential for understanding the characteristics of biomass that contribute to wildfire risk. The presence of numerous variables with lower frequencies, such as Enhanced Vegetation Index (EVI) and Normalized Difference Water Index (NDWI), each used only once, highlights the complexity of this category. This diversity of variables reflects the multifaceted nature of fuel dynamics, requiring a broad range of factors to be considered in fire risk modeling, as depicted in Fig. 3(a).

In the "Climate and Weather Conditions" category, Temperature emerges as the dominant variable, with a frequency of 65. Precipitation follows closely with 53 occurrences, and Wind is also significantly utilized, with a frequency of 42. These variables are fundamental in understanding fire behavior, particularly in their influence on fire ignition, spread, and intensity.

Humidity, used 27 times, and Moisture, used 16 times, further contribute to this category, reflecting the central role of atmospheric conditions in fire risk assessments. Other variables, such as Fuel Moisture Code, utilized 11 times, and Vapor Pressure, with 9 occurrences, are less frequently employed but remain crucial in specific contexts. The data presented in Fig. 3(b) emphasizes that climate variables, particularly Temperature and Precipitation, are among the most critical factors in fire dynamics, with a wide array of related variables also contributing to detailed climatic modeling.

Land Use and Land Cover (LULC) stands out as the most frequently utilized socio-economic variable, appearing 32 times, underscoring its importance in assessing how human activities and changes in land use influence fire risk. Road Proximity, with 23 occurrences, and Settlement Proximity, with 18, follow, indicating the significance of infrastructure and human settlement patterns in fire studies. Population Density, appearing 16 times, and Road Density, with a frequency of 4, also play roles, although to a lesser extent. The data in Fig. 3(c) suggest that while variables like Gross Domestic Product (GDP), used 5 times, and Distance to Cropland, also used 5 times, are relevant, they are more context-specific. This analysis indicates that socio-economic factors are essential for understanding the human impact on fire dynamics, particularly in areas where land use and human infrastructure intersect with natural landscapes.

In the "Terrain and Hydrological Features" category, Slope is the most frequently used variable, appearing 46 times. This reflects the critical role of slope in influencing fire spread and intensity. Aspect, with a frequency of 34, and Elevation, with 32, are also key factors in understanding how topography affects fire behavior. These variables are particularly important in regions with complex terrain, where physical landscape features significantly impact fire dynamics. Plan Curvature, used 11 times, and Topographic Wetness Index (TWI), used 10 times, are less frequently applied but remain relevant in specific contexts, often related to hydrological modeling. Other variables like Latitude, used 5 times, and Landform, with 3 occurrences, indicate their more specialized application. The analysis of these features highlights that while terrain and hydrological factors are crucial for understanding the physical environment's impact on fires, certain variables like Slope, Aspect, and Elevation consistently prove to be more influential.

Overall, when comparing the categories, climate and weather conditions emerge as the most frequently utilized, with Temperature and Precipitation leading the way. Fuel conditions follow closely, with NDVI being the most prominent indicator of vegetation health and fuel availability. Socio-economic factors, while important, are used more selectively, with LULC, Road Proximity, and Settlement Proximity being the primary variables. Finally, terrain and hydrological features, particularly Slope, Aspect, and Elevation, are critical for understanding how the physical landscape influences fire behavior. However, it is worth noting that the frequency of use of the aforementioned features is not solely dependent on their importance but also on their ease of availability. For example, in the "Fuel Conditions" category, NDVI is more readily accessible compared to other features; similarly, variables like Temperature, LULC, Slope,

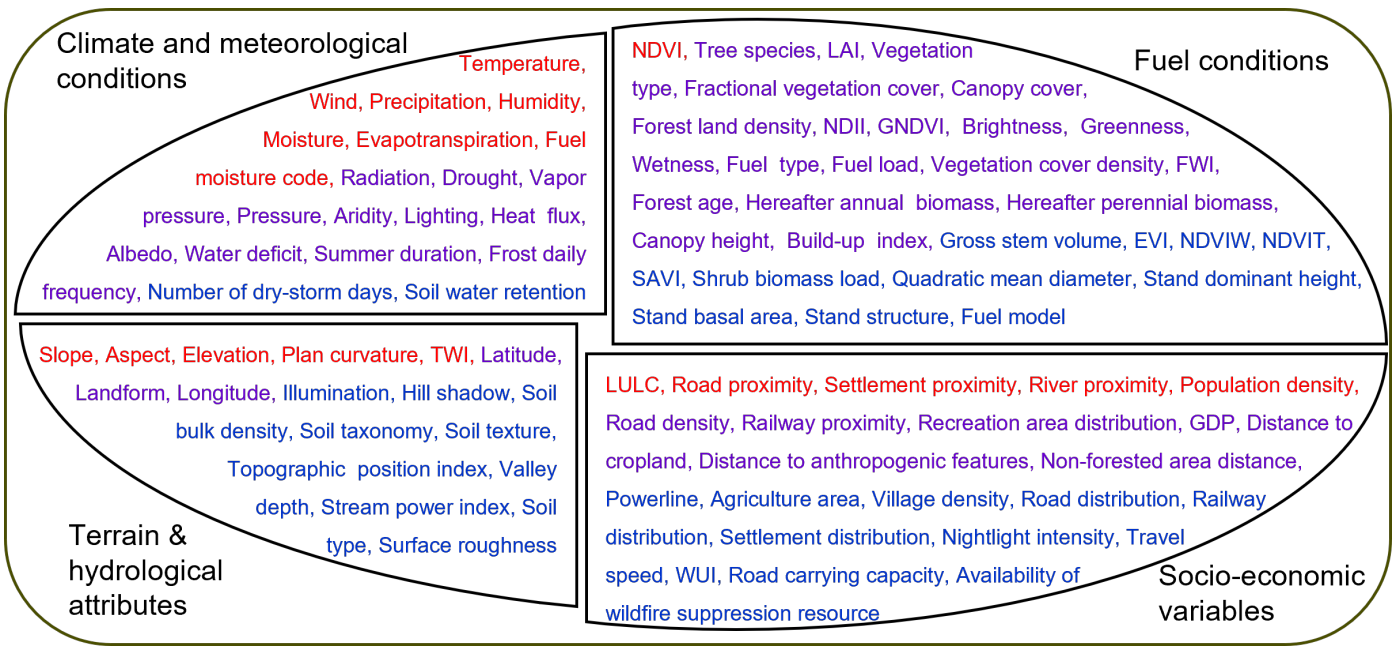


Figure 3: The allocation of feature utilization frequencies is classified into four categories: fuel conditions, weather and climate conditions, socio-economic variables, and terrain and hydrological attributes. The color scheme in this visual representation signifies the prevalence of these features, with red, green, and blue denoting utilization frequencies exceeding 20, 10, and 0 occurrences, respectively.

Aspect, and Elevation are also more easily obtained.

4.6. Open-source wildfire spread prediction datasets

As research on wildfire risk prediction models increasingly relies on traditional machine learning methods or deep learning approaches, there is a growing need for both quantitative and qualitative evaluations of the proposed models' effectiveness. Comparisons between different models' performances are also essential. However, studies confined to specific regions can compromise the fairness of these comparisons and hinder the assessment of the generalization capabilities of different models. To address these challenges and support the development of machine learning-based wildfire risk prediction algorithms, several wildfire spread datasets with varying research areas and data sources have been made publicly available.

The datasets presented in the Table 2, including FireCube (Prapas et al., 2022; Kondylatos et al., 2023), Next Day Wildfire Spread (Huot et al., 2022), WildfireDB (Singla et al., 2020), WildfireSpreadTS (Gerard et al., 2023), CFSDS (Barber et al., 2024), and SeasFire Cube (Alonso et al., 2023), encompass various factors critical to wildfire spread prediction. These factors include spatial-temporal coverage, fuel conditions, climate and weather conditions, socio-economic factors, terrain, and historical records. Each dataset differs in the extent, spatial-temporal coverage, and resolution of these factors, providing diverse perspectives and data for wildfire modeling.

The datasets vary significantly in their spatial and temporal resolutions. For instance, FireCube and Next Day Wildfire Spread focus on high-resolution data with a spatial coverage of 1 km for daily observations. WildfireDB offers more localized coverage at 375 m but over a broader temporal range (2012-2018). The CFSDS dataset provides highly detailed data

at 180m resolution, though its temporal span is longer (2002-2021). SeasFire Cube offers the broadest coverage globally, albeit at a coarser resolution of 0.25 degrees and 8-day intervals.

Regarding fuel conditions, the datasets primarily utilize vegetation indices such as MODIS EVI and NDVI. FireCube combines MODIS EVI, LAI, and NDVI to provide a detailed view of vegetation. Similarly, Next Day Wildfire Spread and WildfireSpreadTS rely on VIIRS NDVI, offering 8-day data at 500m resolution. WildfireDB stands out by incorporating LANDFIRE data, which includes specific details like canopy base density and height, providing a more comprehensive fuel description, although at a lower temporal resolution. CFSDS uses specialized Canadian forest inventory data, adding complexity by considering forest composition and peatland presence.

For climate and weather conditions, most datasets rely on reanalysis products. FireCube integrates ERA5-Land data, covering a broad range of climatic variables, including temperature, precipitation, and soil moisture. Next Day Wildfire Spread and WildfireSpreadTS use GRIDMET data for similar parameters, with WildfireSpreadTS further incorporating Global Forecast System data for temperature and wind predictions. WildfireDB uses NOAA Ground Station data, focusing on ground-based observations, which may offer more accuracy but less spatial coverage.

The inclusion of socio-economic factors varies widely among the datasets. FireCube incorporates multiple socio-economic variables, including LULC, population distribution, and proximity to roads and waterways, offering a comprehensive view of human impact on wildfire spread. Next Day Wildfire Spread and SeasFire Cube focus solely on population density, while WildfireSpreadTS considers only LULC. WildfireDB does not include socio-economic factors, limiting its

ability to account for human influences on wildfire spread.

Terrain and hydrological features, primarily derived from DEM products for elevation, slope, and aspect. FireCube uses the EU-DEM, while Next Day Wildfire Spread and Wildfire-SpreadTS rely on SRTM products. CFSDS employs ASTER data for terrain variables, while WildfireDB and SeasFire Cube use various unspecified sources for elevation data. Despite different products, all datasets achieve similar resolutions of around 30m, ensuring consistency in terrain representation.

Historical wildfire records are crucial for validating wildfire spread models. FireCube incorporates both MODIS and EFFIS records, offering detailed fire occurrence accounts. Next Day Wildfire Spread relies on the MOD14A1 product, while WildfireDB and WildfireSpreadTS use VIIRS data at 375m resolution. SeasFire Cube integrates multiple sources, including FireCCI, GWIS, and MODIS, to provide a comprehensive historical dataset, though at a coarser resolution.

It is important to note that we only consider time series wildfire observation datasets stored in a spatially explicit format and encompassing multiple wildfire impact factors. Datasets that do not have a clearly defined spatial distribution (Sayad et al., 2019), datasets containing only historical wildfire extent (Short, 2014; Andela et al., 2019; Artés et al., 2019; Lizundia-Loiola et al., 2020; Hargrove et al., 2022; Gincheva et al., 2024), fire detection datasets (Chino et al., 2015; Toulouse et al., 2017; Shamsoshoara et al., 2020; Mou et al., 2020; El-Madafri et al., 2023), and simulation datasets (Wang et al., 2024), are not included.

As shown in Table 2, the number of available open-source wildfire spread datasets is limited, with most coverage concentrated in the United States, while other regions, such as the wildfire-prone Mediterranean, Canada, and Australia, are underrepresented. Additionally, some studies using these datasets have overly simplistic considerations of fuel conditions, such as relying solely on vegetation indices as proxies. This approach fails to accurately and comprehensively describe the state of fuel load, moisture content, and continuity. Similarly, using MODIS or VIIRS to record historical burned areas lacks precision, potentially overlooking small fire spots, offering low spatial and temporal resolution, and being prone to false alarms (Zubkova et al., 2024). Furthermore, there is a lack of quantitative evaluation of how the accuracy, variability, and spatiotemporal resolution of different products impact the accuracy of wildfire spread predictions.

5. Features Collinearity and Attribution

The relationships between wildfires and driving environmental factors have always been a focal point in wildfire prediction research. Considering the interplay between wildfire occurrences and factors such as fuel conditions, climate, meteorological variables, topographical features, and human activities is crucial. However, including highly collinear independent variables in a model may impair its performance (Chen et al., 2019). Moreover, when two or more independent variables are significantly correlated, they provide redundant information in regression analysis, complicating the interpretation

of each variable's individual impact on the dependent variable. Therefore, it is essential to examine the collinearity and contributions of different features to provide decision support for wildfire management.

5.1. Assessment of Feature Collinearity

Common metrics for assessing data collinearity in wildfire risk prediction include the Variance Inflation Factor (VIF) and tolerance. Nami et al. (2018) conducted a collinearity analysis using VIF and tolerance in their study on wildfire risk mapping in the northern Hyrcanian ecoregion of Iran. They found significant collinearity between the Topographic Wetness Index (TWI) and slope with other parameters, leading to their exclusion from subsequent modeling efforts. Similarly, Jaafari et al. (2019) assessed the collinearity of various predictors using VIF and tolerance in their study in the western Zagros ecoregion of Iran. They discovered that the VIF values for TWI and slope were below 5, and tolerance values were above 0.2, indicating insignificant collinearity with other predictors (Liao and Valiant, 2012). Hong et al. (2019), in their modeling of wildfire susceptibility in Huichang County, China, used VIF and tolerance to assess the collinearity of multiple predictors and found no significant collinearity between slope and other features. Li et al. (2022a) in their study of the drivers of forest fires in Yunnan Province, China, found that six meteorological factors (daily average atmospheric pressure, daily minimum atmospheric pressure, daily average temperature, daily minimum temperature, daily average surface temperature, and daily minimum surface temperature) had VIF values exceeding 10 and tolerance values below 0.1, indicating significant correlations. The study also used the Pearson correlation algorithm to analyze the correlations of the remaining variables, finding a correlation coefficient of 0.77 between surface temperature and air temperature. Similarly, Rezaie et al. (2023) in their wildfire prediction model for Maui Island in Hawaii analyzed the correlation and collinearity among independent variables (altitude, slope, aspect, valley depth, TWI, slope length, plan curvature, distance from rivers, distance from roads, NDVI, average monthly rainfall, average annual wind speed, and average annual temperature) using Pearson correlation coefficients, VIF, and tolerance. They found the strongest correlations between average annual temperature and altitude, and the most significant collinearity between average annual temperature and distance from roads. However, the collinearity and correlations among all variables were not statistically significant.

5.2. Feature attribution

In wildfire risk prediction algorithms, explicit definition methods can predict wildfire risk by defining the contributions of different features to the ignition and spread of wildfires. However, these methods often have poor fitting capabilities and struggle to handle the nonlinearity and randomness characteristic of wildfire risk prediction tasks. On the other hand, machine learning models, such as deep learning and ensemble learning models (e.g., XGBoost, LightGBM), can extract patterns from highly complex datasets and demonstrate superior predictive performance. However, their decision-making processes

Table 2: Open-access Wildfire Spread Prediction Datasets

Dataset	Spatial-temporal Coverage and Resolution	Fuel Conditions	Climate and Weather Conditions	Socio-economic Factors	Fac-	Terrain and Hydrological Features	Historical Records
FireCube	Greece and Eastern Mediterranean (1 km), 2009-2021 (Daily)	MODIS : EVI (MOD13A2, 16d, 1 km), LAI (MOD12A2H, 500 m, 8d), NDVI (16d, 1 km)	ERA5-Land : Avg, max, min of dew point temperature, relative humidity, surface pressure, air temperature, total precipitation, U and V wind components (1d, 9 km); MODIS : Total evapotranspiration (MOD16A2, 8d, 500 m), day and night LST (MOD11A1, 1d, 1 km), FPAR (8d, 500 m); European EDO : Soil moisture index anomaly, Soil moisture (10d, 5 km)	Corine Land Cover : LULC (2006, 2012, 2018); WorldPop : Population density (2009-2021), distance from roads, distance from waterways	EU-DEM : Elevation, aspect, roughness, slope (2016, 30m)	EFFIS & MODIS : Ignition points, burn area, daily fire count	
Next Day Wildfire Spread	USA (1 km), 2012-2020 (Daily)	VIIRS : NDVI (VNP13A1) (8d, 500 m)	GRIDMET : Wind direction and speed, minimum and maximum temperatures, humidity, precipitation (1d, 4 km), drought index, energy release component (ERC) (5d, 4 km)	GPWv4 : Population density (1 km)	SRTM : Elevation (30 m)	MODIS : MOD14A1 V6 (1d, 1 km)	
WildfireDB	California, USA (375 m), 2012-2018 (Daily)	LANDFIRE : Canopy base density, base height, cover, canopy height, and existing vegetation cover, height, and type (2012, 2014, 2016, 30 m)	NOAA Ground Station Data : Temperature (avg, min, max), total precipitation, atmospheric pressure, and wind speed (1d, 5787 stations)		Elevation and slope (2016, 30 m)	VIIRS : Active Fire (1d, 375 m)	
WildfireSpreadTS	USA, 2018-2021 (Daily)	VIIRS : EVI (VNP13A1) and NDVI (8d, 500 m)	GRIDMET : Surface temperature (min, max), total precipitation, wind speed and direction, specific humidity, Palmer Drought Severity Index (PDSI) (1d, 4.6 km); Global Forecast System : Temperature and wind (avg, direction, speed) (1d, 27.83 km)	MODIS : Land Cover Type Yearly Global product (MCD12Q1, 1y, 500 m)	SRTM : Elevation, slope, and aspect (2013, 30m)	VIIRS : Active Fire (1d, 375 m)	
CFSDS	Canada (180m), 2002-2021 (Daily)	SCNFI : Percentage deciduous component, percentage coniferous component, biomass in tonnes/ha, and crown closure percentage (30m); Peatland presence and class (250m); ERA5-Land : FFMC, DMC, DC, ISI, BUI (1d, 0.1deg)	ERA5-Land : The maximum daily temperature, 24 hr precipitation, noon wind speed, noon relative humidity, and 24hr maximum vapour pressure deficit (1d, 0.1deg)	CanVec Transport Features : Road density, distance to road	ASTER : elevation, slope, aspect, and TWI; National Ecological Framework for Canada : Ecozones	National Burned Area Composite ; VIIRS : VNP14IMGT (375m); MODIS : MCD14ML (1km)	
SeasFire Cube	Global (0.25deg), 2001-2021 (8d)	MODIS : NDVI (MCD15A2, 8d, 500m), LAI (MOD13C1, 16d, 5600m)	ERA5 : Mean sea level pressure, total precipitation, relative humidity, vapor pressure deficit, sea surface temperature, skin temperature, wind speed, 2m temperature (mean, min, max), surface net solar radiation, surface net solar radiation, surface solar radiation downward, volumetric soil water (level1-4), land-sea mask (0.25deg); Copernicus CEMS : Drought code (max, avg), fire weather index (max, avg) (1d, 0.25deg); CAMS : Carbon dioxide emission from wildfire, fire radiative power (1d, 0.1deg); MODIS : LST (MOD11C1, 1d, 0.05deg); NOAA climate indices	GPWv4 : Population density (1km); ESA CCI : LULC (7d, 300m/1km); Biomes	FireCCI : Burned areas (area, mask, fraction) (250m/300m); GFED : Burned areas (area, mask) (1month, 0.25deg); GWIS : Burned areas (area, mask)		

are opaque, earning them the label of "black box models." In wildfire risk prediction, this lack of transparency undermines the credibility of the predictions and makes it difficult for researchers and fire management agencies to understand the factors inducing wildfire ignition and spread. This, in turn, hinders the understanding of wildfire mechanisms and the prevention and management of wildfires. The interpretation of the decision-making processes in machine learning models is generally referred to as explainable AI. In this paper, we define XAI as the attribution of causal responsibility or feature attribution (Josephson and Josephson, 1996), as XAI in wildfire risk prediction algorithms mainly focuses on explaining the influence of different wildfire risk factors on model predictions. Currently, common XAI methods in wildfire risk prediction include Permutation Feature Importance (PFI), Explainable Feature Engineering (Ali et al., 2023), and SHapley Additive exPlanations (SHAP).

Firstly, PFI quantitatively analyzes feature importance by randomly permuting each feature and evaluating the change in model performance. For example, Rubí and Gondim (2023) used PFI to assess the contributions of meteorological, fuel, terrain, and socioeconomic factors in models such as ANN, SVM, NB, KNN, LR, LogLR, and AdaBoost in their study in the Federal District of Brazil. They found that analyzing individual variables might lead to contradictory results. For instance, NDVI was more important for models like AdaBoost and ANN, whereas its influence was relatively low or nonexistent in other models such as LR and SVM. This finding highlights the necessity of considering multiple variables in predictive modeling and the varying importance of different models. Additionally, Shadrin et al. (2024a) evaluated the impact of specific feature values on the final test results by setting them to zero during model testing. Similarly, Chen et al. (2024b) calculated the importance of each feature by measuring the reduction in prediction error when feature values were perturbed.

Secondly, Explainable Feature Engineering (Ali et al., 2023) methods have also been applied to wildfire risk prediction. For example, Rezaie et al. (2023) used the Information Gain Ratio (IGR) to select the optimal subset of variables in their wildfire prediction model for Maui, Hawaii. They found that the distance to roads had the highest IGR value of 0.903, indicating its significant impact on mapping fire-prone areas. The next important variables were annual average temperature (0.724), elevation (0.715), and slope (0.665). Similarly, Zhang et al. (2019) used IGR to evaluate the importance of different factors in assessing forest fire risk in Yunnan Province, China. They found that temperature and wind speed contributed the most to the risk, while the importance of distance to roads and rivers was the lowest. In modeling the spatial distribution of wildfire susceptibility in Huichang County, China, Hong et al. (2019) used the Analytic Hierarchy Process to assign weights to a logistic regression model and found that elevation was the most influential indicator of fire occurrence, followed by land use, NDVI, and distance to human settlements.

Finally, compared to the aforementioned methods, SHAP analysis (Shapley, 1953), which is based on game theory, is more commonly used, especially for explaining complex mod-

els, because it considers both feature importance and feature interactions while offering higher computational efficiency. SHAP explains the impact of each feature on model predictions by assigning SHAP values to them. Common SHAP methods include Kernel SHAP, Deep SHAP, and Tree SHAP (Lundberg and Lee, 2017). For instance, to address the challenge of explaining deep learning models, Abdollahi and Pradhan (2023) introduced SHAP to study the contribution of different features to the model. The authors found that relatively high NDVI, temperature, and elevation, as well as relatively low NDMI and precipitation, increased wildfire risk, while relatively high humidity reduced this risk. They also identified elevation, NDMI, and precipitation as the three most critical factors influencing wildfire occurrence. Similarly, Wang et al. (2021) used SHAP to evaluate the drivers of large-scale wildfires in the contiguous United States and found that coordinate variables (including longitude and latitude) and local meteorological variables (such as ERC, RH, temperature, and VPD) were important predictors of burned area across the domain. This is because coordinate variables carry crucial geographic information that broadly reflects climate, land use, human activity, and other key geographic factors, helping to distinguish temporal characteristics of different fire regimes and thus aiding in predicting burned areas. Using SHAP's local interpretability, they also explained the driving factors of large burned areas in different regions and months within the contiguous United States. For example, ERC was identified as the most important indicator of large burned areas in the western US. Iban and Aksu (2024) conducted a local SHAP importance analysis in the Izmir region of Turkey and found that wind speed, LULC, slope, temperature, and NDVI were the five most important influencing factors. Wind speeds above 3.5 m/s, forests in LULC, slopes greater than 8 degrees, annual average temperatures above 14 degrees, and NDVI values below 0.2 all promoted wildfires, while higher NDVI reduced the likelihood of wildfire occurrence. In the wildfire risk assessment for Hawai'i Island, Tran et al. (2024) considered 14 factors, including meteorological, topographic, anthropogenic, and vegetation-related variables: elevation, slope, aspect, plan curvature, profile curvature, TWI, valley depth, annual average wind speed, NDVI, annual average precipitation, annual average temperature, distance to roads, distance to rivers, and land use. SHAP analysis revealed that the distance from a road, annual temperature, and elevation were the most influential factors, with wildfire risk increasing as distance from roads decreased and temperature increased. Additionally, low- to mid-elevation areas were generally associated with a higher likelihood of fire occurrence due to their relatively high temperatures and accessibility. Kondylatos et al. (2022) conducted a SHAP analysis for the Eastern Mediterranean region and found that soil moisture index, humidity indicators, temperature variables, NDVI, and wind speed were the most important factors influencing wildfire risk. Notably, the study found that the relationship between NDVI and fire risk was U-shaped, meaning that both very low and very high NDVI levels were associated with lower wildfire risk.

Currently, explainability analysis in wildfire prediction faces several challenges, such as insufficient exploration of alterna-

tive explainability methods, dependency on models and explanation techniques, unclear attribution analysis, and the uncertainty of the explanations provided.

Firstly, techniques like activation maximization analysis (Erhan et al., 2009), Partial Dependence Plot (Greenwell et al., 2017), Integrated Gradients, and other additive feature attribution methods beyond SHAP—such as Local Interpretable Model-agnostic Explanations (LIME), Integrated Gradients, DeepLIFT, and Layer-Wise Relevance Propagation—have not been adequately explored in the context of wildfire risk prediction. The limited application of these XAI methods leaves gaps in our understanding of how different approaches might enhance model transparency in this domain.

Secondly, many studies select the best-performing model through comparative experiments and then conduct explainability analysis based on that model. The explanations provided by these methods often estimate how a specific machine learning (ML) model derives predictions from input data (Good and Hardin, 2012). However, treating these analyses as direct insights into real-world phenomena can lead to misleading or erroneous conclusions, particularly if the model’s learned decision rules do not align with the actual underlying data relationships (Jiang et al., 2024a). For instance, using a single explainability method to interpret different ML models, or using different explainability methods to interpret the same ML model, might result in varying or even contradictory observations. Therefore, any inferences drawn from these post-hoc explanations should be approached with caution (Ploton et al., 2020).

Furthermore, wildfire prediction studies often employ multiple input variables and model the relationships between these variables and wildfire risk. While such models may perform well, they do not necessarily explain whether causal relationships exist between independent and dependent variables, as the modeled relationships often result from correlations among various features (Rogger et al., 2017; Molnar et al., 2020). An example of this is multicollinearity among features, which is very common in Earth sciences due to the highly complex interactions and interdependencies between geological, meteorological, ecological, and other factors in the Earth system. For instance, features commonly used in wildfire risk prediction, such as NDVI, soil moisture, precipitation, temperature, and evapotranspiration, often exhibit complex interrelationships. A crucial condition for ML models to produce valid causal effect estimates is that their input variables must be independent of unobserved confounders. Therefore, in most cases, ML should not be considered a definitive source of causal knowledge (Jiang et al., 2024a). This highlights the need for further research into the application of causal ML (Tesch et al., 2023) in wildfire risk prediction.

Lastly, while explainability analysis enhances model transparency, these explanations are still subject to uncertainty, unreliability, and low robustness due to the influence of model selection, choice of explainability method, and the correlations within input data (Jiang et al., 2024a). Thus, it is important to explore how insights from related fields can be applied to quantitatively assess the validity of explainability analysis results in

wildfire risk assessment models (Bommer et al., 2024).

6. Fire danger rating systems

Wildfire hazards are characterized by strong nonlinearity and randomness, making it challenging to calculate wildfire risk using simple statistical models. At the same time, developing accurate physical models to precisely estimate the relationship between wildfire risk and factors such as fuel, weather, terrain, and human activities is also difficult. Consequently, adaptive and scientifically grounded wildfire rating systems have been proposed and have remained a critical component of global fire management for over a century (Hardy and Hardy, 2007). These systems have evolved from early dryness indices into complex models that predict spatial and temporal variations in wildfire ignition probability, spread rate, and heat release/fire intensity by characterizing the interactions among fuel, weather, and terrain. This evolution has provided crucial decision support for wildfire management at local, regional, national, and sometimes even international scales (Jolly et al., 2024). According to Zacharakis and Tsihrintzis (2023a), commonly used wildfire danger rating models today include systems developed in Canada, the United States, and Australia.

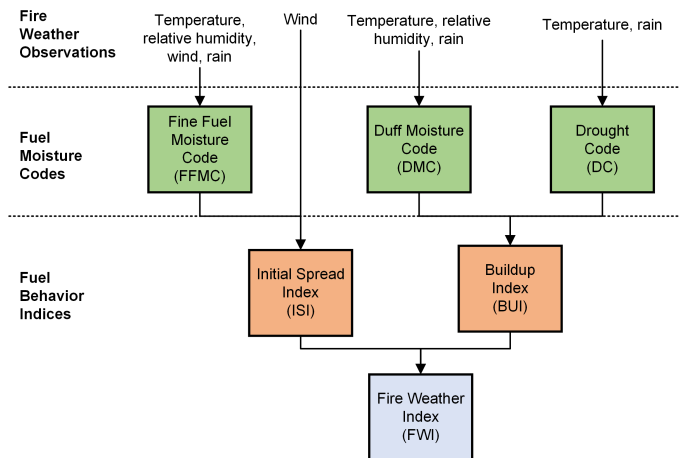


Figure 4: Illustration of FWI system.

For example, Canada developed a meteorology-based fire danger rating method in 1968, known as the Canadian Forest Fire Danger Rating System (CFFDRS). This system comprises four main subsystems: the Fire Weather Index (FWI), Fire Behavior Prediction (FBP), Fire Occurrence Prediction (FOP), and Auxiliary Fuel Moisture (AFM) (Van Wagner et al., 1974; Stocks et al., 1989b; Lawson and Armitage, 2008). Among these, the FWI system is the most widely used (Fig. 4). The FWI system, based on the theory of time lag and equilibrium moisture content, calculates changes in fuel moisture codes (i.e., Fine Fuel Moisture Code (FFMC), Duff Moisture Code (DMC), and Drought Code (DC)) and fire behavior indices (i.e., Initial Spread Index (ISI) and Buildup Index (BI)) according to weather conditions. These indices are then used to classify

potential wildfire danger levels in forests based on the moisture content of fuels at different locations or sizes (Stocks et al., 1989a).

Furthermore, the FWI system has been proven applicable in other countries or regions (Alexander, 1989; Fogarty et al., 1998; López et al., 2002; Taylor and Alexander, 2006; Dimitrakopoulos et al., 2011; Giannakopoulos et al., 2012). For instance, (Viegas et al., 1999) demonstrated that the FWI system is suitable for Europe, and it has been widely adopted by European countries as the optimal method for assessing wildfire danger (San-Miguel-Ayanz et al., 2018). Some countries have also developed their wildfire rating systems based on the FWI system. For example, South Africa developed the Lowveld Fire Danger Index (LFDI) based on the FWI, as shown in Eq. (5). Research has proven that this index is also applicable to the Mediterranean region of Greece (Cavalcante et al., 2021). New Zealand's wildfire rating system incorporates the Rate of Spread (ROS) and Head Fire Intensity (HFI) into the FWI system (Gregor and David, 2017). Similarly, Groot et al. (2007) developed an early wildfire risk warning system for Indonesia and Malaysia based on the FWI and FBP subsystems of the CFFDRS. This system includes a smoke potential indicator based on the DC, an ignition potential indicator based on the FFMC, and a difficulty of control indicator for grassland fires based on the ISI of the FWI System. The ISI-based indicator was developed using the grass fuel model of the FBP System, along with a standard grass fuel load and curing level estimated from previous Indonesian studies.

In comparison, the United States National Fire Danger Rating System (USNFDRS) (Deeming, 1972) evaluates fire risk by considering not only meteorological factors but also various terrain types, fuel types, and fuel models. By inputting meteorological data, fuel moisture, and terrain into the model, four output components are obtained: the Spread Component (SC), Energy Release Component (ERC), Burning Index (BI), and Ignition Component (IC). The first three indices, based on combustion physics, correspond to fire behavior characteristics, while the IC provides an estimate of fire danger levels (Zacharakis and Tsihrintzis, 2023a). The system was revised in 1978 and 1988 to address issues such as poor response to prolonged droughts and the inability to capture real-time fuel dynamics (Deeming et al., 1977) and inadequate performance in moist environments (Burgan, 1988). Recently, Jolly et al. (2024) updated the USNFDRS introduced in 1988 by emphasizing the provision of more detailed, fuel-type-dependent combustion condition assessments, proposing a new fuel moisture model, and simplifying the fuel model.

In Australia, widely used fire danger rating systems include the early McArthur's Forest Fire Danger Model (McArthur, 1966, 1967, 1973; Noble et al., 1980) and the Australia Fire Danger Rating System (AFDRS) introduced in 2022. The first system derived fire danger ratings based on predicted wildfire spread rates and the difficulty of suppressing fires burning in grasslands (McArthur, 1960) and dry sclerophyll forests (McArthur, 1958). This index, originally designed for eastern Australia in the 1950s and 1960s, underwent several revisions, culminating in the final Mark 5 version. Depending on vegeta-

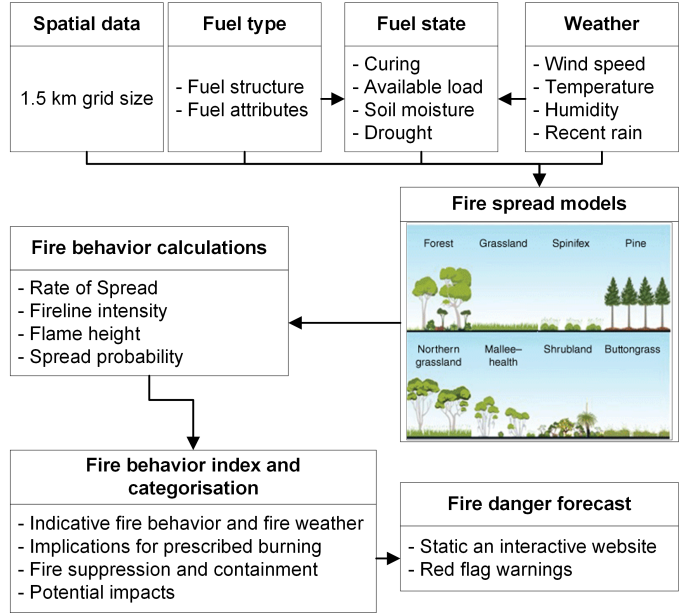


Figure 5: Illustration of AFDRS system (Hollis et al., 2024).

tion type, it is divided into the Forest Fire Danger Index (FFDI) and the Grassland Fire Danger Index (GFDI) (Zacharakis and Tsihrintzis, 2023a). However, Hollis et al. (2024) pointed out that McArthur's Forest Fire Danger Model could not utilize contemporary knowledge of fire behavior, such as new wildfire spread models (Cheney et al., 2012; Cruz et al., 2013; Anderson et al., 2015) and fire-atmosphere coupling (Mills and McCaw, 2010), and that its application has extended beyond its original design (Fogarty et al., 2010). Additionally, this system, with its low spatial resolution, cannot provide specific location-based wildfire risk recommendations. Finally, FFDI and GFDI cannot describe wildfire risks for vegetation types like shrublands (Anderson et al., 2015) and Spinifex (Burrows et al., 2018). Therefore, scientists and representatives from fire and land management agencies across all Australian jurisdictions collaborated to develop the new AFDRS. This system includes six factors: weather, fuel, fire behavior, ignition likelihood, suppression capability, and fire impact. It is designed for consistent and standardized use across Australia's states and territories, eliminating the need for ad hoc local adjustments. The main components of this system are shown in Fig. (5), which determines fire danger by establishing a forward spread rate model (Cruz et al., 2015) and incorporating hourly forecast weather data on a 1.5 km grid across Australia, as well as fuel type and fuel state, to calculate forward spread rates, fireline intensity, and other relevant information.

7. Deep Learning Methods for Wildfire Risk Prediction

Currently, popular methods for predicting wildfire risk include fire rating systems, statistical methods, traditional machine learning methods, and deep learning approaches. Fire rating systems, developed and extensively applied in regions like Canada, the USA, and Australia, are based on a combination of

empirical and mathematical modeling principles involving fluid dynamics, combustion, energy transfer, and considerations of fuel, weather, and terrain conditions (Rezaie et al., 2023; Mell et al., 2007). These models are known for their interpretability and generalizability, particularly suitable when training data are limited. However, physical models heavily rely on implicit assumptions about soil moisture, fuel load, land cover types, landscape structure, air humidity, and associated fire behaviors, which could adversely affect prediction accuracy (Rezaie et al., 2023; Bar Massada et al., 2011).

For small-scale or specific target analyses of wildfire risk, three additional methods are commonly employed. Firstly, statistical methods use various regression models to establish relationships between observed wildfire risks and factors such as fuel conditions, meteorological and climatic conditions, and terrain features. These methods are relatively simple but have limited learning capabilities and tolerance for the randomness and high nonlinearity typical of wildfire prediction tasks (Li et al., 2022a). In contrast, traditional machine learning methods like Random Forests (RF), Support Vector Machines (SVM), ensemble learning models, and Bayesian models automate the modeling of patterns and regularities in historical fire data and various wildfire risk factors through data-driven approaches and manual feature engineering. They handle non-linearities with higher interpretability and significantly better predictive capabilities than statistical methods. However, many of these models lack good interpretability.

Over the past decade, wildfire modeling has evolved from using statistical algorithms to more advanced machine learning methods that can automatically improve through experience (Jain et al., 2020; Oliveira et al., 2021b). The advantages of statistical methods include simplicity in modeling, low data requirements, and strong interpretability. However, limited by a small number of parameters, statistical methods often have poor predictive performance and generalization capabilities. Machine learning methods are increasingly used due to their ability to identify distributions in large datasets without the need for prior knowledge of the phenomena and to model in a non-parametric and non-linear manner (Oliveira et al., 2021b). Yet, their high dimensionality and complexity pose challenges in interpreting the importance of independent variables compared to traditional statistical regression methods. According to the classification proposed by Jain et al. (2020), common machine learning models used for wildfire prediction include decision trees, SVM, ANN, Bayesian methods, reward-based methods, clustering methods, and others. Some researchers have found that decision tree methods, such as Random Forests, perform better in wildfire prediction than other models. For instance, Malik et al. (2021) observed that Random Forest algorithms outperformed all other tested algorithms in terms of accuracy across various target labels and dataset subsets. However, some researchers argue that different methods have their advantages and disadvantages, and it is not conclusive that a single model is superior to others (Jaafari et al., 2019; Razavi Termeh et al., 2018). Therefore, some studies combine predictions from two or more models to improve final prediction accuracy. Since Jain et al. (2020); Zacharakis and Tsirhrintzis (2023b) have already

extensively reviewed the application of statistical methods and machine learning algorithms in wildfire prediction, detection, fuel characteristics, and other aspects of wildfire science and management up to the years 2020 and 2023, this section will not repeat those details.

The traditional machine learning methods mentioned earlier typically use shallow architectures and fail to fully leverage the spatial patterns inherent in images (Zhang et al., 2018). These classifiers directly categorize input data, lacking an effective feature extraction process, which limits their ability to extract representative features and improve classification accuracy (Zhang et al., 2019). Compared to traditional machine learning, deep learning models, although requiring more training data, can automatically extract more discriminative predictive features and learn more complex relationships and distributions through hierarchical structures and activation functions. This reduces reliance on manual feature engineering and enhances generalizability, making them better suited for complex real-world conditions. Additionally, deep learning algorithms have a larger parameter capacity, enabling them to handle larger datasets and reducing the risk of model overfitting. While deep learning models have become an increasingly popular tool for predicting wildfire risks and represent a new trend in the field, current literature reviews, such as those by Jain et al. (2020); Zacharakis and Tsirhrintzis (2023b), provide only a limited overview of methods including Recurrent Neural Network (RNN) and CNN, lacking a comprehensive systematization of their use.

To address this gap, this section systematically reviews the latest advancements in deep learning-based wildfire risk prediction models. Currently, wildfire risk prediction using deep learning methods generally transforms the task into segmentation or classification challenges, where models are trained using historical wildfire data and driving factors affecting fire ignition or spread as inputs, with future wildfire occurrences or risk levels as ground truth. For segmentation tasks, models can be categorized based on how they use the data into three types: time series prediction, classic semantic segmentation, and spatio-temporal prediction. Time series prediction uses 1D feature vectors of time series as input and employs recurrent neural network methods like RNN, LSTM, and GRU, as well as attention-based Transformer methods, to predict wildfire risks at the next time step. Classic semantic segmentation methods take 2D feature maps of wildfire influencing factors or wildfire data from a previous time step as inputs to predict the next time step's wildfire risks, outputting results in 2D. These models are typically CNNs or Transformers. Spatio-temporal prediction methods combine the above approaches, using 2D time series data of wildfire influencing factors or wildfire data as inputs to predict the next time step's wildfire risks. Deep learning models used for spatio-temporal prediction often combine models such as CNNs, Transformers, GCNs, and GNNs with RNNs, LSTM, and GRU in various ways. Thus, this section will introduce models based on time series prediction methods (including RNN, LSTM, GRU, and Transformers), classic semantic segmentation methods (CNNs), and spatio-temporal prediction methods for wildfire risk. Furthermore, since deep learning

models are often considered black box models, making it difficult to interpret the contribution of various features to model predictions and the prediction process itself, this section also establishes techniques for explainability of deep learning models to support decision-making in wildfire management and model development.

7.1. Wildfire risk rating and probability calibration

Even though [Jain et al. \(2020\)](#); [Zacharakis and Tsihrintzis \(2023b\)](#) systematically reviewed the application of various machine learning methods in wildfire risk research, but they did not provide a description of the post-processing techniques required to convert the predictions of machine learning models into actual wildfire risk. Directly using the output of these models as the probability of wildfire risk may lack theoretical foundation and stability. This is because the machine learning model, trained using the wildfire coverage at time $t + n$ as the ground truth and input data from time t such as fuel and environmental conditions, inherently outputs a probability map that reflects the likelihood of a specific location being within the wildfire area at time $t + n$, rather than representing actual risk. Additionally, even with identical inputs, different models may produce significantly divergent probability maps.

Moreover, wildfire historical data sets typically suffer from severe class imbalance, where the spatial and temporal scope of fire occurrences is considerably smaller compared to non-fire events. To expedite model convergence, many machine learning datasets are often constructed with a balanced class ratio, typically 1:1, 1:1.5, or 1:2 ([Huot et al., 2021](#); [Kondylatos et al., 2022](#)) between fire and non-fire instances. This may lead to an overestimation of false positives during model evaluation ([Bakke et al., 2023](#)). However, actual wildfire risk probabilities are usually much lower. For example, in wildfire risk assessments for the Mediterranean region and the United States, [Ager et al. \(2014a\)](#) and [Preisler et al. \(2004\)](#) respectively, used probabilities in the thousandths range.

Using the probability output of machine learning models as wildfire risk could be misleading to non-experts. Therefore, many studies convert continuous wildfire risk probabilities into risk levels to support wildfire management, such as conveying public warnings and guiding fire suppression measures. Among the methods for risk level classification, the Jenks natural breaks classification ([Jenks and Caspall, 1971](#)) is most commonly used. For instance, [Xie et al. \(2022b\)](#) trained an ensemble machine learning model using binary wildfire ignition records and then classified the predicted probabilities into five groups using the Jenks method. Similarly, [Iban and Sekertekin \(2022\)](#) and [Moayedi and Khasmakhi \(2023\)](#) also classified the hazard maps generated by machine learning models into five categories using the Jenks method. Along the same lines, [Chen et al. \(2024c\)](#) used the Jenks method to divide the estimated potential rate of spread and fire radiative power into five levels for wildfire risk assessment. Other methods have also been employed for risk level classification. For example, [Liang et al. \(2019\)](#) used the Kennard-Stone method combined with standardized duration and fire size to categorize the wildfire risk predicted by an RNN into five levels. [Jalilian and Jouibary](#)

(2023) applied natural discontinuity classification methods to group the probabilities predicted by machine learning models into three classes. [Bjånes et al. \(2021\)](#) and [Chicas et al. \(2022\)](#) divided the wildfire ignition probability maps produced by the models into five levels using an equal-interval method, with intervals of 0.2. Similarly, [Trucchia et al. \(2022\)](#) manually defined five risk levels.

Furthermore, some methods aim to recalibrate probability outputs to obtain actual wildfire risk probabilities. For instance, [Pelletier et al. \(2023\)](#) constructed a semi-balanced dataset for model training, in which the numbers of burned and never-burned sites were 3,268 and 60,146, respectively. They then used the method proposed by [Elkan \(2001\)](#) (Eq. (10)) to convert the wildfire probabilities predicted by a time series XG-Boost model into actual probability values:

$$p' = \frac{BR2 \times (p - p \times BR1)}{BR1 - p \times BR1 + p \times BR2 - BR1 \times BR2} \quad (10)$$

where p' represents the revised probability for a prediction, $BR1$ stands for the base rate of the predicted probability estimates (the average of predicted probabilities for that class), and $BR2$ denotes the base rate of the actual probability estimates derived from the target population. Here, the target population refers to the average probability of fires across all observations within the training dataset, including the unburned observations that were not utilized in model training. Similarly, [Phelps and Woolford \(2021\)](#) used the function proposed by [Dal Pozzolo et al. \(2015\)](#) to correct the neural network's probability output:

$$p_k = \frac{\pi \gamma_k}{\pi \gamma_k - \gamma_k + 1} \quad (11)$$

where p_k and γ_k represent the wildfire probabilities modeled from the original and sampled distributions, respectively, and π denotes the proportion of non-fire observations sampled.

From the above analysis, it is evident that the natural breaks method is commonly used to classify machine learning-predicted probability maps into multiple levels. However, there is still limited exploration on how to map these probability maps into continuous probability distributions and establish a relationship between predicted probabilities and actual risk probabilities.

7.2. Time series prediction

7.2.1. Recurrent neural network

As discussed in previous sections, the occurrence and spread of wildfires are influenced by various factors, including meteorological conditions, fuel status, and historical wildfire data. These factors exhibit cumulative effects. Therefore, utilizing time series data enables models to capture the gradual changes in influencing factors, thus facilitating the prediction of future wildfire risks. The most classical methods in time series prediction tasks are Recurrent Neural Networks (RNNs), which include RNN, LSTM, and Gated Recurrent Unit (GRU).

RNN is a basic neural network structure with recurrent connections, designed to process sequential data. As shown in

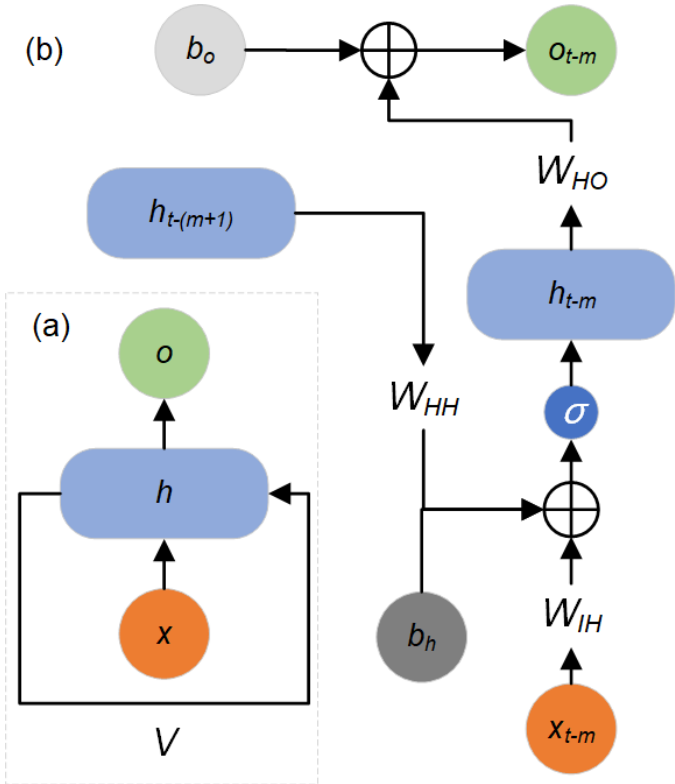


Figure 6: The architecture of RNN where (a) and (b) represent the overall architecture and detailed hiddenlayer calculation.

Fig. 6, it integrates input from the current time step with output from the previous time step to model and predict sequence data. A simple RNN structure consists of an input layer, hidden layer, and output layer. Input data are time series data, i.e., feature vectors with dimensions $f \times d$. The hidden layer includes several hidden units, where each hidden unit outputs \mathbf{h}_{t-m} , the 'memory' at any intermediate time $t - m$ ($m < n$), as a weighted sum of its previous 'memory' and current time step's input features:

$$\begin{cases} \mathbf{h}_{t-m} = \sigma_h(\mathbf{W}_{IN}\mathbf{x}_{t-m} + \mathbf{W}_{HH}\mathbf{h}_{t-(m+1)} + \mathbf{b}_h) \\ \mathbf{y}_{t-m} = \sigma_o(\mathbf{W}_{HO}\mathbf{h}_{t-m} + \mathbf{b}_o) \end{cases} \quad (12)$$

where \mathbf{W}_{IN} and \mathbf{W}_{HH} represent weight matrices for processing input to the hidden layer and from hidden layer to hidden layer, respectively; \mathbf{x}_{t-m} and $\mathbf{h}_{t-(m+1)}$ represent the input feature vector at time $t - m$ and 'memory' from the previous time step, respectively; \mathbf{b}_h and \mathbf{b}_o represent bias vectors for the hidden units and output layer, respectively. Ultimately, the output \mathbf{y}_t at time $(t - m)$ ($m < n$) is a weighted sum of all hidden units. By iteratively repeating the above process, each timestep of the entire time series data ($t - n, t - (n - 1), \dots, t - 1$) is predicted. Finally, a loss function (Eq. 13) estimates the discrepancy between the prediction and labels, and model weight parameters are iteratively updated through backpropagation.

$$\ell(\mathbf{y}, \mathbf{GT}) = \sum_{t=n}^{t-1} \ell_t((\mathbf{y}_t, \mathbf{GT}_t)) \quad (13)$$

where \mathbf{GT}_t represents the label value at time t .

In wildfire risk prediction, classic RNN networks and their variants have been employed. For instance, Elman RNN designed a spatiotemporal prediction framework integrating historical wildfire and weather data to predict the annual average burned area in Canadian forests. Experiments demonstrated a prediction error of less than 0.5ha on areas of 500ha, validating the feasibility of using RNN for fire prediction. Similarly, a comparative study of ten artificial neural networks (ANNs) based on meteorological data for predicting wildfire incidence in Australia found that Elman RNN exhibited the best performance, with average accuracy, sensitivity, and specificity exceeding 93%. Further, a network composed of a dynamic autoencoder and RNN was used to predict the next month's burned area in five U.S. regions, where the dynamic autoencoder was employed to transform multidimensional time series data into RNN input features, and dual decoders were used for predicting fire spot likelihood over different time spans, i.e., one week and one month. Comparative experiments showed that their method was slightly superior to comparative methods, generative network, and GRU.

While [Jain et al. \(2020\)](#) and others have highlighted the limited use of classical RNNs, our findings are consistent with these observations. The underutilization of RNNs may be attributed to their difficulties in handling long sequence data, where they are prone to gradient vanishing or exploding, making it challenging to capture long-term dependencies ([Hochreiter, 1997](#); [Gers et al., 2000](#)). To address these issues, LSTM networks were developed. As illustrated in Fig. 7, LSTMs incorporate three gating units: input gate, forget gate, and output gate, which control the flow and retention of information. These gates, with trainable weights, decide whether to pass, forget, or output information based on the current input and the output from the previous timestep. This gating mechanism effectively resolves the issues of vanishing and exploding gradients, thereby enabling better handling of long sequences and capturing of long-term dependencies. Consequently, LSTMs are more prevalently applied in wildfire risk prediction than classical RNNs. The specific configuration of an LSTM cell is depicted in Fig. 7b and Eq.14 ([Monner and Reggia, 2012](#); [Liang et al., 2019](#)).

- For the forget gate (f_t), the output from the hidden layer of the previous timestep $\mathbf{h}_{t-(m+1)}$ is concatenated with the input features at the current timestep \mathbf{x}_{t-m} , then multiplied by the forget gate weight matrix \mathbf{W}_f and added to the forget gate bias b_f . This sum is then passed through a sigmoid activation function σ , resulting in the output of the forget gate.
- The input gate has two branches. The first branch (i_t) is similar to the forget gate, involving concatenation followed by multiplication with the input gate weight matrix \mathbf{W}_i and addition of the bias b_i . The second branch uses a weight matrix \mathbf{W}_c that represents candidate cell states to multiply with the concatenated result, added to the bias b_c , and activated using the hyperbolic tangent function \tanh . The outputs of these two branches are multiplied together

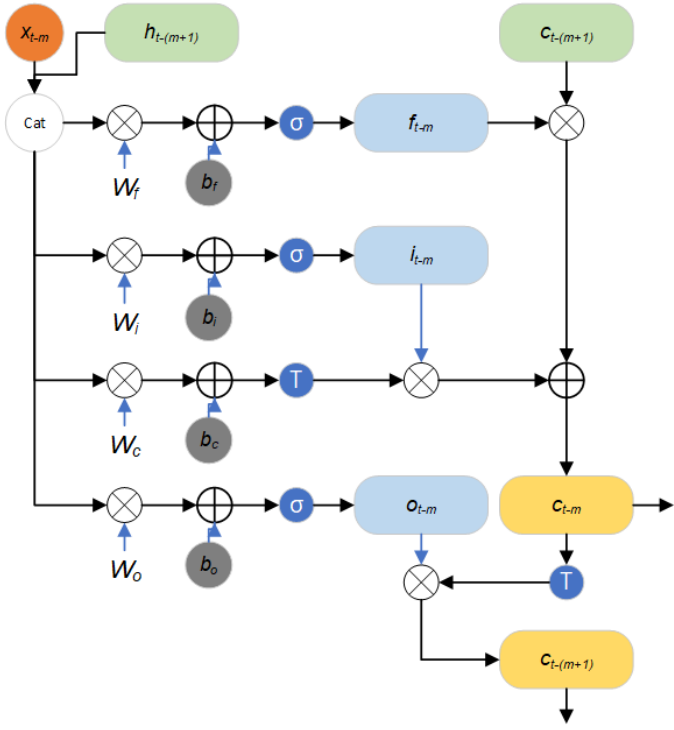


Figure 7: Schematic diagram of the LSTM architecture illustrating the flow of data through input, forget, and output gates.

and added to the product of the forget gate output and the output of the input gate from the previous timestep ($c_{t-(m+1)}$) to produce the output for the current timestep (c_{t-m}).

- Similarly, the output gate includes two branches. The first branch multiplies the concatenated input by the output gate weight matrix W_o , adds the bias b_o , and activates it. For the second branch, the output of the input gate at the current timestep (c_t) is activated using tanh. The final output of the hidden layer at the current timestep is obtained by multiplying the results of these two branches.

$$f_{t-m} = \sigma(W_f \cdot [h_{t-(m+1)}, x_{t-m}] + b_f) \quad (14)$$

$$i_{t-m} = \sigma(W_i \cdot [h_{t-(m+1)}, x_{t-m}] + b_i) \quad (15)$$

$$c_{t-m} = f_{t-m} \odot c_{t-(m+1)} + i_{t-m} \odot \tanh(W_c \cdot [h_{t-(m+1)}, x_{t-m}] + b_c) \quad (16)$$

$$o_{t-m} = \sigma(W_o \cdot [h_{t-(m+1)}, x_{t-m}] + b_o) \quad (17)$$

$$h_{t-m} = o_{t-m} \odot \tanh(c_{t-m}) \quad (18)$$

Studies utilizing LSTM for wildfire risk prediction often model various risk factors, including weather and climate conditions, fuel conditions, and socio-economic factors. For instance, Liang et al. (2019) found that LSTM outperformed RNN and Back Propagation Neural Network (BPNN) in predicting the class of wildfires in Alberta, Canada, based on meteorological conditions, achieving an overall accuracy of 90.9%.

Similar findings were reported by Natekar et al. (2021), who assessed the wildfire risk in Indian forests using meteorological parameters and LSTM methods. The accuracy and RMSE were 94.77% and 37.5%, respectively, surpassing other benchmark methods like CNN and SVM. Additionally, Kondylatos et al. (2022) compared RF, XGBoost, and deep learning methods (LSTM and ConvLSTM) and found that deep learning significantly outperformed traditional machine learning methods in predicting next day wildfires in the Mediterranean using ERA5-Land meteorological data, MODIS NDVI, and diurnal LST data along with soil moisture, terrain data, land cover types, and distances from infrastructure. Li et al. (2023a) further integrated attention mechanisms and deep learning interpretability into an LSTM network, using monthly-scale climate, socio-economic, fuel variables, and oceanic indices to predict short-term (1–4 months) and long-term (5–8 months) wildfire burning areas in tropical regions. Experimental results demonstrated that the enhanced LSTM model outperformed traditional machine learning methods and the baseline LSTM model. Additionally, interpretability analysis revealed that precipitation and vapor pressure deficit were critical driving factors, while oceanic indices provided more significant contributions to long-term wildfire burning area predictions.

Moreover, some studies use only historical wildfire occurrence data combined with LSTM to predict future regional wildfire risks. For example, Kadir et al. (2023) used historical MODIS wildfire data combined with LSTM to predict the spatiotemporal distribution of wildfires in Indonesia for the following year, with a success rate exceeding 90% and an error rate of only 6.94%. Notably, to reduce the amount of data, this study grouped several days' worth of data into single days for training and testing. Furthermore, Hu et al. (2023) combined LSTM with autoencoders, using historical wildfire data from 1992–2018 to predict the level of wildfire occurrence in high-risk areas such as California. The autoencoder was employed to generalize wildfire events from the overall dataset, enhancing the accuracy of anomaly event predictions through reconstruction errors.

Similar to the LSTM, the GRU addresses the challenges of gradient vanishing and explosion inherent in traditional RNNs and involving the gate mechanisms. GRU reduces the number of gating units found in LSTM, containing only a reset gate and an update gate, as shown in Eq.19, which simplifies the model architecture and enhances computational efficiency (Chung et al., 2014). The structure of the GRU model is depicted in Fig. 8. Despite its simpler configuration, GRU retains the capability to model long-term dependencies with performance comparable to that of LSTM (Jin et al., 2020a).

$$r_t = \sigma(W_r \cdot [h_{t-1}, x_t] + b_r) \quad (19)$$

$$z_t = \sigma(W_z \cdot [h_{t-1}, x_t] + b_z) \quad (20)$$

$$\tilde{h}_t = \tanh(W_h \cdot [r_t h_{t-1}, x_t] + b_h) \quad (21)$$

$$h_t = (1 - z_t) h_{t-1} + z_t \tilde{h}_t \quad (22)$$

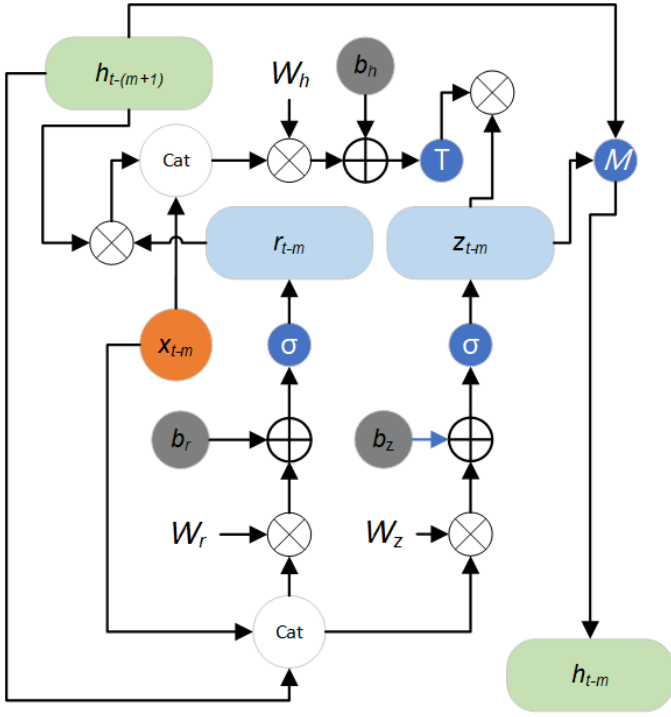


Figure 8: Schematic representation of the GRU architecture highlighting its reset and update gates.

Studies such as [Dzulhijjah et al. \(2023\)](#) have compared the performance of LSTM, BiLSTM, CNN-LSTM, Stacked-LSTM, and GRU in predicting wildfire risk in the Indonesian region of Kalimantan, finding that GRU slightly outperforms the other models, though the advantage is not significant. In contrast, [Gopu et al. \(2023\)](#) observed better results with LSTM in a comparative study of wildfire prediction in the Montesinho Natural Park, Portugal. Additionally, [Chavalithumrong et al. \(2021\)](#) found that models integrating a dynamic autoencoder with RNN outperformed standard GRU models, suggesting that enhanced RNN architectures can offer superior performance.

7.2.2. Transformers for Wildfire Risk Prediction

Transformers utilize multi-head self-attention mechanisms to calculate attention scores, enabling them to capture dependencies at any position within the sequence. The attention mechanism is defined as:

$$\text{Attention}(Q, K, V) = \text{softmax}\left(\frac{QK^T}{\sqrt{d_k}}\right)V \quad (23)$$

where d_k represents the dimensionality of the key. The architecture of a Transformer, as illustrated in Fig. 9, comprises encoders, decoders, positional encoding, and multiple attention mechanisms.

Transformers operate on sequences transformed into tokens, which are then embedded with positional encoding to maintain the sequence order absent in traditional RNNs. The sequence of embedded tokens is processed by the encoder, which transforms it into a context vector using layers of multi-head self-attention

and feed-forward networks. The decoder similarly processes the context vector to predict the output sequence.

The ability of Transformers to process sequence data without relying on sequential processing allows for parallel computation during training, significantly speeding up the learning process compared to RNNs ([Vaswani et al., 2017](#)). This makes them particularly effective for long-sequence predictions or complex scenarios requiring modeling of long-range dependencies ([Zerveas et al., 2021; Prapas et al., 2023](#)).

Transformers have been adapted for several predictive tasks in wildfire risk assessment. For example, [Miao et al. \(2023\)](#) developed a Transformer model with a window-based attention mechanism to predict forest fire risks in Chongli District, Beijing, using time-series data of meteorological, topographical, vegetation, and anthropogenic factors. The window mechanism confines attention to a fixed-size window centered on each element, reducing computational complexity and memory usage. Similarly, [Cao et al. \(2024\)](#) employed a Transformer to predict next-day wildfire risks in Quanzhou County, Guangxi Province, based on three days of meteorological, topographical, and human activity data. The model's performance, analyzed using IGR, outperformed LSTM, RNN, and SVM in terms of generalization, noise resistance, and overfitting mitigation.

In addition, [Prapas et al. \(2023\)](#) introduced a TeleViT model that incorporates teleconnections to model long-range spatio-temporal interactions globally, aiming to predict subseasonal to seasonal wildfire patterns. This model combines fine-grained local-scale inputs with coarse-grained global-scale data, improving prediction accuracy for global wildfire patterns up to four months in advance.

These examples illustrate the growing importance and versatility of Transformers in addressing the complexities of wildfire risk prediction, offering advancements over traditional models in handling long-range dependencies and large-scale data integration.

From the analysis above, it is evident that both RNNs and GRUs are less frequently used in wildfire risk prediction, which includes forecasting occurrences, susceptibility, and spread. In contrast, LSTM networks have a relatively higher usage rate. RNNs, compared to LSTMs, are particularly challenged by issues such as vanishing and exploding gradients and exhibit weaker capabilities in modeling long-distance dependencies. Furthermore, although some researchers argue that GRUs perform comparably to LSTMs ([Viswanathan et al., 2019; Gao et al., 2020; Liu et al., 2021; Gao et al., 2021; Zarzycki and Ławryńczuk, 2022](#)), the simplified structure of GRUs may result in inferior performance when processing highly complex sequences or capturing intricate relationships ([Cahuantzi et al., 2023](#)), especially in wildfire risk prediction tasks that do not require high real-time processing capabilities or are intended for edge computing devices. Recently, however, with the advent of Transformers, these models are gaining popularity in wildfire risk prediction due to their complex architecture, larger parameter capacity, and the advantages of parallel computation.

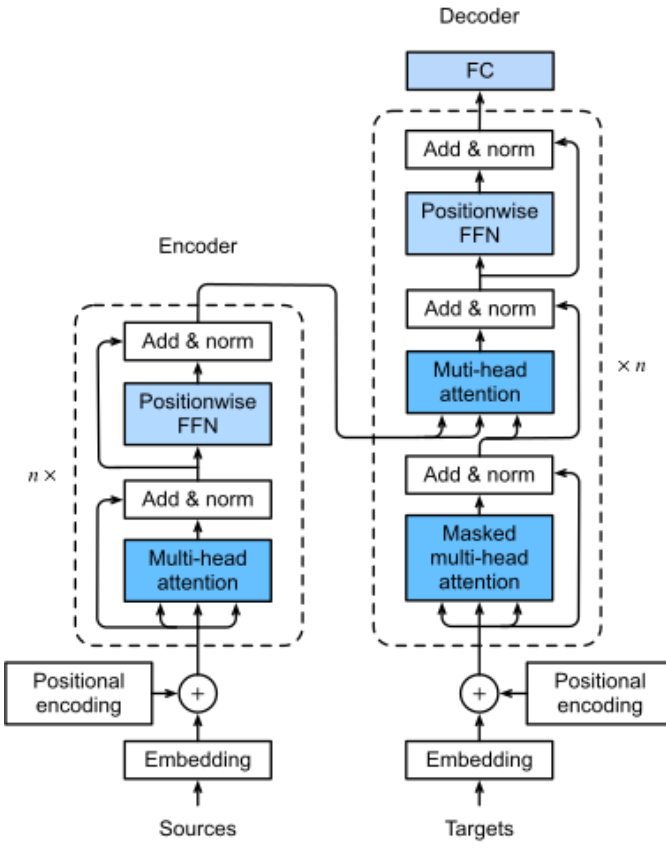


Figure 9: Schematic diagram of the Transformer architecture, highlighting its main components.

7.3. Image Semantic Segmentation and Classification Methods

Although RNNs and Transformers excel at capturing temporal dependencies for sequence-to-sequence learning tasks, these methods primarily classify individual pixels' temporal sequence data. However, wildfire occurrences are not only influenced by local conditions but also by neighboring areas (e.g., wind propagation) (?). When RNNs use 1D data inputs, the spatial structure of the image is often lost (Hu et al., 2020). Consequently, several studies have explored the use of classical image semantic segmentation and classification methods, such as CNNs, GNNs, and Transformers, to predict wildfire risk at time t using the influencing factors (e.g., fuel, weather) from time $t' < t$. These methods rely on 2D image inputs, which explicitly model the spatial dependencies of input features, while also implicitly modeling the influence of current driving factors on future wildfire risk by having different input features and predicted time steps. In wildfire risk prediction, convolutional neural networks (CNNs) are commonly used, with graph neural networks (GNNs) and Transformers increasingly adopted in recent studies.

7.3.1. Convolutional Neural Networks

CNNs are foundational network structures in deep learning, designed to extract local spatial features through convolution operations, making them well-suited for capturing the

spatial information necessary for wildfire risk prediction, as shown in Fig.10. Zhang et al. (2019) employed a modified AlexNet (Krizhevsky et al., 2012) using annual fire point maps and springtime mean influencing factors for Yunnan Province, China, to classify image patches as wildfire-prone areas. The model outputs a probability map of wildfire risk through softmax mapping in the final CNN layer. The authors compared the performance of the CNN model with RF, SVM, MLP, and kernel logistic regression models, finding that CNN achieved the highest overall accuracy. They also explored the contributions of various wildfire drivers using information gain ratio, identifying temperature, wind speed, surface roughness, precipitation, and elevation as the most influential factors.

Subsequently, they extended the modified AlexNet to generate a global quarterly wildfire susceptibility map (Zhang et al., 2021), comparing its performance with MLP-2D, CNN-1D, and MLP-1D models. Results indicated that CNN-2D and MLP-1D models outperformed CNN-1D and MLP-2D. Additionally, the authors applied an improved permutation importance (PI) method and partial dependence plots (PDP) to investigate the interpretability of the CNN-2D model. PI analysis revealed that maximum monthly temperature, soil temperature, NDVI, and soil moisture were significant factors affecting the model. PDP analysis further indicated a negative relationship between cumulative precipitation and wildfire probability, while maximum monthly temperature and soil temperature positively influenced wildfire occurrence.

Furthermore, they used a similar CNN method to predict the spatiotemporal variation of wildfire risk under different climate scenarios, discovering that global warming would lead to an increase in burned areas and a northward shift of wildfire-prone regions (Zhang et al., 2024a). Kanwal et al. (2023) similarly explored CNN-1D and CNN-2D classification models and machine learning algorithms for evaluating seasonal wildfire risks in Pakistan, finding that CNN-2D outperformed CNN-1D and other machine learning algorithms.

Some studies have employed deeper or structurally and parameter-optimized CNN networks. For example, Oak et al. (2024) used VGG16 combined with ReLU, BatchNorm, Dropout, and a sigmoid layer to predict wildfire susceptibility in Quebec, Canada. Comparative experiments demonstrated that this model outperformed Xception, VGG16, ResNet50, and In-

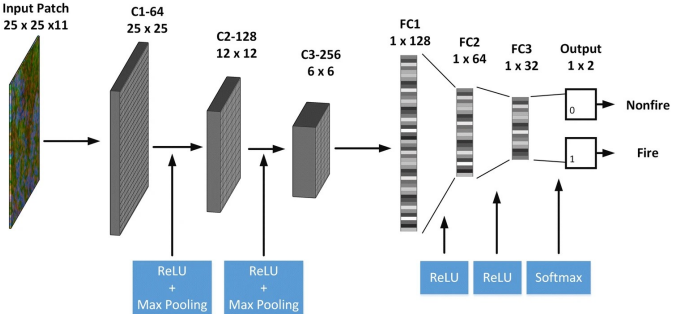


Figure 10: The architecture of CNN classification network where the center pixel is classified using surrounding information (Zhang et al., 2019).

ception V3. Similarly, Nur et al. (2022) applied a meta-heuristic optimization algorithm to fine-tune the hyperparameters of a CNN model for wildfire susceptibility mapping in the Plumas National Forest, USA. Their IGR analysis of 16 driving factors revealed that land use, drought index, and maximum temperature had the greatest impact on wildfire susceptibility. After applying the meta-heuristic optimization algorithm, CNN performance improved significantly. Likewise, (You et al., 2023) employed particle swarm optimization to optimize the structure and parameters of a CNN classification model to assess annual forest fire risk across China. Comparative analysis showed that this approach outperformed both CNN and traditional machine learning methods. Using SHAP for interpretability analysis, the most significant factors were found to be NDVI, land cover, and temperature. Eddin et al. (2023) introduced location information to the CNN by adding a separate convolution branch, highlighting the distinction between dynamic variables (those changing over time) and static variables (those that remain constant over the study period). To address the causal effects of static variables on dynamic ones, they introduced a LOAN layer to adjust the activation maps in the dynamic branch based on static features. Additionally, they used a sinusoidal encoding of Julian days to provide the model with explicit time information. Their experiments on the FireCube dataset, covering parts of the Mediterranean (Prapas et al., 2022; Kondylatos et al., 2023), demonstrated that the proposed model's predictions of $t + 1$ wildfire spread outperformed baseline models, including LSTM, ConvLSTM, RF, and XGBoost. Dong et al. (2024) proposed a similar architecture where dynamic and static variables are modeled separately in the encoding phase, resulting in improved accuracy in predicting fire radiative power.

Beyond classification-based approaches, some studies have adopted end-to-end models to provide higher-resolution predictions. For instance, Hodes and Lattimer (2019) proposed a deep convolutional inverse graphic network comprising convolution and deconvolution layers to simulate wildfire spread over homogeneous and heterogeneous landscapes for 6-hour and 24-hour intervals. The study demonstrated the high efficiency of CNNs in wildfire spread prediction. Similarly, Santopaolo et al. (2021) used an end-to-end CNN image segmentation model to predict wildfire risk in Sicily, Italy, and California, USA, based on driving factors from 8 days prior. Likewise, Bergado et al. (2021) designed an AllConvNet, a fully convolutional network, to predict wildfire burn probability for the next 7 days in Victoria, Australia, based on pre-fire driving factors. Overall, the proposed AllConvNet achieved higher prediction accuracy than logistic regression, SegNet, and MLP models. Feature extraction and normalization of LR coefficients revealed that total rainfall, lightning density, and surface temperature were among the most influential variables across all models. Additionally, Li et al. (2023b) introduced spatial and channel attention mechanisms to help the end-to-end CNN model focus on critical features while suppressing irrelevant ones to predict the next moment's wildfire spread. Unlike previous studies, this model's input also included the burning map from the prior time step. Comparative results demonstrated that this model outperformed other CNN models and ConvLSTM. Similarly, Shadrin et al.

(2024b) employed the MA-Net segmentation model, which includes position attention and multi-scale attention blocks, to predict wildfire extent for the next 1-5 days. In contrast to previous studies, they also incorporated short-term weather forecasts for the next 1-5 days along with various wildfire driving factors. Experimental results showed accurate wildfire spread predictions within 3 days, with wind component, land cover, NDVI, EVI, and LAI being the most influential factors. Marjani et al. (2024a) combined CNN with atrous spatial pyramid pooling to model wildfires at different scales and shapes, adopting an end-to-end approach to model wildfire spread for the next day. They also used linear regression and Grad-CAM heatmap correlations to show that larger and smaller dilation rates help extract large-scale and small-scale wildfires, respectively. Similar to Eddin et al. (2023), Jiang et al. (2023) employed three branches to process static DEM and fuel data, dynamic wind speed, wind direction, temperature, and humidity data, as well as the previous time step's wildfire status. The experiments demonstrated that this model's inference efficiency was significantly higher than that of cellular automata and Farsite models. Furthermore, the model accurately predicted burned areas in real wildfire scenarios.

7.3.2. Other Methods

In addition to CNNs, other image segmentation methods, such as Graph Neural Networks (GNNs) and Transformers, have also been applied to wildfire risk prediction. GNNs, compared to CNNs, are better suited for handling non-Euclidean structured data (Asif et al., 2021), while Transformers' multi-head self-attention mechanisms are more effective in modeling long-range semantic dependencies within images (Vaswani et al., 2017). For example, Jiang et al. (2022) proposed using an irregular graph network to simulate wildfire spread in variable-scale landscapes, addressing the issue of fixed-grid data being unable to adaptively differentiate landscape heterogeneity. The model adjusts graph node density based on terrain complexity to achieve uniformity in nodes and edges at varying scales. Comparative experiments with cellular automata and FARSITE demonstrated that the proposed model exhibits competitive accuracy and efficiency.

Additionally, Chen et al. (2022) incorporated a GNN into the knowledge graph framework proposed by Ge et al. (2022) to enable automated learning and prediction of burn areas. Specifically, the model first constructs a knowledge graph in the form of triples, then uses RotaE to compute representation vectors for each entity. These entity vectors are associated with nodes in the graph, and the vectors are subsequently fed into the GNN to facilitate automatic updates. Finally, link prediction algorithms are employed to predict the burn areas associated with the recorded nodes. Experiments conducted in Portugal's Montesinho Natural Park demonstrated that this algorithm significantly outperformed traditional machine learning algorithms such as RF, SVM, and MLP.

Moreover, Li and Rad (2024) introduced spatial attention mechanisms and focal modulation into a U-shaped encoder-decoder network based on Transformers, known as Swin Unet. This end-to-end image segmentation approach utilizes wildfire

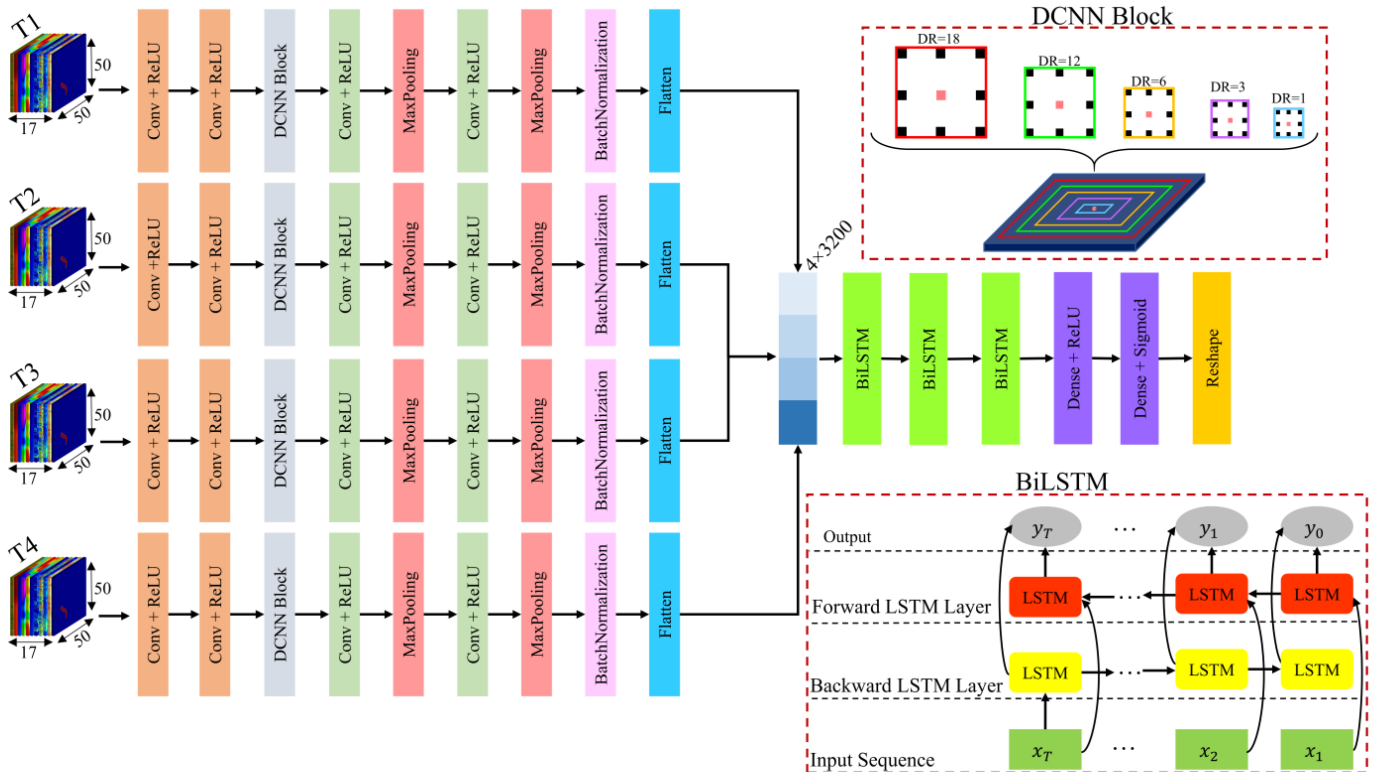


Figure 11: The sample architecture of the separated spatial and temporal modeling method (Marjani et al., 2024b)

risk driving factors from the previous day to predict wildfire risk for the following day across the continental United States. Comparative experiments using the extended Next Day Wildfire Spread dataset (Huot et al., 2022) showed that this model outperforms baseline models, including the standard UNet and Swin Unet.

7.4. Spatiotemporal Prediction Methods

The previously discussed time series prediction methods and image segmentation/classification methods each have their strengths in capturing temporal and spatial dependencies, respectively. However, they are unable to simultaneously handle both spatial and temporal dependencies and capture the complex cross-spatiotemporal interaction patterns. For instance, [Prapas et al. \(2021\)](#) pointed out that focusing only on spatial scale modeling could overestimate a model’s real-world performance. To integrate spatial structure and time series data, many studies have attempted to combine CNN, GNN, and Transformer models with RNN, LSTM, and GRU methods. This transforms the task of time series prediction or localized optimization between consecutive wildfire states ([Jiang et al., 2023](#)) into spatiotemporal sequence prediction tasks. There are three primary approaches to achieving this combination: separated spatial and temporal modeling, coupled spatiotemporal modeling, and spatially enhanced coupled spatiotemporal modeling.

Specifically, separated spatial and temporal modeling involves abstracting spatial features into 1D feature vectors using spatial modeling methods, which are then input into tempo-

ral prediction models. Coupled spatiotemporal modeling converts the 1D tensors in RNNs into 3D tensors, incorporating spatial dimensions (rows and columns) and using convolutions or graphs (instead of weight matrix multiplication) to determine a grid cell's future state based on its neighbors' current and past states. Lastly, spatially enhanced coupled spatiotemporal modeling introduces CNNs or graph-based methods to extract spatial features before the temporal modeling stage.

7.4.1. Separated Spatial and Temporal Modeling Methods

The approach of separately extracting spatial and temporal features is quite common. The structure of a typical spatiotemporal wildfire risk prediction model is illustrated in the Fig.11. In this model, multiple CNNs are employed to process multi-dimensional spatial images at each time step, with dimensionality reduction applied before feeding the data into the LSTM. Finally, the output from the LSTM is mapped to output probabilities using a CNN, or directly without it, along with the application of a sigmoid function.

For example, Jin et al. (2020b) proposed enhancing spatial feature extraction by employing CNNs and GCNs to extract spatial information, which is then passed through a feed-forward network (FFN) to unify the data into a 1D vector before being input into a GRU. The output 1D vector is then restored to its original size using deconvolution layers, performing urban fire situation prediction through an end-to-end semantic segmentation approach. Compared to traditional machine learning methods like RF, XGBoost, as well as GRUN and Conv-GRUN,

this model showed significant performance improvements.

Similarly, [Huot et al. \(2021\)](#) used the Next Day Wildfire Spread dataset and categorized wildfire risk prediction into two tasks: next-day wildfire probability prediction and final burning area prediction. They experimented with four models: convolutional autoencoder and residual UNet for segmentation, and convolutional autoencoder and residual UNet combined with LSTM for temporal prediction. The results showed that, among the segmentation models, the convolutional autoencoder outperformed UNet. When combining the two models with LSTM for final burning area prediction, there was no significant performance difference between the models.

[Zhang et al. \(2022\)](#) designed and compared four deep neural networks with identical structures but different depths, combining 2D CNN and LSTM models to predict global monthly burned area maps using seven meteorological and two biophysical predictors from the previous 12 months. Each model reduced spatial dimensions through convolution, ReLU, and max-pooling operations and used fully connected layers to flatten the input patches into 1D features before feeding them into LSTM layers. The primary difference among the models was the number of CNN and LSTM layers. Ultimately, the CNN-LSTM network with two convolutional layers and two LSTM layers was selected for its balance of performance and efficiency. The results showed that the combination of convolution and LSTM methods outperformed standalone LSTM and CNN models.

Furthermore, [Marjani et al. \(2024b\)](#) combined CNN with bidirectional LSTM (BiLSTM) for a study in Australia, using wildfire driving factors from the previous four days and wildfire masks to predict next-day wildfire spread. The method first employed four CNN layers to extract spatial features, which were then flattened and input into a three-layer BiLSTM. The model produced binary outputs through dilated convolution, dense layers, and sigmoid activation functions. Comparative experiments demonstrated that this approach outperformed LSTM and Conv-LSTM methods, and the study also confirmed that using longer time steps improved prediction capabilities. In another study, [Li et al. \(2021b\)](#) not only introduced CNN before the LSTM but also incorporated an attention mechanism within the LSTM to assign different weights to the hidden states, reducing information loss and improving prediction accuracy. Applied in Portugal's Montesinho Natural Park, the model used various meteorological factors from the Fire Weather Index (FWI), historical burned areas, and time and location data to predict future wildfire risk. Comparisons with SVM, XGBoost, neural networks, RNN, and basic LSTM showed that deep learning models significantly outperformed machine learning models, with LSTM surpassing RNN and the CNN-attention LSTM performing best overall.

[Rösch et al. \(2024\)](#) applied graph convolution combined with GRU to develop Spatiotemporal Graph Neural Networks (ST-GNNs) for predicting wildfire spread in Portugal and the Mediterranean region. These models used an H3 grid system built from weather data, land cover, fuel types, DEM, and fire weather indices. However, the models exhibited high false positive rates.

In another study, [Bhowmik et al. \(2023\)](#) proposed a U-shaped

LSTM network combining UNet and LSTM, using seven days of meteorological, environmental, vegetation, and geological data to predict wildfire risk. The U-shaped LSTM network first used a three-layer UNet encoder to extract semantic information, which was then flattened and input into an LSTM. The LSTM output was passed through a UNet decoder to produce end-to-end pixel-level predictions of wildfire heatmaps for the next 24 hours to two weeks. This model achieved over 97

Similarly, [Yoon and Voulgaris \(2022\)](#) conducted research on wildfire risk prediction in the western United States, using a convolutional encoder to reduce the dimensionality of input time series data into vectors, which were then fed into a GRU model. A dual deconvolution decoder was designed to restore image size, predicting wildfire risk at different time steps (one, two, three, and four weeks). Compared to logistic regression, generative networks, and GRU, the combination of CNN and GRU showed significant performance improvement.

Lastly, [Marjani et al. \(2023\)](#) developed a spatiotemporal prediction model combining CNNs and RNNs to predict wildfire spread at time step $t + 1$, using environmental variables and burned areas from time steps t and $t - 1$. Data were divided into three blocks: hourly block (6-hour averaged wind speed and direction), daily block (temperature, precipitation, and wildfire burning map), and constant variables (land cover type, population, terrain, etc.). Each block was processed by CNNs and flattened into 1D features, then fed into RNNs with 64 and 31 neurons, respectively. Constant variables were similarly processed and flattened. The RNN outputs were concatenated with the constant variables and passed through convolution, reshape, dropout, and sigmoid layers to produce a burning probability map. Comparative results showed the superiority of this spatiotemporal modeling approach over CNN and the deep convolutional inverse graphics network proposed by [Hodges and Latimer \(2019\)](#). Additionally, experiments assessing data availability, noise addition, and Monte Carlo dropout were conducted to evaluate model uncertainty.

7.4.2. Coupled Spatiotemporal Modeling Methods

Compared to the separated spatial and temporal modeling methods, event sequence prediction algorithms like ConvLSTM are also widely used. For instance, [Burge et al. \(2021\)](#) evaluated the feasibility of using ConvLSTM to simulate wildfire propagation dynamics on three simulated datasets with varying terrain, wind, humidity, and vegetation density distributions. The experiments demonstrated that ConvLSTM's predictive capability surpassed that of CNN. In the study by [Prapas et al. \(2021\)](#), which compared traditional machine learning models (RF), time series prediction algorithms (LSTM), image classification methods (CNN), and spatiotemporal modeling methods (ConvLSTM) for next-day wildfire danger prediction across Greece, several key findings emerged. For the RF model, training data was constructed by averaging each driving factor for the 10 days preceding the prediction date at each spatial location, resulting in a dataset with dimensions $f \times 1$, where f is the number of driving factors. The LSTM model used time series input, with data dimensions of $f \times t$, where t represents the time series length (10 days). For the image classification task, the

spatial data was constructed as spatial patches centered on the target point, with dimensions $f \times h \times w$, where h and w are the height and width of the image. Lastly, for the spatiotemporal prediction task using ConvLSTM, the dataset dimensions were $f \times h \times w \times t$. The results showed that LSTM and ConvLSTM performed better than RF and CNN. Evaluating the binary classification results, LSTM outperformed ConvLSTM overall, but when using the area under the ROC curve as the evaluation metric, ConvLSTM slightly surpassed LSTM, with AUC scores of 0.926 and 0.920, respectively.

Similarly, [Khalaf et al. \(2024\)](#) compared ConvLSTM with cellular automata and FlamMap in simulating wildfire spread in Iran's Golestan National Park. The results indicated that ConvLSTM had the highest accuracy in predicting burned areas, but for spread rate evaluation, the CA algorithm performed better than the other models. In another study, [Michail et al. \(2024\)](#) compared temporally-enabled GNN, GRU, and ConvLSTM using the SeasFire Datacube ([Alonso et al., 2023](#)), finding that GNN was better at capturing global information, thus improving the understanding of complex patterns. The study also emphasized the importance of long time series information and a large receptive field in global wildfire risk prediction, especially for seasonal forecasts. It showed that longer input sequences provided more reliable predictions, and integrating spatial information to capture the spatiotemporal dynamics of wildfires improved model performance. Therefore, to improve predictions over longer forecast horizons, it is essential to consider a larger spatial receptive field.

[Masrur and Yu \(2023\)](#); [Masrur et al. \(2024\)](#) further proposed two ConvLSTM models based on spatiotemporal attention to predict wildfire spread over the next 10 days using the previous 10 days' NDVI, wind components, and soil moisture. These models were designed to capture local-to-global and short-to-long-term spatiotemporal dependencies. The models were trained and tested on both simulated and real-world datasets. Pairwise self-attention was used to calculate attention scores for input variables, while patchwise self-attention replaced convolution operations in ConvLSTM. Comparisons on simulated datasets showed that the pairwise self-attention model performed better, while the standard ConvLSTM outperformed the patchwise self-attention model. Moreover, they employed integrated gradients ([Sundararajan et al., 2017](#)) to enhance the interpretability of the contributions of time steps and driving factors to the model's predictions. The spatial patterns from integrated gradients confirmed the importance of capturing both local and global spatial dependencies. However, in real-world scenarios, replacing ConvLSTM's convolution operations with patchwise self-attention significantly improved the standard ConvLSTM's prediction accuracy and model transferability, surpassing even the pairwise self-attention ConvLSTM in both aspects.

7.4.3. Spatially Enhanced Coupled Spatiotemporal Modeling Methods

In addition, there are studies that combine convolutional layers with ConvLSTM to further emphasize spatial feature extraction. Similar to the separated spatial and temporal sequence

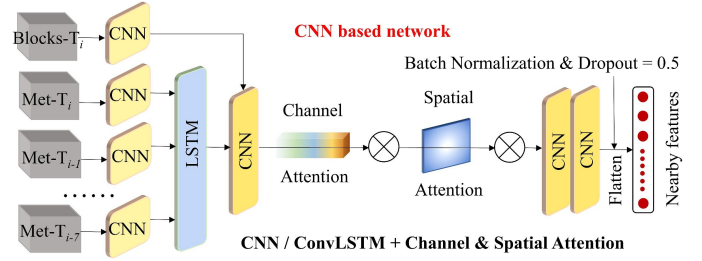


Figure 12: A typical spatial feature-enhanced coupled spatiotemporal wildfire risk prediction model proposed by [He et al. \(2024\)](#).

wildfire risk prediction models, the spatially enhanced coupled spatiotemporal wildfire risk prediction method, as shown in the Fig.12, first extracts spatial features using convolution operations and reduces dimensionality before feeding the data into a ConvLSTM. For the output of the ConvLSTM, either a CNN is further applied followed by sigmoid mapping, or the sigmoid mapping is directly applied to the output.

For example, [Deng et al. \(2023\)](#) used terrain, vegetation, climate, and human activity factors in Yunnan Province, China, to build a 3D CNN and ConvLSTM hybrid model for next-day wildfire prediction. During data preprocessing, Pearson correlation analysis was used to exclude the minimum and average temperatures from the dataset. Variance inflation factors and tolerance were then employed to assess multicollinearity among wildfire driving factors. Information gain ratio analysis revealed that precipitation and slope had the highest impact. In the proposed model, 3D CNN was primarily responsible for extracting spatial features and reducing the input patch's spatial dimensions, which were then fed into a many-to-many ConvLSTM for prediction. The results showed that the combined 3D CNN and ConvLSTM model outperformed both standalone ConvLSTM and 3D CNN models.

Similarly, [Burge et al. \(2023\)](#) built upon the model proposed by [Hodges and Lattimer \(2019\)](#) by introducing fuel embedding layers and inserting ConvLSTM between the encoder and decoder for end-to-end wildfire spread simulation. The experimental results demonstrated that incorporating LSTM improved prediction accuracy.

Furthermore, [Ji et al. \(2024\)](#), following a similar branch structure to [Eddin et al. \(2023\)](#) and [Jiang et al. \(2023\)](#), proposed a static location-aware model based on ConvLSTM. This model aimed to integrate global static features (sine and cosine values of longitude and latitude, along with climate variables) with dynamic variables (e.g., meteorological, human, and vegetation cover factors) to predict global wildfire probability on sub-seasonal to seasonal scales. In this model, global static features were first convolved and max-pooled, and the resulting feature maps were multiplied with climate variables for data fusion. SKNet was then employed to extract higher-order features, which were upsampled and merged with the static features generated by the encoder. Finally, upsampling and skip connections were used to restore the image size and supplement the spatial details of global static location variables. The dynamic and static variables were concatenated and input into

ConvLSTM. The hidden state output from the last time step of ConvLSTM was combined with the static and global features, and a 1×1 convolution was applied to produce the final wildfire probability prediction. Comparing accuracy, recall, F1 score, precision, and Kappa coefficient with different variants of vision Transformer and ConvLSTM demonstrated the effectiveness of incorporating global location information and climate variables for enhancing predictive capabilities.

Similarly, [He et al. \(2024\)](#) developed a next-day wildfire risk prediction model for eastern China by combining CNN, ConvLSTM, and vision Transformer models, also employing a branch structure. In this model, eight CNN modules were used to model eight meteorological variables, while another CNN module modeled terrain, vegetation, and anthropogenic factors from the last day. The sequence feature maps generated by the temporal meteorological variables were input into LSTM, and its output was merged with the other variables' CNN outputs. Channel attention, spatial attention, and CNN were used to extract higher-order features. To emphasize the high-resolution structural features of vegetation and scattered small settlements, Landsat data were used to generate 30-meter monthly high-resolution NDVI products, and vision Transformer was applied to extract these structural features. The flattened outputs from the vision Transformer and CNN were concatenated and classified using an artificial neural network (ANN) binary classifier. Ablation studies demonstrated the effectiveness of incorporating attention mechanisms, high-resolution spatial structure features, and vision Transformer. Sensitivity analysis also confirmed that meteorological factors were the most important among wildfire drivers.

Finally, [Chen et al. \(2024a\)](#) designed an end-to-end encoder-decoder network structure similar to that of [Bhowmik et al. \(2023\)](#) and [Yoon and Voulgaris \(2022\)](#), combining GCN and ConvLSTM. The GCN component was introduced to model the long-distance spatial dependencies required for global wildfire risk prediction, while mitigating the impact of missing data from ocean regions. Explicitly modeling information flow through the graph edges improved the interpretability of the prediction results. Specifically, the Earth's land surface pixels, as simulated by the JULES-INFERNO model, were treated as graph nodes, and the correlation coefficients between nodes were used to establish the graph's edges. Spatial dependencies were modeled using a spatial graph convolution model, followed by LSTM for long-term temporal dependencies. The model was trained and validated using 30 years of simulated data from 1961 to 1990 in the JULES-INFERNO dataset, and its performance was compared against LSTM, ConvLSTM, and convolutional autoencoder with LSTM. The proposed model demonstrated superior performance, with ConvLSTM being the best among the comparative models. Additionally, the study used the Louvain method to identify potential wildfire communities, and integrated gradient analysis revealed that short-term (one-month) wildfire risk is primarily driven by lightning, while long-term (11-month) risk is more influenced by temperature, followed by lightning. Node importance analysis also showed that even geographically distant locations could have strong interactions regarding wildfire risk. Similarly, [Zhao et al. \(2024\)](#)

aimed to improve model interpretability by combining causal GNN with LSTM, comparing its performance with LSTM and GRU in predicting future.

7.5. Promising New Methods

The aforementioned deep learning-based methods for spatial, temporal, and spatiotemporal modeling face challenges in capturing long-term and spatial dependencies. As a result, when these methods are applied to wildfire risk prediction on a regional scale, they often neglect the influence of climate factors outside the study area. Furthermore, global-scale wildfire risk prediction is limited by computational capacity, resulting in relatively low spatial resolution in the predictions. Additionally, whether modeling wildfire risk on a regional or global scale, the time series of driving factors considered is often short (a few days) or constructed using monthly or yearly averages for long-term sequences. This calls for more efficient models capable of handling longer temporal scales and higher spatial resolution.

One potential solution is Mamba ([Gu and Dao, 2024](#)), a parameter-efficient model designed to handle long sequence modeling ([Xu et al., 2024](#)) such as videos or remote sensing imagery over long temporal scales. Mamba's architecture reduces the number of parameters through optimized dimensionality reduction and hierarchical attention mechanisms, allowing it to focus on key spatial and temporal features. This makes Mamba particularly promising for constructing wildfire risk prediction models that require high-resolution spatial and temporal data over extended time periods. The architecture of Mamba is shown below.

Moreover, pre-trained models and foundation models offer new opportunities for building more generalizable and robust wildfire risk assessment models. In various fields, domain-specific pre-trained or foundation models have been developed. Examples include the Segment Anything series ([Kirillov et al., 2023; Ravi et al., 2024](#)) for image segmentation, and the DINO series ([Caron et al., 2021; Oquab et al., 2024](#)) for general vision tasks. In the remote sensing field, foundation models have been proposed for image generation, segmentation, classification, and retrieval tasks ([Li et al., 2024a; Zhang et al., 2024b; Hong et al., 2024; Li et al., 2024b; Kuckreja et al., 2024](#)). These models, compared to traditional deep learning-based segmentation, classification, and retrieval models, can handle multi-modal data and establish relationships between semantic reasoning and visual concept modeling ([Li et al., 2024a](#)).

Wildfire risk prediction studies frequently highlight the importance of weather and climate factors, and in this context, several foundational models, such as FourCastNet ([Kurth et al., 2023](#)), Pangu-Weather ([Bi et al., 2023](#)), and GraphCast ([Lam et al., 2023](#)), have been developed specifically for weather and climate forecasting.

These foundation models, initially designed for image processing or remote sensing applications, can be easily adapted for downstream tasks like wildfire risk prediction and detection. A key research question is how to integrate these weather and climate forecasting products to enhance short-term wildfire risk predictions and improve the feasibility of large-scale, long-term wildfire risk forecasting.

Moreover, multi-source remote sensing satellites, including the Landsat series, Sentinel series, MODIS Terra and Aqua, and various meteorological satellites, provide long time series, large spatial coverage, and multi-band Earth observation products. These products are foundational for building wildfire detection algorithms, historical wildfire datasets, and quantitative estimation methods for wildfire driving factors. They also provide a rich dataset for training deep learning models or wildfire risk prediction foundation models. Thus, leveraging these multi-source, multi-modal, long-term Earth observation data and foundation model methodologies could lead to the development of foundational models for wildfire risk prediction. Ultimately, this approach aims to achieve high temporal-spatial resolution, large-scale, and long-term wildfire risk forecasting.

8. Conclusion

In the pursuit of wildfire prediction, researchers have employed a variety of data sources, proposing diverse models and methodologies. However, a comprehensive and systematic review of these data and methods remains lacking, particularly in the case of deep learning techniques, which have seen rapid development and widespread application in wildfire risk prediction in recent years. This paper presents a thorough review of various wildfire driving factor data, feature collinearity, machine learning model interpretability, and wildfire risk prediction algorithms.

First, the development of wildfire prediction models requires multiple input data sources, as well as ground truth data for training and validation. These input data include fuel, weather, and climate conditions, topographical variables, hydrological features, and socio-economic factors. Researchers select different data sources and design appropriate data preprocessing workflows based on the characteristics of the study area and the availability of data. It has been found that most studies prioritize meteorological and climatic parameters, followed by fuel and terrain conditions, with socio-economic and hydrological factors being considered to a lesser extent. Additionally, to facilitate modeling for deep learning-based wildfire risk assessments, we introduced several publicly available wildfire burn prediction datasets, such as FireCube, Next Day Wildfire Spread, Wildfire DB, WildfireSpreadTS, CFSDS, and the SeasFire Datacube. Regarding feature collinearity and the interpretability of deep learning models, this review also highlighted the use of feature collinearity evaluation methods, including Variance Inflation Factor (VIF), tolerance, and Pearson correlation coefficients, as well as interpretability methods for deep learning, such as Permutation Feature Importance, Explainable Feature Engineering, and SHapley Additive exPlanations.

Another crucial aspect of wildfire prediction models is the choice of algorithms. The most commonly used models include traditional machine learning models, wildfire danger rating systems, and deep learning models. While traditional machine learning models have been extensively reviewed in the literature, deep learning models, despite their growing attention, have lacked a systematic overview. In this paper, deep learning

models have been categorized into three types: time series prediction, image segmentation and classification, and spatiotemporal prediction models. The review of these models revealed a growing trend towards the consideration of longer time series and the development of higher spatiotemporal resolution wildfire risk assessment models.

Looking ahead, we foresee the potential for more efficient architectures, such as Mamba, and more generalized pre-trained and foundational models to further enhance the performance and scalability of deep learning-based wildfire risk prediction systems.

References

Abatzoglou, J.T., Kolden, C.A., 2011. Relative importance of weather and climate on wildfire growth in interior alaska. *International Journal of Wildland Fire* 20, 479–486.

Abatzoglou, J.T., Kolden, C.A., 2013. Relationships between climate and macroscale area burned in the western united states. *International Journal of Wildland Fire* 22, 1003–1020.

Abatzoglou, J.T., Kolden, C.A., Balch, J.K., Bradley, B.A., 2016. Controls on interannual variability in lightning-caused fire activity in the western us. *Environmental Research Letters* 11, 045005.

Abdollahi, A., Pradhan, B., 2023. Explainable artificial intelligence (XAI) for interpreting the contributing factors feed into the wildfire susceptibility prediction model. *SCIENCE OF THE TOTAL ENVIRONMENT* 879, 163004. URL: <https://www.webofscience.com/api/gateway?GWVersion=2&SrcAuth=DynamicDOIArticle&SrcApp=WOS&KeyID=10.1016%2Fj.scitotenv.2023.163004&DestApp=DOI&SrcAppSID=USW2EC0D7EfQ4jdthTkoDVukmMmGx&SrcJTitle=SCIENCE+OF+THE+TOTAL+ENVIRONMENT&DestDOIRegistrantName=Elsevier>, doi:10.1016/j.scitotenv.2023.163004. num Pages: 14 Place: Amsterdam Publisher: Elsevier Web of Science ID: WOS:000973651700001.

Adhikari, B., Xu, C., Hodza, P., Minckley, T., 2021. Developing a geospatial data-driven solution for rapid natural wildfire risk assessment. *Applied Geography* 126, 102382. URL: <https://www.sciencedirect.com/science/article/pii/S0143622820314818>, doi:10.1016/j.apgeog.2020.102382.

Agee, J.K., Skinner, C.N., 2005. Basic principles of forest fuel reduction treatments. *Forest ecology and management* 211, 83–96.

Ager, A.A., Day, M.A., McHugh, C.W., Short, K., Gilbertson-Day, J., Finney, M.A., Calkin, D.E., 2014a. Wildfire exposure and fuel management on western US national forests. *Journal of Environmental Management* 145, 54–70. URL: <https://linkinghub.elsevier.com/retrieve/pii/S0301479714002916>, doi:10.1016/j.jenvman.2014.05.035.

Ager, A.A., Preisler, H.K., Arca, B., Spano, D., Salis, M., 2014b. Wildfire risk estimation in the mediterranean area. *Environmetrics* 25, 384–396.

Ager, A.A., Vaillant, N.M., Finney, M.A., 2010. A comparison of landscape fuel treatment strategies to mitigate wildland fire risk in the urban interface and preserve old forest structure. *Forest Ecology and Management* 259, 1556–1570. URL: <https://www.sciencedirect.com/science/article/pii/S0378112710000514>, doi:10.1016/j.foreco.2010.01.032.

Albini, F.A., 1976. Estimating wildfire behavior and effects. volume 30. Department of Agriculture, Forest Service, Intermountain Forest and Range

Aldersley, A., Murray, S.J., Cornell, S.E., 2011. Global and regional analysis of climate and human drivers of wildfire. *Science of The Total Environment* 409, 3472–3481. URL: <https://www.sciencedirect.com/science/article/pii/S0048969711005353>, doi:10.1016/j.scitotenv.2011.05.032.

Alexander, M., 1989. Fiji adopts canadian system of fire danger rating. *International Forest Fire News* 2, 3.

Ali, S., Abuhmed, T., El-Sappagh, S., Muhammad, K., Alonso-Moral, J.M., Confalonieri, R., Guidotti, R., Del Ser, J., Díaz-Rodríguez, N., Herrera, F., 2023. Explainable artificial intelligence (xai): What we know and what is left to attain trustworthy artificial intelligence. *Information fusion* 99, 101805.

Alonso, L., Gans, F., Karasante, I., Ahuja, A., Prapas, I., Kondylatos, S., Poulosis, I., Panagiotou, E., Mihail, D., Cremer, F., Weber, U., Carvalhais, N., 2023. SeasFire Cube: A Global Dataset for Seasonal Fire Modeling in the Earth System. URL: <https://doi.org/10.5281/zenodo.8055879>, doi:10.5281/zenodo.8055879.

Alonso-Rego, C., Arellano-Pérez, S., Cabo, C., Ordoñez, C., Álvarez-González, J.G., Díaz-Varela, R.A., Ruiz-González, A.D., 2020. Estimating fuel loads and structural characteristics of shrub communities by using terrestrial laser scanning. *Remote Sensing* 12, 3704.

Andela, N., Morton, D.C., Giglio, L., Pausas, J., Chen, Y., Hantson, S., Van Der Werf, G.R., Randerson, J.T., 2019. The global fire atlas of individual fire size, duration, speed and direction. *Earth System Science Data* 11, 529–552.

Andersen, H.E., McGaughey, R.J., Reutebuch, S.E., 2005. Estimating forest canopy fuel parameters using lidar data. *Remote sensing of Environment* 94, 441–449.

Anderson, W.R., Cruz, M.G., Fernandes, P.M., McCaw, L., Vega, J.A., Bradstock, R.A., Fogarty, L., Gould, J., McCarthy, G., Marsden-Smedley, J.B., et al., 2015. A generic, empirical-based model for predicting rate of fire spread in shrublands. *International Journal of Wildland Fire* 24, 443–460.

Aragoneses, E., Chuvieco, E., 2021. Generation and mapping of fuel types for fire risk assessment. *Fire* 4, 59.

Aragoneses, E., García, M., Ruiz-Benito, P., Chuvieco, E., 2024. Mapping forest canopy fuel parameters at european scale using spaceborne lidar and satellite data. *Remote Sensing of Environment* 303, 114005.

Arellano-Pérez, S., Castedo-Dorado, F., López-Sánchez, C.A., González-Ferreiro, E., Yang, Z., Díaz-Varela, R.A., Álvarez-González, J.G., Vega, J.A., Ruiz-González, A.D., 2018. Potential of sentinel-2a data to model surface and canopy fuel characteristics in relation to crown fire hazard. *Remote Sensing* 10, 1645.

Arroyo, L.A., Pascual, C., Manzanera, J.A., 2008. Fire models and methods to map fuel types: The role of remote sensing. *Forest ecology and management* 256, 1239–1252.

Artés, T., Oom, D., De Rigo, D., Durrant, T.H., Maiani, P., Libertà, G., San-Miguel-Ayanz, J., 2019. A global wildfire dataset for the analysis of fire regimes and fire behaviour. *Scientific data* 6, 296.

Asif, N.A., Sarker, Y., Chakrabortty, R.K., Ryan, M.J., Ahamed, M.H., Saha, D.K., Badal, F.R., Das, S.K., Ali, M.F., Moyeen, S.I., Islam, M.R., Tasneem, Z., 2021. Graph neural network: A comprehensive review on non-euclidean space. *IEEE Access* 9, 60588–60606. doi:10.1109/ACCESS.2021.3071274.

Badia-Perpinyà, A., Pallares-Barbera, M., 2006. Spatial distribution of ignitions in mediterranean periurban and rural areas: the case of catalonia. *International journal of Wildland fire* 15, 187–196.

Bakke, S.J., Wanders, N., Van Der Wiel, K., Tallaksen, L.M., 2023. A data-driven model for Fennoscandian wildfire danger. *Natural Hazards and Earth System Sciences* 23, 65–89. URL: <https://www.duo.uio.no/handle/10852/108719>, doi:10.5194/nhess-23-65-2023. accepted: 2024-02-27T18:29:41Z.

Balch, J.K., Bradley, B.A., Abatzoglou, J.T., Nagy, R.C., Fusco, E.J., Mahood, A.L., 2017. Human-started wildfires expand the fire niche across the united states. *Proceedings of the National Academy of Sciences* 114, 2946–2951.

Bar Massada, A., Syphard, A.D., Hawbaker, T.J., Stewart, S.I., Radeloff, V.C., 2011. Effects of ignition location models on the burn patterns of simulated wildfires. *Environmental Modelling & Software* 26, 583–592. URL: <https://www.sciencedirect.com/science/article/pii/S1364815210003233>, doi:10.1016/j.envsoft.2010.11.016.

Barber, Q.E., Jain, P., Whitman, E., Thompson, D.K., Guindon, L., Parks, S.A., Wang, X., Hethcoat, M.G., Parisien, M.A., 2024. The canadian fire spread dataset. *Scientific data* 11, 764.

Benali, A., Russo, A., Sá, A.C., Pinto, R.M., Price, O., Koutsias, N., Pereira, J.M., 2016. Determining fire dates and locating ignition points with satellite data. *Remote Sensing* 8, 326.

Bergado, J.R., Persello, C., Reinke, K., Stein, A., 2021. Predicting wildfire burns from big geodata using deep learning. *Safety Science* 140, 105276. URL: <https://www.sciencedirect.com/science/article/pii/S0925753521001211>, doi:10.1016/j.ssci.2021.105276.

Bergonse, R., Oliveira, S., Gonçalves, A., Nunes, S., DaCamara, C., Zêzere, J.L., 2021. Predicting burnt areas during the summer season in Portugal by combining wildfire susceptibility and spring meteorological conditions. *Geomatics, Natural Hazards and Risk* 12, 1039–1057.

URL: <https://doi.org/10.1080/19475705.2021.1909664>, doi:10.1080/19475705.2021.1909664. publisher: Taylor & Francis _eprint: <https://doi.org/10.1080/19475705.2021.1909664>.

Bessie, W., Johnson, E., 1995. The relative importance of fuels and weather on fire behavior in subalpine forests. *Ecology* 76, 747–762.

Bhowmik, R.T., Jung, Y.S., Aguilera, J.A., Prunicki, M., Nadeau, K., 2023. A multi-modal wildfire prediction and early-warning system based on a novel machine learning framework. *Journal of Environmental Management* 341, 117908. URL: <https://www.sciencedirect.com/science/article/pii/S0301479723006965>, doi:10.1016/j.jenvman.2023.117908.

Bi, K., Xie, L., Zhang, H., Chen, X., Gu, X., Tian, Q., 2023. Accurate medium-range global weather forecasting with 3d neural networks. *Nature* 619, 533–538.

Bianchi, L.O., Defossé, G.E., 2015. Live fuel moisture content and leaf ignition of forest species in Andean Patagonia, Argentina. *International Journal of Wildland Fire* 24, 340–348. URL: <https://www.publish.csiro.au/wf/WF13099>, doi:10.1071/WF13099. publisher: CSIRO PUBLISHING.

Bjånes, A., De La Fuente, R., Mena, P., 2021. A deep learning ensemble model for wildfire susceptibility mapping. *Ecological Informatics* 65, 101397.

Bommer, P.L., Kretschmer, M., Hedström, A., Bareeva, D., Höhne, M.M.C., 2024. Finding the right xai method—a guide for the evaluation and ranking of explainable ai methods in climate science. *Artificial Intelligence for the Earth Systems* 3, e230074.

Botequim, B., Garcia-Gonzalo, J., Marques, S., Ricardo, A., Borges, J.G., Tomé, M., Oliveira, M.M., 2013. Developing wildfire risk probability models for Eucalyptus globulus stands in Portugal. *iForest - Biogeosciences and Forestry* 6, 217. URL: <https://iforest.sisef.org/contents/?id=ifor0821-006>, doi:10.3832/ifor0821-006. publisher: SISEF - Italian Society of Silviculture and Forest Ecology Section: Forest Dynamics and Natural Disturbances.

Bowyer, P., Danson, F., 2004. Sensitivity of spectral reflectance to variation in live fuel moisture content at leaf and canopy level. *Remote Sensing of Environment* 92, 297–308.

Bradshaw, L.S., Deeming, J.E., Burgan, R.E., Cohen, J.D., 1984. The 1978 National Fire-Danger Rating System: technical documentation. Technical Report. U.S. Department of Agriculture, Forest Service, Intermountain Forest and Range Experiment Station. URL: <http://dx.doi.org/10.2737/INT-GTR-169>, doi:10.2737/int-gtr-169.

Braun, W.J., Jones, B.L., Lee, J.S., Woolford, D.G., Wotton, B.M., 2010. Forest fire risk assessment: an illustrative example from ontario, canada. *Journal of Probability and Statistics* 2010, 823018.

Bright, B.C., Hudak, A.T., Meddens, A.J., Hawbaker, T.J., Briggs, J.S., Kennedy, R.E., 2017. Prediction of forest canopy and surface fuels from lidar and satellite time series data in a bark beetle-affected forest. *Forests* 8, 322.

Brillinger, D.R., Preisler, H.K., Benoit, J.W., 2003. Risk assessment: a forest fire example. *Lecture Notes-Monograph Series* , 177–196.

Burgan, R.E., 1984. Behave: fire behavior prediction and fuel modeling system, fuel subsystem. volume 167. US Department of Agriculture, Forest Service, Intermountain Forest and Range

Burgan, R.E., 1988. 1988 revisions to the 1978 national fire-danger rating system. volume 273. US Department of Agriculture, Forest Service, Southeastern Forest Experiment

Burge, J., Bonanni, M., Ihme, M., Hu, L., 2021. Convolutional lstm neural networks for modeling wildland fire dynamics. URL: <https://arxiv.org/abs/2012.06679>, arXiv:2012.06679.

Burge, J., Bonanni, M.R., Hu, R.L., Ihme, M., 2023. Recurrent convolutional deep neural networks for modeling time-resolved wildfire spread behavior. *Fire Technology* 59, 3327–3354.

Burrows, N., Gill, M., Sharples, J., 2018. Development and validation of a model for predicting fire behaviour in spinifex grasslands of arid australia. *International Journal of Wildland Fire* 27, 271–279.

Caccamo, G., Chisholm, L., Bradstock, R., Puotinen, M.L., Pippen, B., 2011. Monitoring live fuel moisture content of heathland, shrubland and sclerophyll forest in south-eastern australia using modis data. *International Journal of Wildland Fire* 21, 257–269.

Cahuanzzi, R., Chen, X., Güttel, S., 2023. A comparison of lstm and gru networks for learning symbolic sequences, in: *Science and Information Conference*, Springer. pp. 771–785.

Calviño-Cancela, M., Chas-Amil, M.L., García-Martínez, E.D., Touza, J.,

2016. Wildfire risk associated with different vegetation types within and outside wildland-urban interfaces. *Forest Ecology and Management* 372, 1–9.

Calviño-Cancela, M., Chas-Amil, M.L., García-Martínez, E.D., Touza, J., 2017. Interacting effects of topography, vegetation, human activities and wildland-urban interfaces on wildfire ignition risk. *Forest Ecology and Management* 397, 10–17.

Canisius, F., Chen, J.M., 2007. Retrieving forest background reflectance in a boreal region from Multi-angle Imaging SpectroRadiometer (MISR) data. *Remote Sensing of Environment* 107, 312–321. URL: <https://www.sciencedirect.com/science/article/pii/S0034425706004184>, doi:10.1016/j.rse.2006.07.023.

Cao, Y., Zhou, X., Yu, Y., Rao, S., Wu, Y., Li, C., Zhu, Z., 2024. Forest fire prediction based on time series networks and remote sensing images. *Forests* 15, 1221.

Capps, S.B., Zhuang, W., Liu, R., Rolinski, T., Qu, X., 2021. Modelling chamise fuel moisture content across California: A machine learning approach. *International Journal of Wildland Fire* 31, 136–148.

Caron, M., Touvron, H., Misra, I., Jégou, H., Mairal, J., Bojanowski, P., Joulin, A., 2021. Emerging properties in self-supervised vision transformers, in: *Proceedings of the IEEE/CVF international conference on computer vision*, pp. 9650–9660.

Castro, F.X., Tudela, A., Sebastià, M.T., 2003. Modeling moisture content in shrubs to predict fire risk in Catalonia (Spain). *Agricultural and Forest Meteorology* 116, 49–59. URL: <https://www.sciencedirect.com/science/article/pii/S0168192302002484>, doi:10.1016/S0168-1923(02)00248-4.

Catchpole, E., Catchpole, W., Viney, N., McCaw, W., Marsden-Smedley, J., 2001. Estimating fuel response time and predicting fuel moisture content from field data. *International Journal of Wildland Fire* 10, 215–222.

Catry, F.X., Rego, F.C., Bação, F.L., Moreira, F., 2009. Modeling and mapping wildfire ignition risk in Portugal. *International Journal of Wildland Fire* 18, 921–931.

Cavalcante, R.B., Souza, B.M., Ramos, S.J., Gastauer, M., NASCIMENTO, W.R., Caldeira, C.F., Souza-Filho, P.W., 2021. Assessment of fire hazard weather indices in the eastern Amazon: a case study for different land uses. *Acta Amazonica* 51, 352–362.

Cawson, J.G., Nyman, P., Schunk, C., Sheridan, G.J., Duff, T.J., Gibos, K., Bovill, W.D., Conedera, M., Pezzatti, G.B., Menzel, A., 2020. Estimation of surface dead fine fuel moisture using automated fuel moisture sticks across a range of forests worldwide. *International Journal of Wildland Fire* 29, 548–559.

Chaparro, D., Jagdhuber, T., Piles, M., Jonard, F., Fluhrer, A., Vall-llossera, M., Camps, A., López-Martínez, C., Fernández-Morán, R., Baur, M., et al., 2024. Vegetation moisture estimation in the western United States using radiometer-radar-lidar synergy. *Remote Sensing of Environment* 303, 113993.

Chavalithumrong, A., Yoon, H.J., Voulgaris, P., 2021. Learning Wildfire Model from Incomplete State Observations. URL: <http://arxiv.org/abs/2111.14038>. arXiv:2111.14038 [cs].

Chen, D., Cheng, S., Hu, J., Kasoar, M., Arcucci, R., 2024a. Explainable global wildfire prediction models using graph neural networks. *arXiv preprint arXiv:2402.07152*.

Chen, J., Yang, Y., Peng, L., Chen, L., Ge, X., 2022. Knowledge graph representation learning-based forest fire prediction. *Remote Sensing* 14, 4391.

Chen, R., He, B., Li, Y., Fan, C., Yin, J., Zhang, H., Zhang, Y., 2024b. Estimation of potential wildfire behavior characteristics to assess wildfire danger in southwest China using deep learning schemes. *Journal of Environmental Management* 351, 120005. URL: <https://linkinghub.elsevier.com/retrieve/pii/S0301479723027937>, doi:10.1016/j.jenvman.2023.120005.

Chen, R., He, B., Li, Y., Fan, C., Yin, J., Zhang, H., Zhang, Y., 2024c. Estimation of potential wildfire behavior characteristics to assess wildfire danger in southwest China using deep learning schemes. *Journal of Environmental Management* 351, 120005.

Chen, R., He, B., Li, Y., Zhang, Y., Liao, Z., Fan, C., Yin, J., Zhang, H., 2024d. Incorporating fire spread simulation and machine learning algorithms to estimate crown fire potential for pine forests in Sichuan, China. *International Journal of Applied Earth Observation and Geoinformation* 132, 104080.

Chen, W., Panahi, M., Khosravi, K., Pourghasemi, H.R., Rezaie, F., Parvinnezhad, D., 2019. Spatial prediction of groundwater potentiality using ANFIS ensembled with teaching-learning-based and biogeography-based optimization. *Journal of Hydrology* 572, 435–448. URL: <https://www.sciencedirect.com/science/article/pii/S0022169419302604>, doi:10.1016/j.jhydrol.2019.03.013.

Chen, Y., Morton, D.C., Andela, N., Giglio, L., Randerson, J.T., 2016. How much global burned area can be forecast on seasonal time scales using sea surface temperatures? *Environmental Research Letters* 11, 045001. URL: <https://dx.doi.org/10.1088/1748-9326/11/4/045001>, doi:10.1088/1748-9326/11/4/045001. publisher: IOP Publishing.

Chen, Y., Zhu, X., Yebra, M., Harris, S., Tapper, N., 2017. Development of a predictive model for estimating forest surface fuel load in Australian eucalypt forests with LiDAR data. *Environmental Modelling & Software* 97, 61–71. URL: <https://www.sciencedirect.com/science/article/pii/S1364815216304418>, doi:10.1016/j.envsoft.2017.07.007.

Cheney, N.P., Gould, J.S., McCaw, W.L., Anderson, W.R., 2012. Predicting fire behaviour in dry eucalypt forest in southern Australia. *Forest Ecology and Management* 280, 120–131.

Chicas, S.D., Østergaard Nielsen, J., Valdez, M.C., Chen, C.F., 2022. Modelling wildfire susceptibility in Belize's ecosystems and protected areas using machine learning and knowledge-based methods. *Geocarto International* 37, 15823–15846.

Chino, D.Y., Avalhais, L.P., Rodrigues, J.F., Traina, A.J., 2015. Bowfire: detection of fire in still images by integrating pixel color and texture analysis, in: 2015 28th SIBGRAPI conference on graphics, patterns and images, IEEE, pp. 95–102.

Chung, J., Gulcehre, C., Cho, K., Bengio, Y., 2014. Empirical evaluation of gated recurrent neural networks on sequence modeling. *arXiv preprint arXiv:1412.3555*.

Chuvieco, E., Aguado, I., Jurdao, S., Pettinari, M.L., Yebra, M., Salas, J., Hantson, S., de la Riva, J., Ibarra, P., Rodrigues, M., et al., 2012. Integrating geospatial information into fire risk assessment. *International Journal of Wildland Fire* 23, 606–619.

Chuvieco, E., Aguado, I., Salas, J., García, M., Yebra, M., Oliva, P., 2020. Satellite remote sensing contributions to wildland fire science and management. *Current Forestry Reports* 6, 81–96.

Chuvieco, E., Cocco, D., Riano, D., Martín, P., Martínez-Vega, J., De La Riva, J., Pérez, F., 2004. Combining NDVI and surface temperature for the estimation of live fuel moisture content in forest fire danger rating. *Remote Sensing of Environment* 92, 322–331.

Chuvieco, E., Congalton, R.G., 1989. Application of remote sensing and geographic information systems to forest fire hazard mapping. *Remote Sensing of Environment* 29, 147–159.

Chuvieco, E., Deshayes, M., Stach, N., Cocco, D., Riaño, D., 1999. Short-term fire risk: foliage moisture content estimation from satellite data, in: Chuvieco, E. (Ed.), *Remote Sensing of Large Wildfires: in the European Mediterranean Basin*. Springer, Berlin, Heidelberg, pp. 17–38. URL: https://doi.org/10.1007/978-3-642-60164-4_3, doi:10.1007/978-3-642-60164-4_3.

Chuvieco, E., Riaño, D., Aguado, I., Cocco, D., 2002. Estimation of fuel moisture content from multitemporal analysis of Landsat thematic mapper reflectance data: applications in fire danger assessment. *International Journal of Remote Sensing* 23, 2145–2162.

Chuvieco, E., Riaño, D., Van Wagendok, J., Morsdof, F., 2003. Fuel loads and fuel type mapping, in: *Wildland fire danger estimation and mapping: The role of remote sensing data*. World Scientific, pp. 119–142.

Clark, K.L., Skowronski, N., Hom, J., Duvaneck, M., Pan, Y., Van Tuyl, S., Cole, J., Patterson, M., Maurer, S., 2009. Decision support tools to improve the effectiveness of hazardous fuel reduction treatments in the New Jersey pine barrens. *International Journal of Wildland Fire* 18, 268–277.

Cohen, J.D., 1985. The national fire-danger rating system: basic equations. volume 82. US Department of Agriculture, Forest Service, Pacific Southwest Forest and ...

Coskuner, K.A., 2022. Assessing the performance of MODIS and VIIRS active fire products in the monitoring of wildfires: a case study in Turkey. *iForest-Biogeosciences and Forestry* 15, 85.

Cruz, M., Gould, J., Alexander, M., Sullivan, A., McCaw, W., Matthews, S., Land, C., Flagship, W., of Alberta, U., of Parks, W.A.D., Wildlife, M., Fire, A., Limited, E.S.A.C., et al., 2015. A Guide to Rate of Fire Spread Models for Australian Vegetation. *Australasian Fire & Emergency Service Authorities*. URL: <https://books.google.ca/books?id=0LR6rgEACAAJ>.

Cruz, M.G., Alexander, M.E., Wakimoto, R.H., 2003. Assessing canopy fuel stratum characteristics in crown fire prone fuel types of western north america. *International Journal of Wildland Fire* 12, 39–50.

Cruz, M.G., Alexander, M.E., Wakimoto, R.H., 2004. Modeling the likelihood of crown fire occurrence in conifer forest stands. *Forest Science* 50, 640–658.

Cruz, M.G., Alexander, M.E., Wakimoto, R.H., 2005. Development and testing of models for predicting crown fire rate of spread in conifer forest stands. *Canadian Journal of Forest Research* 35, 1626–1639.

Cruz, M.G., McCaw, W.L., Anderson, W.R., Gould, J.S., 2013. Fire behaviour modelling in semi-arid mallee-heath shrublands of southern australia. *Environmental Modelling & Software* 40, 21–34.

Cunill Camprubi, A., González-Moreno, P., Resco de Dios, V., 2022. Live fuel moisture content mapping in the mediterranean basin using random forests and combining modis spectral and thermal data. *Remote Sensing* 14, 3162.

Dal Pozzolo, A., Caelen, O., Johnson, R.A., Bontempi, G., 2015. Calibrating probability with undersampling for unbalanced classification, in: 2015 IEEE symposium series on computational intelligence, IEEE. pp. 159–166.

Danson, F.M., Bowyer, P., 2004. Estimating live fuel moisture content from remotely sensed reflectance. *Remote Sensing of Environment* 92, 309–321.

De Roo, R.D., Du, Y., Ulaby, F.T., Dobson, M.C., 2001. A semi-empirical backscattering model at l-band and c-band for a soybean canopy with soil moisture inversion. *IEEE Transactions on Geoscience and Remote Sensing* 39, 864–872.

Deeming, J.E., 1972. National fire-danger rating system. volume 84. Rocky Mountain Forest and Range Experiment Station, Forest Service, US

Deeming, J.E., Burgan, R.E., Cohen, J.D., 1977. The national fire-danger rating system, 1978. volume 39. Department of Agriculture, Forest Service, Intermountain Forest and Range

Deng, J., Wang, W., Gu, G., Chen, Z., Liu, J., Xie, G., Weng, S., Ding, L., Li, C., 2023. Wildfire susceptibility prediction using a multisource and spatiotemporal cooperative approach. *Earth Science Informatics* 16, 3511–3529.

Depicker, A., De Baets, B., Baetens, J.M., 2020. Wildfire ignition probability in belgium. *Natural hazards and earth system sciences* 20, 363–376.

Dimitrakopoulos, A., Bemmerzouk, A., Mitsopoulos, I., 2011. Evaluation of the canadian fire weather index system in an eastern mediterranean environment. *Meteorological Applications* 18, 83–93.

Dong, Z., Zhao, F., Wang, G., Tian, Y., Li, H., 2024. A deep learning framework: Predicting fire radiative power from the combination of polar-orbiting and geostationary satellite data during wildfire spread. *IEEE Journal of Selected Topics in Applied Earth Observations and Remote Sensing* .

Donovan, V.M., Wonkka, C.L., Wedin, D.A., Twidwell, D., 2020. Land-use type as a driver of large wildfire occurrence in the us great plains. *Remote Sensing* 12, 1869.

Dorigo, W., Wagner, W., Albergel, C., Albrecht, F., Balsamo, G., Brocca, L., Chung, D., Ertl, M., Forkel, M., Gruber, A., et al., 2017. Esa cci soil moisture for improved earth system understanding: State-of the art and future directions. *Remote Sensing of Environment* 203, 185–215.

Duff, T.J., Bell, T.L., York, A., 2012. Predicting continuous variation in forest fuel load using biophysical models: a case study in south-eastern Australia. *International Journal of Wildland Fire* 22, 318–332. URL: <https://www.publish.csiro.au/wf/WF11087>, doi:10.1071/WF11087. publisher: CSIRO PUBLISHING.

Duff, T.J., Keane, R.E., Penman, T.D., Tolhurst, K.G., 2017. Revisiting wildland fire fuel quantification methods: the challenge of understanding a dynamic, biotic entity. *Forests* 8, 351.

Dzulhijjah, D.A., Majid, M.N., Alwanda, A.Y., Kusuma, D.C., Zakaria, F., Kusrini, K., Kusnawi, K., 2023. Comparative analysis of hybrid long short-term memory models for fire danger index forecasting with weather data, in: 2023 6th International Conference on Information and Communications Technology (ICOIACT), pp. 165–170. doi:10.1109/ICOIACT59844.2023.10455879.

D'Este, M., Elia, M., Giannico, V., Spano, G., Laforteza, R., Sanesi, G., 2021. Machine learning techniques for fine dead fuel load estimation using multi-source remote sensing data. *Remote Sensing* 13, 1658.

Eames, T., Russell-Smith, J., Yates, C., Edwards, A., Vernooy, R., Ribeiro, N., Steinbruch, F., van der Werf, G.R., 2021. Instantaneous pre-fire biomass and fuel load measurements from multi-spectral uas mapping in southern african savannas. *Fire* 4, 2.

Eddin, M.H.S., Roscher, R., Gall, J., 2023. Location-aware adaptive normalization: a deep learning approach for wildfire danger forecasting. *IEEE Transactions on Geoscience and Remote Sensing* 61, 1–18.

El-Madafri, I., Peña, M., Olmedo-Torre, N., 2023. The wildfire dataset: Enhancing deep learning-based forest fire detection with a diverse evolving open-source dataset focused on data representativeness and a novel multi-task learning approach. *Forests* 14, 1697.

Elia, M., Giannico, V., Spano, G., Laforteza, R., Sanesi, G., 2020. Likelihood and frequency of recurrent fire ignitions in highly urbanised mediterranean landscapes. *International journal of wildland fire* 29, 120–131.

Elkan, C., 2001. The foundations of cost-sensitive learning, in: International joint conference on artificial intelligence, Lawrence Erlbaum Associates Ltd. pp. 973–978.

Erhan, D., Bengio, Y., Courville, A., Vincent, P., 2009. Visualizing higher-layer features of a deep network. Ph.D. thesis, University of Montreal.

Fan, C., He, B., 2021. A physics-guided deep learning model for 10-h dead fuel moisture content estimation. *Forests* 12, 933.

Fan, C., He, B., Yin, J., Chen, R., Zhang, H., 2024. Process-based and geostationary meteorological satellite-enhanced dead fuel moisture content estimation. *GIScience & Remote Sensing* 61, 2324556.

Fan, L., Wigneron, J.P., Xiao, Q., Al-Yaari, A., Wen, J., Martin-StPaul, N., Dupuy, J.L., Pimont, F., Al Bitar, A., Fernandez-Moran, R., et al., 2018. Evaluation of microwave remote sensing for monitoring live fuel moisture content in the mediterranean region. *Remote Sensing of Environment* 205, 210–223.

FAO, 2006. Fire management-Global assessment 2006. Technical Report. Food and Agriculture Organization of the United Nations.

Fensholt, R., Sandholt, I., 2003. Derivation of a shortwave infrared water stress index from MODIS near- and shortwave infrared data in a semiarid environment. *Remote Sensing of Environment* 87, 111–121. URL: <https://www.sciencedirect.com/science/article/pii/S0034425703001895>, doi:10.1016/j.rse.2003.07.002.

Ferguson, S.A., Rutherford, J.E., McKay, S.J., Wright, D., Wright, C., Ottmar, R., 2002. Measuring moisture dynamics to predict fire severity in longleaf pine forests. *International Journal of Wildland Fire* 11, 267–279.

Fernandes, P.M., Botelho, H., Rego, F., Loureiro, C., 2008. Using fuel and weather variables to predict the sustainability of surface fire spread in maritime pine stands. *Canadian Journal of Forest Research* 38, 190–201.

Fernandes, P.M., Botelho, H.S., 2003. A review of prescribed burning effectiveness in fire hazard reduction. *International Journal of wildland fire* 12, 117–128.

Finney, M.A., 1998. FARSITE, Fire Area Simulator—model development and evaluation. 4, US Department of Agriculture, Forest Service, Rocky Mountain Research Station.

Finney, M.A., 2002. Fire growth using minimum travel time methods. *Canadian Journal of Forest Research* 32, 1420–1424.

Fogarty, L., Pearce, H., Catchpole, W., Alexander, M., 1998. Adoption vs. adaptation: lessons from applying the canadian forest fire danger rating system in new zealand, in: Proceedings, 3rd International Conference on Forest Fire Research and 14th Fire and Forest Meteorology Conference, Luso, Coimbra, Portugal, pp. 1011–1028.

Fogarty, L., Sullivan, A., Heemstra, S., Chladil, M., 2010. Review of grassland fire danger indices for scaled bushfire advice warning. Technical Report. Science sub group.

Forkel, M., Schmidt, L., Zotta, R.M., Dorigo, W., Yebra, M., 2023. Estimating leaf moisture content at global scale from passive microwave satellite observations of vegetation optical depth. *Hydrology and Earth System Sciences* 27, 39–68. URL: <https://hess.copernicus.org/articles/27/39/2023/>, doi:10.5194/hess-27-39-2023. publisher: Copernicus GmbH.

Frandsen, W.H., Andrews, P.L., Forest, I., Range Experiment Station (Ogden, U., 1979. Fire behavior in nonuniform fuels. volume no.232. Ogden, Utah, Intermountain Forest and Range Experiment Station, Forest Service, U.S. Dept. of Agriculture, 1979. URL: <https://www.biodiversitylibrary.org/item/136922>. https://www.biodiversitylibrary.org/bibliography/68702.

Fuller, M., 1991. Forest fires: an introduction to wildland fire behavior, management, firefighting, and prevention. John Wiley & Sons, Inc.

Fusco, E.J., Finn, J.T., Abatzoglou, J.T., Balch, J.K., Dadashi, S., Bradley, B.A., 2019. Detection rates and biases of fire observations from modis and agency reports in the conterminous united states. *Remote Sensing of Environment* 220, 30–40.

Gao, S., Huang, Y., Zhang, S., Han, J., Wang, G., Zhang, M., Lin, Q., 2020.

Short-term runoff prediction with gru and lstm networks without requiring time step optimization during sample generation. *Journal of Hydrology* 589, 125188.

Gao, Y., Wang, R., Zhou, E., 2021. Stock prediction based on optimized lstm and gru models. *Scientific Programming* 2021, 4055281.

García, M., Popescu, S., Riaño, D., Zhao, K., Neuenschwander, A., Agca, M., Chuvieco, E., 2012. Characterization of canopy fuels using icesat/glas data. *Remote Sensing of Environment* 123, 81–89.

García, M., Riaño, D., Yebra, M., Salas, J., Cardil, A., Monedero, S., Ramirez, J., Martín, M.P., Vilar, L., Gajardo, J., et al., 2020. A live fuel moisture content product from landsat tm satellite time series for implementation in fire behavior models. *Remote Sensing* 12, 1714.

García-Llamas, P., Suárez-Seoane, S., Taboada, A., Fernández-García, V., Fernández-Guisuraga, J.M., Fernández-Manso, A., Quintano, C., Marcos, E., Calvo, L., 2019. Assessment of the influence of biophysical properties related to fuel conditions on fire severity using remote sensing techniques: a case study on a large fire in NW Spain. *International Journal of Wildland Fire* 28, 512–520. URL: <https://www.publish.csiro.au/wf/WF18156>, doi:10.1071/WF18156. publisher: CSIRO PUBLISHING.

Ge, X., Yang, Y., Peng, L., Chen, L., Li, W., Zhang, W., Chen, J., 2022. Spatio-temporal knowledge graph based forest fire prediction with multi source heterogeneous data. *Remote Sensing* 14, 3496.

Gentilucci, M., Barbieri, M., Younes, H., Rihab, H., Pambianchi, G., 2024. Analysis of Wildfire Susceptibility by Weight of Evidence. Using Geomorphological and Environmental Factors in the Marche Region, Central Italy. *Geosciences* 14, 112. URL: <https://www.mdpi.com/2076-3263/14/5/112>, doi:10.3390/geosciences14050112. number: 5 Publisher: Multidisciplinary Digital Publishing Institute.

Gerard, S., Zhao, Y., Sullivan, J., 2023. Wildfirespreads: A dataset of multi-modal time series for wildfire spread prediction. *Advances in Neural Information Processing Systems* 36, 74515–74529.

Gers, F.A., Schmidhuber, J., Cummins, F., 2000. Learning to forget: Continual prediction with lstm. *Neural computation* 12, 2451–2471.

Ghorbanzadeh, O., Blaschke, T., Gholamnia, K., Aryal, J., 2019. Forest Fire Susceptibility and Risk Mapping Using Social/Infrastructural Vulnerability and Environmental Variables. *Fire* 2, 50. URL: <https://www.mdpi.com/2571-6255/2/3/50>, doi:10.3390/fire2030050. number: 3 Publisher: Multidisciplinary Digital Publishing Institute.

Giannakopoulos, C., LeSager, P., Moriondo, M., Bindi, M., Karali, A., Hatzaki, M., Kostopoulou, E., 2012. Comparison of fire danger indices in the mediterranean for present day conditions. *Iforest-Biogeosciences and Forestry* 5, 197.

Giglio, L., Descloitres, J., Justice, C.O., Kaufman, Y.J., 2003. An enhanced contextual fire detection algorithm for modis. *Remote Sensing of Environment* 87, 273–282. URL: <https://www.sciencedirect.com/science/article/pii/S0034425703001846>, doi:[https://doi.org/10.1016/S0034-4257\(03\)00184-6](https://doi.org/10.1016/S0034-4257(03)00184-6).

Giglio, L., Schroeder, W., Justice, C.O., 2016. The collection 6 modis active fire detection algorithm and fire products. *Remote Sensing of Environment* 178, 31–41. URL: <https://www.sciencedirect.com/science/article/pii/S0034425716300827>, doi:<https://doi.org/10.1016/j.rse.2016.02.054>.

Gilreath, J., 2006. Validation of Variables for the Creation of a Descriptive Fire Potential Model for the Southeastern Fire District of Mississippi. Theses and Dissertations URL: <https://scholarsjunction.msstate.edu/td/4942>.

Gincheva, A., Pausas, J.G., Edwards, A., Provenzale, A., Cerdà, A., Hanes, C., Royé, D., Chuvieco, E., Mouillet, F., Vissio, G., et al., 2024. A monthly gridded burned area database of national wildland fire data. *Scientific data* 11, 352.

Good, P.I., Hardin, J.W., 2012. Common errors in statistics (and how to avoid them). John Wiley & Sons.

Gopu, A., Ramakrishnan, A., Balasubramanian, G., Srinidhi, K., 2023. A comparative study on forest fire prediction using arima, sarima, lstm, and gru methods, in: 2023 IEEE International Conference on Contemporary Computing and Communications (InC4), IEEE. pp. 1–5.

Gould, J.S., McCaw, W.L., Cheney, N.P., 2011. Quantifying fine fuel dynamics and structure in dry eucalypt forest (*eucalyptus marginata*) in western australia for fire management. *Forest ecology and management* 262, 531–546.

Greenwell, B.M., et al., 2017. pdp: An r package for constructing partial dependence plots. *R J* 9, 421.

Gregor, M., David, S., 2017. Fire Risk Assessment: A measure to quantify fire risk for New Zealand locations. Technical Report. Ministry for the Environment, National Institute of water & Atmospheric Research Ltd.

de Groot, W.J., Hanes, C.C., Wang, Y., 2022. Crown fuel consumption in canadian boreal forest fires. *International Journal of Wildland Fire* 31, 255–276.

Groot, W.J.d., Field, R.D., Brady, M.A., Roswintarti, O., Mohamad, M., 2007. Development of the indonesian and malaysian fire danger rating systems. *Mitigation and Adaptation Strategies for Global Change* 12, 165–180.

Group, C.F.C.F.D., Science, C.F.C., Directorate, S.D., 1992. Development and structure of the Canadian forest fire behavior prediction system. volume 3. Forestry Canada, Science and Sustainable Development Directorate.

Gu, A., Dao, T., 2024. Mamba: Linear-time sequence modeling with selective state spaces. URL: <https://arxiv.org/abs/2312.00752>, arXiv:2312.00752.

Guerra-Hernández, J., Pereira, J.M., Stovall, A., Pascual, A., 2024. Impact of fire severity on forest structure and biomass stocks using nasa gedi data. insights from the 2020 and 2021 wildfire season in spain and portugal. *Science of Remote Sensing* 9, 100134.

Hall, J.V., Argueta, F., Zubkova, M., Chen, Y., Randerson, J.T., Giglio, L., 2024. Glocab: global cropland burned area from mid-2002 to 2020. *Earth System Science Data* 16, 867–885.

Hall, S.A., Burke, I.C., 2006. Considerations for characterizing fuels as inputs for fire behavior models. *Forest Ecology and Management* 227, 102–114.

Hantson, S., Padilla, M., Corti, D., Chuvieco, E., 2013. Strengths and weaknesses of MODIS hotspots to characterize global fire occurrence. *Remote Sensing of Environment* 131, 152–159. URL: <https://www.sciencedirect.com/science/article/pii/S0034425712004610>, doi:10.1016/j.rse.2012.12.004.

Hao, X., Qu, J.J., 2007. Retrieval of real-time live fuel moisture content using modis measurements. *Remote Sensing of Environment* 108, 130–137.

Hardy, C.C., 2005. Wildland fire hazard and risk: Problems, definitions, and context. *Forest ecology and management* 211, 73–82.

Hardy, C.C., Hardy, C.E., 2007. Fire danger rating in the united states of america: an evolution since 1916. *International journal of wildland fire* 16, 217–231.

Hargrove, W.W., Kumar, J., Norman, S.P., Hoffman, F.M., 2022. Statistically determined global fire regimes (gfrs) empirically characterized using historical modis hotspots. URL: <https://doi.org/10.5281/zenodo.6522071>, doi:10.5281/zenodo.6522071.

Harris, L.B., Taylor, A.H., Kassa, H., Leta, S., Powell, B., 2023. Humans and climate modulate fire activity across ethiopia. *Fire Ecology* 19, 15.

Harrison, S.P., Prentice, I.C., Bloomfield, K.J., Dong, N., Forkel, M., Forrest, M., Ningthoujam, R.K., Pellegrini, A., Shen, Y., Baudena, M., et al., 2021. Understanding and modelling wildfire regimes: an ecological perspective. *Environmental Research Letters* 16, 125008.

He, Z., Fan, G., Li, Z., Li, S., Gao, L., Li, X., Zeng, Z.C., 2024. Deep learning modeling of human activity affected wildfire risk by incorporating structural features: A case study in eastern china. *Ecological Indicators* 160, 111946.

Helman, D., Lensky, I.M., Tessler, N., Osem, Y., 2015. A Phenology-Based Method for Monitoring Woody and Herbaceous Vegetation in Mediterranean Forests from NDVI Time Series. *Remote Sensing* 7, 12314–12335. URL: <https://www.mdpi.com/2072-4292/7/9/12314>, doi:10.3390/rs70912314. number: 9 Publisher: Multidisciplinary Digital Publishing Institute.

Hochreiter, S., 1997. Long short-term memory. *Neural Computation* MIT-Press .

Hodges, J.L., Lattimer, B.Y., 2019. Wildland fire spread modeling using convolutional neural networks. *Fire technology* 55, 2115–2142.

Holdrege, M.C., Schlaepfer, D.R., Palmquist, K.A., Crist, M., Doherty, K.E., Lauenroth, W.K., Remington, T.E., Riley, K., Short, K.C., Tull, J.C., Wiechman, L.A., Bradford, J.B., 2024. Wildfire probability estimated from recent climate and fine fuels across the big sagebrush region. *Fire Ecology* 20, 22. URL: <https://doi.org/10.1186/s42408-024-00252-4>, doi:10.1186/s42408-024-00252-4.

Hollis, J.J., Matthews, S., Fox-Hughes, P., Grootemaat, S., Heemstra, S., Kenny, B.J., Sauvage, S., 2024. Introduction to the australian fire danger rating system. *International Journal of Wildland Fire* 33.

Hong, D., Zhang, B., Li, X., Li, Y., Li, C., Yao, J., Yokoya, N., Li, H., Ghamisi, P., Jia, X., Plaza, A., Gamba, P., Benediktsson, J.A., Chanussot, J., 2024. Spectralgpt: Spectral remote sensing foundation model. IEEE

Transactions on Pattern Analysis and Machine Intelligence 46, 5227–5244. doi:[10.1109/TPAMI.2024.3362475](https://doi.org/10.1109/TPAMI.2024.3362475).

Hong, H., Jaaafari, A., Zenner, E.K., 2019. Predicting spatial patterns of wildfire susceptibility in the Huichang County, China: An integrated model to analysis of landscape indicators. Ecological Indicators 101, 878–891. URL: <https://www.sciencedirect.com/science/article/pii/S1470160X19300792>, doi:[10.1016/j.ecolind.2019.01.056](https://doi.org/10.1016/j.ecolind.2019.01.056).

Hu, P., Tanchak, R., Wang, Q., 2023. Developing Risk Assessment Framework for Wildfire in the United States – A Deep Learning Approach to Safety and Sustainability. Journal of Safety and Sustainability URL: <https://www.sciencedirect.com/science/article/pii/S2949926723000033>, doi:[10.1016/j.jsasus.2023.09.002](https://doi.org/10.1016/j.jsasus.2023.09.002).

Hu, W.S., Li, H.C., Pan, L., Li, W., Tao, R., Du, Q., 2020. Spatial-spectral feature extraction via deep convlstm neural networks for hyperspectral image classification. IEEE Transactions on Geoscience and Remote Sensing 58, 4237–4250. doi:[10.1109/TGRS.2019.2961947](https://doi.org/10.1109/TGRS.2019.2961947).

Hua, L., Shao, G., 2017. The progress of operational forest fire monitoring with infrared remote sensing. Journal of Forestry Research 28, 215–229. URL: <https://doi.org/10.1007/s11676-016-0361-8>, doi:[10.1007/s11676-016-0361-8](https://doi.org/10.1007/s11676-016-0361-8).

Hunt Jr, E.R., Rock, B.N., Nobel, P.S., 1987. Measurement of leaf relative water content by infrared reflectance. Remote sensing of environment 22, 429–435.

Huot, F., Hu, R.L., Goyal, N., Sankar, T., Ihme, M., Chen, Y.F., 2022. Next day wildfire spread: A machine learning dataset to predict wildfire spreading from remote-sensing data. IEEE Transactions on Geoscience and Remote Sensing 60, 1–13.

Huot, F., Hu, R.L., Ihme, M., Wang, Q., Burge, J., Lu, T., Hickey, J., Chen, Y.F., Anderson, J., 2021. Deep Learning Models for Predicting Wildfires from Historical Remote-Sensing Data. URL: <http://arxiv.org/abs/2010.07445>. arXiv:2010.07445 [cs].

Iban, M.C., Aksu, O., 2024. Shap-driven explainable artificial intelligence framework for wildfire susceptibility mapping using modis active fire pixels: An in-depth interpretation of contributing factors in izmir, türkiye. Remote Sensing 16, 2842.

Iban, M.C., Sekertekin, A., 2022. Machine learning based wildfire susceptibility mapping using remotely sensed fire data and gis: A case study of adana and mersin provinces, turkey. Ecological Informatics 69, 101647.

Jaaafari, A., Gholami, D.M., Zenner, E.K., 2017. A Bayesian modeling of wildfire probability in the Zagros Mountains, Iran. Ecological Informatics 39, 32–44. URL: <https://linkinghub.elsevier.com/retrieve/pii/S1574954117300912>, doi:[10.1016/j.ecoinf.2017.03.003](https://doi.org/10.1016/j.ecoinf.2017.03.003).

Jaaafari, A., Mafi-Gholami, D., Thai Pham, B., Tien Bui, D., 2019. Wildfire Probability Mapping: Bivariate vs. Multivariate Statistics. Remote Sensing 11, 618. URL: <https://www.mdpi.com/2072-4292/11/6/618>, doi:[10.3390/rs11060618](https://doi.org/10.3390/rs11060618). number: 6 Publisher: Multidisciplinary Digital Publishing Institute.

Jain, P., Barber, Q.E., Taylor, S.W., Whitman, E., Castellanos Acuna, D., Boulanger, Y., Chavardès, R.D., Chen, J., Englefield, P., Flannigan, M., et al., 2024. Drivers and impacts of the record-breaking 2023 wildfire season in canada. Nature Communications 15, 6764.

Jain, P., Coogan, S.C., Subramanian, S.G., Crowley, M., Taylor, S., Flannigan, M.D., 2020. A review of machine learning applications in wildfire science and management. Environmental Reviews 28, 478–505. URL: <https://cdnsciencepub.com/doi/10.1139/er-2020-0019>, doi:[10.1139/er-2020-0019](https://doi.org/10.1139/er-2020-0019). publisher: NRC Research Press.

Jalilian, S., Jouibary, S.S., 2023. Forest wildfire risk mapping, performance comparison of machine learning algorithms. Research Square .

Jenks, G.F., Caspall, F.C., 1971. Error on choroplethic maps: definition, measurement, reduction. Annals of the Association of American Geographers 61, 217–244.

Ji, Y., Wang, D., Li, Q., Liu, T., Bai, Y., 2024. Global wildfire danger predictions based on deep learning taking into account static and dynamic variables. Forests 15, 216.

Jia, S., Kim, S.H., Nghiem, S.V., Kafatos, M., 2019. Estimating live fuel moisture using smap l-band radiometer soil moisture for southern california, usa. Remote Sensing 11, 1575.

Jiang, S., Sweet, L.b., Blougouras, G., Brenning, A., Li, W., Reichstein, M., Denzler, J., Shangguan, W., Yu, G., Huang, F., et al., 2024a. How interpretable machine learning can benefit process understanding in the geosciences. Earth's Future 12, e2024EF004540.

Jiang, W., Qiao, Y., Su, G., Li, X., Meng, Q., Wu, H., Quan, W., Wang, J., Wang, F., 2023. Wfnet: A hierarchical convolutional neural network for wildfire spread prediction. Environmental Modelling & Software 170, 105841.

Jiang, W., Qiao, Y., Zheng, X., Zhou, J., Jiang, J., Meng, Q., Su, G., Zhong, S., Wang, F., 2024b. Wildfire risk assessment using deep learning in Guangdong Province, China. International Journal of Applied Earth Observation and Geoinformation 128, 103750. URL: <https://www.sciencedirect.com/science/article/pii/S1569843224001043>, doi:[10.1016/j.jag.2024.103750](https://doi.org/10.1016/j.jag.2024.103750).

Jiang, W., Wang, F., Su, G., Li, X., Wang, G., Zheng, X., Wang, T., Meng, Q., 2022. Modeling wildfire spread with an irregular graph network. Fire 5, 185.

Jin, G., Wang, Q., Zhu, C., Feng, Y., Huang, J., Hu, X., 2020a. Urban fire situation forecasting: Deep sequence learning with spatio-temporal dynamics. Applied Soft Computing 97, 106730.

Jin, G., Zhu, C., Chen, X., Sha, H., Hu, X., Huang, J., 2020b. Ufsp-net: a neural network with spatio-temporal information fusion for urban fire situation prediction, in: IOP Conference Series: Materials Science and Engineering, IOP Publishing, p. 012050.

Jolly, W.M., Cochrane, M.A., Freeborn, P.H., Holden, Z.A., Brown, T.J., Williamson, G.J., Bowman, D.M., 2015. Climate-induced variations in global wildfire danger from 1979 to 2013. Nature communications 6, 7537.

Jolly, W.M., Freeborn, P.H., Bradshaw, L.S., Wallace, J., Brittain, S., 2024. Modernizing the us national fire danger rating system (version 4): Simplified fuel models and improved live and dead fuel moisture calculations. Environmental Modelling & Software , 106181.

Jolly, W.M., Johnson, D.M., 2018. Pyro-ecophysiology: shifting the paradigm of live wildland fuel research. Fire 1, 8.

Jones, M.W., Kelley, D.I., Burton, C.A., Di Giuseppe, F., Barbosa, M.L.F., Brambleby, E., Hartley, A.J., Lombardi, A., Mataveli, G., McNorton, J.R., et al., 2024. State of wildfires 2023–2024. Earth System Science Data 16, 3601–3685.

Josephson, J.R., Josephson, S.G., 1996. Abductive inference: Computation, philosophy, technology. Cambridge University Press.

Kadir, E.A., Kung, H.T., AlMansour, A.A., Irie, H., Rosa, S.L., Fauzi, S.S.M., 2023. Wildfire hotspots forecasting and mapping for environmental monitoring based on the long short-term memory networks deep learning algorithm. Environments 10, 124.

Kanwal, R., Rafaqat, W., Iqbal, M., Weiguo, S., 2023. Data-Driven Approaches for Wildfire Mapping and Prediction Assessment Using a Convolutional Neural Network (CNN). Remote Sensing 15, NA–NA. URL: <https://go.gale.com/ps/i.do?p=AONE&sw=w&issn=20724292&v=2.1&it=r&id=GALE%7CA772535779&sid=googleScholar&linkaccess=abs>, doi:[10.3390/rs15215099](https://doi.org/10.3390/rs15215099). publisher: MDPI AG.

Keane, R.E., Burgan, R., Wagendron, J.v., 2001. Mapping wildland fuels for fire management across multiple scales: Integrating remote sensing, GIS, and biophysical modeling. International Journal of Wildland Fire 10, 301–319. URL: <https://www.publish.csiro.au/wf/wf01028>, doi:[10.1071/wf01028](https://doi.org/10.1071/wf01028). publisher: CSIRO PUBLISHING.

Khalaf, M.W.A., Jouibary, S.S., Jahdi, R., 2024. Performance analysis of convlstm, flammmap, and ca algorithms to predict wildfire spread in golestan national park, ne iran. Environmental Modeling & Assessment , 1–14.

Kilgore, B.M., Sando, R.W., 1975. Crown-fire potential in a sequoia forest after prescribed burning. Forest Science 21, 83–87.

Kim, D.W., Chung, W., Lee, B., 2016. Exploring tree crown spacing and slope interaction effects on fire behavior with a physics-based fire model. Forest Science and Technology 12, 167–175.

Kim, Y., Jackson, T., Bindlish, R., Lee, H., Hong, S., 2012. Radar vegetation index for estimating the vegetation water content of rice and soybean. IEEE Geoscience and Remote Sensing Letters 9, 564–568. doi:[10.1109/LGRS.2011.2174772](https://doi.org/10.1109/LGRS.2011.2174772).

Kirillov, A., Mintun, E., Ravi, N., Mao, H., Rolland, C., Gustafson, L., Xiao, T., Whitehead, S., Berg, A.C., Lo, W.Y., Dollár, P., Girshick, R., 2023. Segment anything. URL: <https://arxiv.org/abs/2304.02643>, arXiv:2304.02643.

Knippling, E.B., 1970. Physical and physiological basis for the reflectance of visible and near-infrared radiation from vegetation. Remote sensing of environment 1, 155–159.

Kondylatos, S., Prapas, I., Camps-Valls, G., Papoutsis, I., 2023. Mesogeos: A multi-purpose dataset for data-driven wildfire modeling in the mediterranean.

ranean, in: Thirty-seventh Conference on Neural Information Processing Systems Datasets and Benchmarks Track. URL: <https://openreview.net/forum?id=VH1vxapUTs>.

Kondylatos, S., Papas, I., Ronco, M., Papoutsis, I., Camps-Valls, G., Piles, M., Fernández-Torres, M.A., Carvalhais, N., 2022. Wildfire Danger Prediction and Understanding With Deep Learning. *Geophysical Research Letters* 49, e2022GL099368. doi:10.1029/2022GL099368. _eprint: <https://onlinelibrary.wiley.com/doi/pdf/10.1029/2022GL099368>.

Kozlowski, T.T., Kramer, P.J., Pallardy, S.G., 1990. *The Physiological Ecology of Woody Plants*. Academic Press. doi:10.1093/treephys/8.2.213.

Kramer, H.A., Collins, B.M., Kelly, M., Stephens, S.L., 2014. Quantifying ladder fuels: A new approach using lidar. *Forests* 5, 1432–1453.

Kriedemann, P.E., Barrs, H.D., 1983. *Photosynthetic Adaptation to Water Stress and Implications for Drought Resistance*, in: *Crop Reactions To Water And Temperature Stresses In Humid, Temperate Climates*. CRC Press. Num Pages: 30.

Krizhevsky, A., Sutskever, I., Hinton, G.E., 2012. Imagenet classification with deep convolutional neural networks. *Advances in neural information processing systems* 25.

Kuckreja, K., Danish, M.S., Naseer, M., Das, A., Khan, S., Khan, F.S., 2024. Geochat: Grounded large vision-language model for remote sensing, in: *Proceedings of the IEEE/CVF Conference on Computer Vision and Pattern Recognition (CVPR)*, pp. 27831–27840.

Kurth, T., Subramanian, S., Harrington, P., Pathak, J., Mardani, M., Hall, D., Miele, A., Kashinath, K., Anandkumar, A., 2023. Fourcastnet: Accelerating global high-resolution weather forecasting using adaptive fourier neural operators, in: *Proceedings of the platform for advanced scientific computing conference*, pp. 1–11.

Labenski, P., Ewald, M., Schmidlein, S., Heinsch, F.A., Fassnacht, F.E., 2023. Quantifying surface fuels for fire modelling in temperate forests using airborne lidar and Sentinel-2: potential and limitations. *Remote Sensing of Environment* 295, 113711. URL: <https://www.sciencedirect.com/science/article/pii/S0034425723002626>, doi:10.1016/j.rse.2023.113711.

Lall, S., Mathibela, B., 2016. The application of artificial neural networks for wildfire risk prediction, in: *2016 International Conference on Robotics and Automation for Humanitarian Applications (RAHA)*, IEEE. pp. 1–6.

Lam, R., Sanchez-Gonzalez, A., Willson, M., Wirsberger, P., Fortunato, M., Alet, F., Ravuri, S., Ewalds, T., Eaton-Rosen, Z., Hu, W., et al., 2023. Learning skillful medium-range global weather forecasting. *Science* 382, 1416–1421.

Lawson, B.D., Armitage, O., 2008. Weather guide for the Canadian forest fire danger rating system. Technical Report. Canadian Forest Service, Northern Forestry Centre.

Lee, S.J., Lee, Y.J., Ryu, J.Y., Kwon, C.G., Seo, K.W., Kim, S.Y., 2022. Prediction of wildfire fuel load for *pinus densiflora* stands in south korea based on the forest-growth model. *Forests* 13, 1372.

Leite, R.V., Amaral, C., Neigh, C.S., Cosenza, D.N., Klauberg, C., Hudak, A.T., Aragão, L., Morton, D.C., Coffield, S., McCabe, T., et al., 2024. Leveraging the next generation of spaceborne earth observations for fuel monitoring and wildland fire management. *Remote Sensing in Ecology and Conservation*.

Leite, R.V., Silva, C.A., Broadbent, E.N., Do Amaral, C.H., Liesenberg, V., De Almeida, D.R.A., Mohan, M., Godinho, S., Cardil, A., Hamamura, C., et al., 2022. Large scale multi-layer fuel load characterization in tropical savanna using gedi spaceborne lidar data. *Remote Sensing of Environment* 268, 112764.

Li, B.S., Rad, R., 2024. Wildfire spread prediction in north america using satellite imagery and vision transformer, in: *2024 IEEE Conference on Artificial Intelligence (CAI)*, IEEE. pp. 1536–1541.

Li, F., Zhu, Q., Riley, W.J., Zhao, L., Xu, L., Yuan, K., Chen, M., Wu, H., Gui, Z., Gong, J., et al., 2023a. Attentionfire_v1. 0: interpretable machine learning fire model for burned-area predictions over tropics. *Geoscientific Model Development* 16, 869–884.

Li, W., Xu, Q., Yi, J., Liu, J., 2022a. Predictive model of spatial scale of forest fire driving factors: a case study of Yunnan Province, China. *Scientific Reports* 12, 19029. doi:10.1038/s41598-022-23697-6. publisher: Nature Publishing Group.

Li, X., Wang, X., Sun, S., Wang, Y., Li, S., Li, D., 2023b. Predicting the wildland fire spread using a mixed-input cnn model with both channel and spatial attention mechanisms. *Fire Technology* 59, 2683–2717.

Li, X., Wen, C., Hu, Y., Yuan, Z., Zhu, X.X., 2024a. Vision-language models in remote sensing: Current progress and future trends. *IEEE Geoscience and Remote Sensing Magazine*.

Li, X., Wen, C., Hu, Y., Yuan, Z., Zhu, X.X., 2024b. Vision-language models in remote sensing: Current progress and future trends. *IEEE Geoscience and Remote Sensing Magazine* 12, 32–66. doi:10.1109/MGRS.2024.3383473.

Li, Y., Chen, R., He, B., Veraverbeke, S., 2022b. Forest foliage fuel load estimation from multi-sensor spatiotemporal features. *International Journal of Applied Earth Observation and Geoinformation* 115, 103101. URL: <https://www.sciencedirect.com/science/article/pii/S1569843222002898>, doi:10.1016/j.jag.2022.103101.

Li, Y., He, B., 2022. A semi-empirical retrieval method of above-ground live forest fuel loads by combining sar and optical data. *Remote Sensing* 15, 5.

Li, Y., Quan, X., Liao, Z., He, B., 2021a. Forest fuel loads estimation from landsat etm+ and alos palsar data. *Remote Sensing* 13, 1189.

Li, Z., Huang, Y., Li, X., Xu, L., 2021b. Wildland Fire Burned Areas Prediction Using Long Short-Term Memory Neural Network with Attention Mechanism. *Fire Technology* 57, 1–23. URL: <https://doi.org/10.1007/s10694-020-01028-3>, doi:10.1007/s10694-020-01028-3.

Li, Z., Shi, H., Vogelmann, J.E., Hawbaker, T.J., Peterson, B., 2020. Assessment of fire fuel load dynamics in shrubland ecosystems in the western united states using modis products. *Remote Sensing* 12, 1911.

Liang, H., Zhang, M., Wang, H., 2019. A Neural Network Model for Wildfire Scale Prediction Using Meteorological Factors. *IEEE Access* 7, 176746–176755. URL: <https://ieeexplore.ieee.org/document/8924693>, doi:10.1109/ACCESS.2019.2957837. conference Name: IEEE Access.

Liang, M., Duncanson, L., Silva, J.A., Sedano, F., 2023. Quantifying above-ground biomass dynamics from charcoal degradation in mozambique using gedi lidar and landsat. *Remote sensing of environment* 284, 113367.

Liao, D., Valliant, R., 2012. Variance inflation factors in the analysis of complex survey data. *Survey Methodology* 38, 53–62.

Liu, X., Lin, Z., Feng, Z., 2021. Short-term offshore wind speed forecast by seasonal arima-a comparison against gru and lstm. *Energy* 227, 120492.

Lizundia-Loiola, J., Otón, G., Ramo, R., Chuvieco, E., 2020. A spatio-temporal active-fire clustering approach for global burned area mapping at 250 m from modis data. *Remote Sensing of Environment* 236, 111493.

López, A.S., San-Miguel-Ayanz, J., Burgan, R.E., 2002. Integration of satellite sensor data, fuel type maps and meteorological observations for evaluation of forest fire risk at the pan-european scale. *International Journal of Remote Sensing* 23, 2713–2719.

Lu, Y., Wei, C., 2021a. Evaluation of microwave soil moisture data for monitoring live fuel moisture content (lfmc) over the coterminous united states. *Science of The Total Environment* 771, 145410.

Lu, Y., Wei, C., 2021b. Evaluation of microwave soil moisture data for monitoring live fuel moisture content (LFMC) over the coterminous United States. *Science of The Total Environment* 771, 145410. URL: <https://www.sciencedirect.com/science/article/pii/S0048969721004782>, doi:10.1016/j.scitotenv.2021.145410.

Lundberg, S.M., Lee, S.I., 2017. A Unified Approach to Interpreting Model Predictions, in: *Advances in Neural Information Processing Systems*, Curran Associates, Inc. URL: <https://proceedings.neurips.cc/paper/2017/hash/8a20a8621978632d76c43df428b67767-Abstract.html>.

Luo, L., Zhai, Q., Su, Y., Ma, Q., Kelly, M., Guo, Q., 2018. Simple method for direct crown base height estimation of individual conifer trees using airborne lidar data. *Optics express* 26, A562–A578.

Malik, A., Rao, M.R., Puppala, N., Koouri, P., Thota, V.A.K., Liu, Q., Chiao, S., Gao, J., 2021. Data-Driven Wildfire Risk Prediction in Northern California. *Atmosphere* 12, 109. URL: <https://www.mdpi.com/2073-4433/12/1/109>, doi:10.3390/atmos12010109. number: 1 Publisher: Multidisciplinary Digital Publishing Institute.

Mansuy, N., Miller, C., Parisien, M.A., Parks, S.A., Batllori, E., Moritz, M.A., 2019. Contrasting human influences and macro-environmental factors on fire activity inside and outside protected areas of North America. *Environmental Research Letters* 14, 064007. URL: <https://dx.doi.org/10.1088/1748-9326/ab1bc5>, doi:10.1088/1748-9326/ab1bc5. publisher: IOP Publishing.

Marino, E., Yebra, M., Guillén-Climent, M., Algeet, N., Tomé, J.L., Madrigal, J., Guijarro, M., Hernando, C., 2020. Investigating live fuel moisture content estimation in fire-prone shrubland from remote sensing using empirical modelling and rtm simulations. *Remote Sensing* 12, 2251.

Marjani, M., Ahmadi, S.A., Mahdianpari, M., 2023. Firepred: A hybrid multi-

temporal convolutional neural network model for wildfire spread prediction. *Ecological Informatics* 78, 102282.

Marjani, M., Mahdianpari, M., Ahmadi, S.A., Hemmati, E., Mohammadi-mahesh, F., Mesgari, M.S., 2024a. Application of explainable artificial intelligence in predicting wildfire spread: an aspp-enabled cnn approach. *IEEE Geoscience and Remote Sensing Letters*.

Marjani, M., Mahdianpari, M., Mohammadi-mahesh, F., 2024b. Cnn-bilstm: A novel deep learning model for near-real-time daily wildfire spread prediction. *Remote Sensing* 16, 1467.

Martell, D.L., Bevilacqua, E., Stocks, B.J., 1989. Modelling seasonal variation in daily people-caused forest fire occurrence. *Canadian Journal of Forest Research* 19, 1555–1563. URL: <https://cdnsciencepub.com/doi/10.1139/x89-237>, doi:10.1139/x89-237. publisher: NRC Research Press.

Martínez, J., Vega-García, C., Chuvieco, E., 2009. Human-caused wildfire risk rating for prevention planning in Spain. *Journal of Environmental Management* 90, 1241–1252. URL: <https://www.sciencedirect.com/science/article/pii/S0301479708001758>, doi:10.1016/j.jenvman.2008.07.005.

Masrur, A., Yu, M., 2023. Chapter 6 - spatiotemporal attention convlstm networks for predicting and physically interpreting wildfire spread, in: Sun, Z., Cristea, N., Rivas, P. (Eds.), *Artificial Intelligence in Earth Science*. Elsevier, pp. 119–156. URL: <https://www.sciencedirect.com/science/article/pii/B9780323917377000098>, doi:<https://doi.org/10.1016/B978-0-323-91737-7.00009-8>.

Masrur, A., Yu, M., Taylor, A., 2024. Capturing and interpreting wildfire spread dynamics: attention-based spatiotemporal models using convlstm networks. *Ecological Informatics* 82, 102760.

Matthews, S., 2013. Dead fuel moisture research: 1991–2012. *International journal of wildland fire* 23, 78–92.

May, N., Ellicott, E., Gollner, M., 2019. An examination of fuel moisture, energy release and emissions during laboratory burning of live wildland fuels. *International Journal of Wildland Fire* 28, 187–197.

Mbow, C., Goitia, K., Bénié, G.B., 2004. Spectral indices and fire behavior simulation for fire risk assessment in savanna ecosystems. *Remote Sensing of Environment* 91, 1–13. doi:10.1016/j.rse.2003.10.019.

McArthur, A.G., 1958. The preparation and use of fire danger tables. Technical Report. Forestry and Timber Bureau: Canberra, Australia.

McArthur, A.G., 1960. Fire danger rating tables for annual grassland. Technical Report. (Forestry and Timber Bureau: Canberra, Australia).

McArthur, A.G., 1966. Weather and grassland fire behaviour. Technical Report. Department of National Development, Forestry and Timber Bureau: Canberra, Australia.

McArthur, A.G., 1967. Fire behaviour in eucalypt forests. Technical Report. Forest Research Institute, Forestry and Timber Bureau: Canberra, Australia.

McArthur, A.G., 1973. Grassland fire danger meter Mk IV. Technical Report. Forest Research Institute, Forestry and Timber Bureau: Canberra, ACT.

McCandless, T.C., Kosovic, B., Petzke, W., 2020. Enhancing wildfire spread modelling by building a gridded fuel moisture content product with machine learning. *Machine Learning: Science and Technology* 1, 035010.

McLauchlan, K.K., Higuera, P.E., Miesel, J., Rogers, B.M., Schweitzer, J., Shuman, J.K., Tepley, A.J., Varner, J.M., Veblen, T.T., Adalsteinsson, S.A., et al., 2020. Fire as a fundamental ecological process: Research advances and frontiers. *Journal of Ecology* 108, 2047–2069.

McNorton, J.R., Di Giuseppe, F., 2024. A global fuel characteristic model and dataset for wildfire prediction. *Biogeosciences* 21, 279–300. doi:10.5194/bg-21-279-2024. publisher: Copernicus GmbH.

Meikle, S., Heine, J., 1987. A fire danger index system for the transvaal lowveld and adjoining escarpment areas. *South African Forestry Journal* 143, 55–56.

Mell, W., Jenkins, M.A., Gould, J., Cheney, P., 2007. A physics-based approach to modelling grassland fires. *International Journal of Wildland Fire* 16, 1–22. URL: <https://www.publish.csiro.au/wf/WF06002>, doi:10.1071/WF06002. publisher: CSIRO PUBLISHING.

Menning, K.M., Stephens, S.L., 2007. Fire climbing in the forest: a semiquantitative, semiquantitative approach to assessing ladder fuel hazards. *Western Journal of Applied Forestry* 22, 88–93.

Miao, X., Li, J., Mu, Y., He, C., Ma, Y., Chen, J., Wei, W., Gao, D., 2023. Time Series Forest Fire Prediction Based on Improved Transformer. *Forests* 14, 1596. URL: <https://www.mdpi.com/1999-4907/14/8/1596>, doi:10.3390/f14081596. number: 8 Publisher: Multidisciplinary Digital Publishing Institute.

Michail, D., Panagiotou, L.I., Davalas, C., Prapas, I., Kondylatos, S., Bountos, N.I., Papoutsis, I., 2024. Seasonal Fire Prediction using Spatio-Temporal Deep Neural Networks. URL: <http://arxiv.org/abs/2404.06437>. arXiv:2404.06437 [cs].

Miller, C., Ager, A.A., 2012. A review of recent advances in risk analysis for wildfire management. *International journal of wildland fire* 22, 1–14.

Miller, C., Parisien, M.A., Ager, A., Finney, M., 2008. Evaluating spatially-explicit burn probabilities for strategic fire management planning. *WIT Transactions on Ecology and the Environment* 119, 245–252.

Miller, L., Zhu, L., Yebra, M., Rüdiger, C., Webb, G.I., 2023. Projecting live fuel moisture content via deep learning. *International Journal of Wildland Fire* 32, 709–727. URL: <https://www.publish.csiro.au/wf/WF22188>, doi:10.1071/WF22188. publisher: CSIRO PUBLISHING.

Mills, G.A., McCaw, W.L., 2010. Atmospheric stability environments and fire weather in Australia: extending the Haines Index. volume 20. Centre for Australian Weather and Climate Research Melbourne, Australia.

Moayedi, H., Khasmakhi, M.A.S.A., 2023. Wildfire susceptibility mapping using two empowered machine learning algorithms. *Stochastic Environmental Research and Risk Assessment* 37, 49–72.

Molnar, C., König, G., Herbinger, J., Freiesleben, T., Dandl, S., Scholbeck, C.A., Casalicchio, G., Grosse-Wentrup, M., Bischl, B., 2020. General pitfalls of model-agnostic interpretation methods for machine learning models, in: *International Workshop on Extending Explainable AI Beyond Deep Models and Classifiers*. Springer, pp. 39–68.

Monner, D., Reggia, J.A., 2012. A generalized lstm-like training algorithm for second-order recurrent neural networks. *Neural Networks* 25, 70–83.

Mou, L., Hua, Y., Jin, P., Zhu, X.X., 2020. Era: A data set and deep learning benchmark for event recognition in aerial videos [software and data sets]. *IEEE Geoscience and Remote Sensing Magazine* 8, 125–133.

Myoung, B., Kim, S.H., Nghiem, S.V., Jia, S., Whitney, K., Kafatos, M.C., 2018. Estimating live fuel moisture from modis satellite data for wildfire danger assessment in southern california usa. *Remote Sensing* 10, 87.

Myroniuk, V., Zibtsev, S., Bogomolov, V., Goldammer, J.G., Soshenskyi, O., Levchenko, V., Matsala, M., 2023. Combining landsat time series and gedi data for improved characterization of fuel types and canopy metrics in wildfire simulation. *Journal of Environmental Management* 345, 118736.

Naderpour, M., Rizeei, H.M., Ramezani, F., 2020. Wildfire Prediction: Handling Uncertainties Using Integrated Bayesian Networks and Fuzzy Logic, in: *2020 IEEE International Conference on Fuzzy Systems (FUZZ-IEEE)*, pp. 1–7. URL: <https://ieeexplore.ieee.org/document/9177700>, doi:10.1109/FUZZ48607.2020.9177700. iSSN: 1558-4739.

Nami, M.H., Jaafari, A., Fallah, M., Nabiuni, S., 2018. Spatial prediction of wildfire probability in the Hycanian ecoregion using evidential belief function model and GIS. *International Journal of Environmental Science and Technology* 15, 373–384. URL: <https://doi.org/10.1007/s13762-017-1371-6>, doi:10.1007/s13762-017-1371-6.

Natekar, S., Patil, S., Nair, A., Roychowdhury, S., 2021. Forest fire prediction using lstm, in: *2021 2nd International Conference for Emerging Technology (INSET)*, pp. 1–5. doi:10.1109/INSET51464.2021.9456113.

Nelson Jr, R.M., 2000. Prediction of diurnal change in 10-h fuel stick moisture content. *Canadian Journal of Forest Research* 30, 1071–1087. URL: <https://cdnsciencepub.com/doi/abs/10.1139/x00-032>, doi:10.1139/x00-032. publisher: NRC Research Press.

Nieto, H., Aguado, I., Chuvieco, E., Sandholt, I., 2010. Dead fuel moisture estimation with msg-seviri data: retrieval of meteorological data for the calculation of the equilibrium moisture content. *Agricultural and Forest Meteorology* 150, 861–870.

Noble, I., Gill, A., Bary, G., 1980. Mcarthur's fire-danger meters expressed as equations. *Australian journal of ecology* 5, 201–203.

Nolan, R.H., de Dios, V.R., Boer, M.M., Caccamo, G., Goulden, M.L., Bradstock, R.A., 2016. Predicting dead fine fuel moisture at regional scales using vapour pressure deficit from modis and gridded weather data. *Remote Sensing of Environment* 174, 100–108.

Nolan, R.H., Price, O.F., Samson, S.A., Jenkins, M.E., Rahmani, S., Boer, M.M., 2022. Framework for assessing live fine fuel loads and biomass consumption during fire. *Forest Ecology and Management* 504, 119830.

Nur, A.S., Kim, Y.J., Lee, C.W., 2022. Creation of wildfire susceptibility maps in plumas national forest using insar coherence, deep learning, and meta-heuristic optimization approaches. *Remote Sensing* 14, 4416.

Oak, O., Nazre, R., Naigaonkar, S., Sawant, S., Joshi, A., 2024. A novel transfer learning based cnn model for wildfire susceptibility prediction, in: *2024 5th International Conference for Emerging Technology (INSET)*, IEEE, pp. 1–

6.

Oliveira, S., Gonçalves, A., Zêzere, J.L., 2021a. Reassessing wildfire susceptibility and hazard for mainland portugal. *Science of the total environment* 762, 143121.

Oliveira, S., Rocha, J., Sá, A., 2021b. Wildfire risk modeling. *Current Opinion in Environmental Science & Health* 23, 100274. URL: <https://www.sciencedirect.com/science/article/pii/S2468584421000465>, doi:10.1016/j.coesh.2021.100274.

Oquab, M., Darzet, T., Moutakanni, T., Vo, H., Szafraniec, M., Khalidov, V., Fernandez, P., Haziza, D., Massa, F., El-Nouby, A., Assran, M., Balas, N., Galuba, W., Howes, R., Huang, P.Y., Li, S.W., Misra, I., Rabbat, M., Sharma, V., Synnaeve, G., Xu, H., Jegou, H., Mairal, J., Labatut, P., Joulin, A., Bojanowski, P., 2024. Dinov2: Learning robust visual features without supervision. URL: <https://arxiv.org/abs/2304.07193>, arXiv:2304.07193.

Ottmar, R.D., Sandberg, D.V., Riccardi, C.L., Prichard, S.J., 2007. An overview of the fuel characteristic classification system—quantifying, classifying, and creating fuelbeds for resource planning. *Canadian Journal of Forest Research* 37, 2383–2393.

Parks, S.A., Abatzoglou, J.T., 2020. Warmer and Drier Fire Seasons Contribute to Increases in Area Burned at High Severity in Western US Forests From 1985 to 2017. *Geophysical Research Letters* 47, e2020GL089858. URL: <https://onlinelibrary.wiley.com/doi/abs/10.1029/2020GL089858>, doi:10.1029/2020GL089858. _eprint: <https://onlinelibrary.wiley.com/doi/pdf/10.1029/2020GL089858>.

Pelletier, N., Millard, K., Darling, S., 2023. Wildfire likelihood in Canadian treed peatlands based on remote-sensing time-series of surface conditions. *Remote Sensing of Environment* 296, 113747. URL: <https://www.sciencedirect.com/science/article/pii/S0034425723002985>, doi:10.1016/j.rse.2023.113747.

Pellizzaro, G., Duce, P., Ventura, A., Zara, P., 2007. Seasonal variations of live moisture content and ignitability in shrubs of the mediterranean basin. *International Journal of Wildland Fire* 16, 633–641.

Peterson, S.H., Roberts, D.A., Dennison, P.E., 2008. Mapping live fuel moisture with modis data: A multiple regression approach. *Remote Sensing of Environment* 112, 4272–4284.

Pettinari, M.L., Chuvieco, E., 2016. Generation of a global fuel data set using the fuel characteristic classification system. *Biogeosciences* 13, 2061–2076.

Pettinari, M.L., Chuvieco, E., 2020. Fire danger observed from space. *Surveys in Geophysics* 41, 1437–1459.

Pettinari, M.L., Ottmar, R.D., Prichard, S.J., Andreu, A.G., Chuvieco, E., 2013. Development and mapping of fuel characteristics and associated fire potentials for south america. *International Journal of Wildland Fire* 23, 643–654.

Phelps, N., Woolford, D.G., 2021. Comparing calibrated statistical and machine learning methods for wildland fire occurrence prediction: a case study of human-caused fires in Lac La Biche, Alberta, Canada. *International Journal of Wildland Fire* 30, 850–870. URL: <https://www.publish.csiro.au/wf/WF20139>, doi:10.1071/WF20139. publisher: CSIRO PUBLISHING.

Pisek, J., Rautiainen, M., Nikopensius, M., Raabe, K., 2015. Estimation of seasonal dynamics of understory NDVI in northern forests using MODIS BRDF data: Semi-empirical versus physically-based approach. *Remote Sensing of Environment* 163, 42–47. URL: <https://www.sciencedirect.com/science/article/pii/S0034425715000991>, doi:10.1016/j.rse.2015.03.003.

Ploton, P., Mortier, F., Réjou-Méchain, M., Barbier, N., Picard, N., Rossi, V., Dormann, C., Cornu, G., Viennois, G., Bayol, N., et al., 2020. Spatial validation reveals poor predictive performance of large-scale ecological mapping models. *Nature communications* 11, 4540.

Pollina, J.B., Colle, B.A., Charney, J.J., 2013. Climatology and Meteorological Evolution of Major Wildfire Events over the Northeast United States. *Weather and Forecasting* 28, 175–193. URL: https://journals.ametsoc.org/view/journals/wefo/28/1/waf-d-12-00009_1.xml, doi:10.1175/WAF-D-12-00009.1. publisher: American Meteorological Society Section: Weather and Forecasting.

Prapas, I., Bountos, N.I., Kondylatos, S., Michail, D., Camps-Valls, G., Papoutsis, I., 2023. TeleViT: Teleconnection-Driven Transformers Improve Subseasonal to Seasonal Wildfire Forecasting, pp. 3754–3759. URL: https://openaccess.thecvf.com/content/ICCV2023W/AIHADR/html/Prapas_TeleViT_Teleconnection-Driven_Transformers_Improve_Subseasonal_to_Seasonal_Wildfire_Forecasting_ICCVW_2023_paper.html.

Prapas, I., Kondylatos, S., Papoutsis, I., 2022. FireCube: A Daily Datacube for the Modeling and Analysis of Wildfires in Greece. URL: <https://doi.org/10.5281/zenodo.6475592>, doi:10.5281/zenodo.6475592.

Prapas, I., Kondylatos, S., Papoutsis, I., Camps-Valls, G., Ronco, M., Ángel Fernández-Torres, M., Guillem, M.P., Carvalhais, N., 2021. Deep learning methods for daily wildfire danger forecasting. URL: <https://arxiv.org/abs/2111.02736>, arXiv:2111.02736.

Preisler, H.K., Brillinger, D.R., Burgan, R.E., Benoit, J., 2004. Probability based models for estimation of wildfire risk. *International Journal of wildland fire* 13, 133–142.

Prior, T., Eriksen, C., 2013. Wildfire preparedness, community cohesion and social-ecological systems. *Global Environmental Change* 23, 1575–1586. URL: <https://www.sciencedirect.com/science/article/pii/S0959378013001684>, doi:10.1016/j.gloenvcha.2013.09.016.

Pye, J.M., Prestemon, J.P., Butry, D.T., Abt, K.L., 2003. Prescribed burning and wildfire risk in the 1998 fire season in florida, in: In: Omi, Philip N.; Joyce, Linda A., technical editors. *Fire, fuel treatments, and ecological restoration: Conference proceedings; 2002 16-18 April; Fort Collins, CO. Proceedings RMRS-P-29*. Fort Collins, CO: US Department of Agriculture, Forest Service, Rocky Mountain Research Station, p. 15-26, pp. 15–26.

Qadir, A., Talukdar, N.R., Uddin, M.M., Ahmad, F., Goparaju, L., 2021. Predicting forest fire using multispectral satellite measurements in Nepal. *Remote Sensing Applications: Society and Environment* 23, 100539. URL: <https://www.sciencedirect.com/science/article/pii/S2352938521000756>, doi:10.1016/j.rsase.2021.100539.

Qiao, Y., Jiang, W., Su, G., Jiang, J., Li, X., Wang, F., 2024. A transformer-based neural network for ignition location prediction from the final wildfire perimeter. *Environmental Modelling & Software* 172, 105915. URL: <https://www.sciencedirect.com/science/article/pii/S1364815223003018>, doi:10.1016/j.envsoft.2023.105915.

Quan, X., Wang, W., Xie, Q., He, B., Resco De Dios, V., Yebra, M., Jiao, M., Chen, R., 2023. Improving wildfire occurrence modelling by integrating time-series features of weather and fuel moisture content. *Environmental Modelling & Software* 170, 105840. doi:10.1016/j.envsoft.2023.105840.

Quan, X., Yebra, M., Riaño, D., He, B., Lai, G., Liu, X., 2021a. Global fuel moisture content mapping from modis. *International Journal of Applied Earth Observation and Geoinformation* 101, 102354.

Quan, X., Yebra, M., Riaño, D., He, B., Lai, G., Liu, X., 2021b. Global fuel moisture content mapping from MODIS. *International Journal of Applied Earth Observation and Geoinformation* 101, 102354. URL: <https://www.sciencedirect.com/science/article/pii/S0303243421000611>, doi:10.1016/j.jag.2021.102354.

Rakhmatulina, E., Stephens, S., Thompson, S., 2021. Soil moisture influences on sierra nevada dead fuel moisture content and fire risks. *Forest Ecology and Management* 496, 119379.

Rao, K., Williams, A.P., Flefil, J.F., Konings, A.G., 2020a. SAR-enhanced mapping of live fuel moisture content. *Remote Sensing of Environment* 245, 111797.

Rao, K., Williams, A.P., Flefil, J.F., Konings, A.G., 2020b. SAR-enhanced mapping of live fuel moisture content. *Remote Sensing of Environment* 245, 111797. URL: <https://www.sciencedirect.com/science/article/pii/S003442572030167X>, doi:10.1016/j.rse.2020.111797.

Ravi, N., Gabeur, V., Hu, Y.T., Hu, R., Ryali, C., Ma, T., Khedr, H., Rädle, R., Rolland, C., Gustafson, L., Mintun, E., Pan, J., Alwala, K.V., Carion, N., Wu, C.Y., Girshick, R., Dollár, P., Feichtenhofer, C., 2024. Sam 2: Segment anything in images and videos. URL: <https://arxiv.org/abs/2408.00714>, arXiv:2408.00714.

Ray, D., Nepstad, D., Brando, P., 2010. Predicting moisture dynamics of fine understory fuels in a moist tropical rainforest system: results of a pilot study undertaken to identify proxy variables useful for rating fire danger. *New Phytologist* 187, 720–732.

Razavi Termeh, S.V., Kornejady, A., Pourghasemi, H.R., Keesstra, S., 2018. Flood susceptibility mapping using novel ensembles of adaptive neuro fuzzy inference system and metaheuristic algorithms. *Science of The Total Environment* 615, 438–451. URL: <https://www.sciencedirect.com/science/article/pii/S0048969717326141>, doi:10.1016/j.scitotenv.2017.09.262.

Rezaie, F., Panahi, M., Bateni, S.M., Lee, S., Jun, C., Trauernicht, C., Neale, C.M.U., 2023. Development of novel optimized deep learning algorithms for wildfire modeling: A case study of Maui, Hawai'i. *Engineering Applications of Artificial Intelligence* 125, 106699. URL: <https://www.sciencedirect.com/science/article/pii/S0952197623008837>, doi:10.1016/j.engappai.2023.106699.

Riaño, D., Chuvieco, E., Salas, J., Palacios-Orueta, A., Bastarrika, A., 2002. Generation of fuel type maps from landsat tm images and ancillary data in mediterranean ecosystems. *Canadian Journal of Forest Research* 32, 1301–1315.

Ritter, S.M., Hoffman, C.M., Battaglia, M.A., Linn, R., Mell, W.E., 2023. Vertical and horizontal crown fuel continuity influences group-scale ignition and fuel consumption. *Fire* 6, 321.

Rodriguez-Jimenez, F., Lorenzo, H., Novo, A., Acuña-Alonso, C., Alvarez, X., 2023. Modelling of live fuel moisture content in different vegetation scenarios during dry periods using meteorological data and spectral indices. *Forest Ecology and Management* 546, 121378.

Rogger, M., Agnoletti, M., Alaoui, A., Bathurst, J., Bodner, G., Borga, M., Chaplot, V., Gallart, F., Glatzel, G., Hall, J., et al., 2017. Land use change impacts on floods at the catchment scale: Challenges and opportunities for future research. *Water resources research* 53, 5209–5219.

Romero-Calcerrada, R., Novillo, C., Millington, J.D., Gomez-Jimenez, I., 2008. Gis analysis of spatial patterns of human-caused wildfire ignition risk in the sw of madrid (central spain). *Landscape ecology* 23, 341–354.

Rösch, M., Nolde, M., Ullmann, T., Riedlinger, T., 2024. Data-driven wildfire spread modeling of european wildfires using a spatiotemporal graph neural network. *Fire* 7, 207.

Rothermel, R.C., Wilson, R., Morris, G.A., Sackett, S.S., 1986. Modeling Moisture Content of Fine Dead Wildland Fuels:. United States Department of Agriculture, Forest Service, Intermountain

Rubí, J.N.S., Gondim, P.R.L., 2023. A performance comparison of machine learning models for wildfire occurrence risk prediction in the Brazilian Federal District region. *Environment Systems and Decisions* URL: <https://doi.org/10.1007/s10669-023-09921-2>, doi:10.1007/s10669-023-09921-2.

Ruffault, J., Martin-StPaul, N., Pimont, F., Dupuy, J.L., 2018. How well do meteorological drought indices predict live fuel moisture content (lfmc)? an assessment for wildfire research and operations in mediterranean ecosystems. *Agricultural and Forest Meteorology* 262, 391–401.

Saatchi, S., Halligan, K., Despain, D.G., Crabtree, R.L., 2007. Estimation of Forest Fuel Load From Radar Remote Sensing. *IEEE Transactions on Geoscience and Remote Sensing* 45, 1726–1740. URL: <https://ieeexplore.ieee.org/abstract/document/4215087>, doi:10.1109/TGRS.2006.887002. conference Name: IEEE Transactions on Geoscience and Remote Sensing.

Sadasivuni, R., Cooke, W.H., Bhushan, S., 2013. Wildfire risk prediction in Southeastern Mississippi using population interaction. *Ecological Modelling* 251, 297–306. URL: <https://www.sciencedirect.com/science/article/pii/S0304380013000070>, doi:10.1016/j.ecolmodel.2012.12.024.

Salis, M., Arca, B., Del Giudice, L., Palaiologou, P., Alcasena-Urdiroz, F., Ager, A., Fiori, M., Pellizzaro, G., Scarpa, C., Schirru, M., Ventura, A., Calsula, M., Duce, P., 2021. Application of simulation modeling for wildfire exposure and transmission assessment in Sardinia, Italy. *International Journal of Disaster Risk Reduction* 58, 102189. URL: <https://linkinghub.elsevier.com/retrieve/pii/S2212420921001552>, doi:10.1016/j.ijdrr.2021.102189.

San-Miguel-Ayanz, J., Durrant, T., Boca, R., Libertà, G., Branco, A., DE, R., Ferrari, D., Maianti, P., ARTES, V.T., PFEIFFER, H., et al., 2018. Forest Fires in Europe, Middle East and North Africa 2018. Publications Office of the European Union, Luxembourg.

Sandberg, D.V., Ottmar, R.D., Cuson, G.H., 2001. Characterizing fuels in the 21st century. *International Journal of Wildland Fire* 10, 381–387.

Santopaolo, A., Saif, S.S., Pietrabissa, A., Giuseppi, A., 2021. Forest fire risk prediction from satellite data with convolutional neural networks, in: 2021 29th Mediterranean Conference on Control and Automation (MED), IEEE. pp. 360–367.

Sayad, Y.O., Mousannif, H., Al Moatassime, H., 2019. Predictive modeling of wildfires: A new dataset and machine learning approach. *Fire safety journal* 104, 130–146.

Scheller, R.M., Domingo, J.B., Sturtevant, B.R., Williams, J.S., Rudy, A., Gustafson, E.J., Mladenoff, D.J., 2007. Design, development, and application of landis-ii, a spatial landscape simulation model with flexible temporal and spatial resolution. *ecological modelling* 201, 409–419.

Schroeder, W., Oliva, P., Giglio, L., Csiszar, I.A., 2014. The new viirs 375 m active fire detection data product: Algorithm description and initial assessment. *Remote Sensing of Environment* 143, 85–96.

Scott, J.H., 2001. Assessing crown fire potential by linking models of surface and crown fire behavior. 29, US Department of Agriculture, Forest Service, Rocky Mountain Research Station.

Shadrin, D., Illarionova, S., Gubanov, F., Evteeva, K., Mironenko, M., Levchunets, I., Belousov, R., Burnaev, E., 2024a. Wildfire spreading prediction using multimodal data and deep neural network approach. *Scientific Reports* 14, 2606. URL: <https://www.ncbi.nlm.nih.gov/pmc/articles/PMC10831103/>, doi:10.1038/s41598-024-52821-x.

Shadrin, D., Illarionova, S., Gubanov, F., Evteeva, K., Mironenko, M., Levchunets, I., Belousov, R., Burnaev, E., 2024b. Wildfire spreading prediction using multimodal data and deep neural network approach. *Scientific Reports* 14, 2606.

Shamsoshoara, A., Afghah, F., Razi, A., Zheng, L., Fulé, P., Blasch, E., 2020. The flame dataset: Aerial imagery pile burn detection using drones (uavs). URL: <https://dx.doi.org/10.21227/qad6-r683>, doi:10.21227/qad6-r683.

Shapley, L.S., 1953. Stochastic games. *Proceedings of the national academy of sciences* 39, 1095–1100.

Short, K.C., 2014. A spatial database of wildfires in the united states, 1992–2011. *Earth System Science Data* 6, 1–27.

Singla, S., Diao, T., Mukhopadhyay, A., Eldawy, A., Shachter, R., Kochenderfer, M., 2020. Wildfiredb: A spatio-temporal dataset combining wildfire occurrence with relevant covariates, in: 34th Conference on Neural Information Processing Systems (NeurIPS 2020).

Skowronski, N.S., Clark, K.L., Duvaneck, M., Hom, J., 2011. Three-dimensional canopy fuel loading predicted using upward and downward sensing LiDAR systems. *Remote Sensing of Environment* 115, 703–714. URL: <https://www.sciencedirect.com/science/article/pii/S0034425710003172>, doi:10.1016/j.rse.2010.10.012.

Song, Y., Wang, Y., 2020. Global Wildfire Outlook Forecast with Neural Networks. *Remote Sensing* 12, 2246. URL: <https://www.mdpi.com/2072-4292/12/14/2246>, doi:10.3390/rs12142246. number: 14 Publisher: Multidisciplinary Digital Publishing Institute.

Sow, M., Mbow, C., Hély, C., Fensholt, R., Sambou, B., 2013. Estimation of herbaceous fuel moisture content using vegetation indices and land surface temperature from modis data. *Remote Sensing* 5, 2617–2638.

Srivastava, S.K., Saran, S., de By, R.A., Dadhwal, V.K., 2014. A geo-information system approach for forest fire likelihood based on causative and anti-causative factors. *International Journal of Geographical Information Science* 28, 427–454. URL: <https://doi.org/10.1080/13658816.2013.797984>, doi:10.1080/13658816.2013.797984. publisher: Taylor & Francis _eprint: https://doi.org/10.1080/13658816.2013.797984.

Stocks, B.J., Lawson, B.D., Alexander, M.E., Wagner, C.E.V., McAlpine, R.S., Lynham, T.J., Dubé, D.E., 1989a. The Canadian Forest Fire Danger Rating System: An Overview. *The Forestry Chronicle* 65, 450–457. URL: <https://pubs.cif-ifc.org/doi/abs/10.5558/tfc65450-6>, doi:10.5558/tfc65450-6. publisher: Canadian Institute of Forestry.

Stocks, B.J., Lynham, T., Lawson, B., Alexander, M., Wagner, C.V., McAlpine, R., Dube, D., 1989b. Canadian forest fire danger rating system: an overview. *The Forestry Chronicle* 65, 258–265.

Stow, D., Niphadkar, M., Kaiser, J., 2006. Time series of chaparral live fuel moisture maps derived from modis satellite data. *International Journal of Wildland Fire* 15, 347–360.

Su, Z., Zheng, L., Luo, S., Tigabu, M., Guo, F., 2021. Modeling wildfire drivers in Chinese tropical forest ecosystems using global logistic regression and geographically weighted logistic regression. *Natural Hazards* 108, 1317–1345. URL: <https://doi.org/10.1007/s11069-021-04733-6>, doi:10.1007/s11069-021-04733-6.

Sundararajan, M., Taly, A., Yan, Q., 2017. Axiomatic attribution for deep networks, in: International conference on machine learning, PMLR. pp. 3319–3328.

Swetnam, T.W., Betancourt, J.L., 1990. Fire-southern oscillation relations in the southwestern united states. *Science* 249, 1017–1020.

Tanase, M., Panciera, R., Lowell, K., Aponte, C., 2015. Monitoring live fuel moisture in semiarid environments using l-band radar data. *International Journal of Wildland Fire* 24, 560–572.

Tanase, M.A., Nova, J.P.G., Marino, E., Aponte, C., Tomé, J.L., Yáñez, L., Madrigal, J., Guijarro, M., Hernando, C., 2022. Characterizing live fuel moisture content from active and passive sensors in a mediterranean environment. *Forests* 13, 1846.

Taneja, R., Hilton, J., Wallace, L., Reinke, K., Jones, S., 2021. Effect of fuel spatial resolution on predictive wildfire models. *International Journal of Wildland Fire* 30, 776–789. URL: <https://www.publish.csiro.au/wf/WF20192>, doi:10.1071/WF20192. publisher: CSIRO PUBLISHING.

Tavakkoli Piralilou, S., Einali, G., Ghorbanzadeh, O., Nachappa, T.G., Gholamnia, K., Blaschke, T., Ghamisi, P., 2022. A Google Earth Engine Approach for Wildfire Susceptibility Prediction Fusion with Remote Sensing Data of Different Spatial Resolutions. *Remote Sensing* 14, 672. URL: <https://www.mdpi.com/2072-4292/14/3/672>, doi:10.3390/rs14030672. number: 3 Publisher: Multidisciplinary Digital Publishing Institute.

Taylor, S.W., Alexander, M.E., 2006. Science, technology, and human factors in fire danger rating: the canadian experience. *International Journal of Wildland Fire* 15, 121–135.

Tesch, T., Kollet, S., Garske, J., 2023. Causal deep learning models for studying the earth system. *Geoscientific Model Development* 16, 2149–2166.

Thompson, M.P., Vaillant, N.M., Haas, J.R., Gebert, K.M., Stockmann, K.D., 2013. Quantifying the potential impacts of fuel treatments on wildfire suppression costs. *Journal of Forestry* 111, 49–58.

Tolhurst, K., Shields, B., Chong, D., 2008. Phoenix: development and application of a bushfire risk management tool. *Australian Journal of Emergency Management*, The 23, 47–54.

Toulouse, T., Rossi, L., Campana, A., Celik, T., Akhlooufi, M.A., 2017. Computer vision for wildfire research: An evolving image dataset for processing and analysis. *Fire Safety Journal* 92, 188–194.

Tran, T.T.K., Janizadeh, S., Bateni, S.M., Jun, C., Kim, D., Trauernicht, C., Rezaie, F., Giambelluca, T.W., Panahi, M., 2024. Improving the prediction of wildfire susceptibility on hawai'i island, hawai'i, using explainable hybrid machine learning models. *Journal of environmental management* 351, 119724.

Trucchia, A., Meschi, G., Fiorucci, P., Gollini, A., Negro, D., 2022. Defining Wildfire Susceptibility Maps in Italy for Understanding Seasonal Wildfire Regimes at the National Level. *Fire* 5, 30. URL: <https://www.mdpi.com/2571-6255/5/1/30>, doi:10.3390/fire5010030. number: 1 Publisher: Multidisciplinary Digital Publishing Institute.

Tymstra, C., Bryce, R., Wotton, B., Taylor, S., Armitage, O., et al., 2010. Development and structure of prometheus: the canadian wildland fire growth simulation model. Natural Resources Canada, Canadian Forest Service, Northern Forestry Centre, Information Report NOR-X-417.(Edmonton, AB) .

Ujjwal, K., Hilton, J., Garg, S., Aryal, J., 2022. A probability-based risk metric for operational wildfire risk management. *Environmental Modelling & Software* 148, 105286.

Umunnakwe, A., Parvania, M., Nguyen, H., Horel, J.D., Davis, K.R., 2022. Data-driven spatio-temporal analysis of wildfire risk to power systems operation. *IET Generation, Transmission & Distribution* 16, 2531–2546.

Ustin, S.L., Middleton, E.M., 2021. Current and near-term advances in earth observation for ecological applications. *Ecological Processes* 10, 1.

Van Wagner, C.E., et al., 1974. Structure of the Canadian forest fire weather index. volume 1333. Environment Canada, Forestry Service Ottawa, ON, Canada.

Vaswani, A., Shazeer, N., Parmar, N., Uszkoreit, J., Jones, L., Gomez, A.N., Kaiser, L., Polosukhin, I., 2017. Attention is all you need, in: *Advances in Neural Information Processing Systems*.

Vega, J.A., Arellano-Pérez, S., Álvarez-González, J.G., Fernández, C., Jiménez, E., Fernández-Alonso, J.M., Vega-Nieva, D.J., Briones-Herrera, C., Alonso-Rego, C., Fontúrbel, T., et al., 2022. Modelling aboveground biomass and fuel load components at stand level in shrub communities in nw spain. *Forest Ecology and Management* 505, 119926.

Verbesselt, J., Fleck, S., Coppin, P., Viegas, D., 2002. Estimation of fuel moisture content towards fire risk assessment: a review. URL: <https://www.semanticscholar.org/paper/Estimation-of-fuel-moisture-content-towards-fire-a-Verbesselt-Fleck/5d7c76a2a1ee4ca7f5984be7a66866def092df59>.

Viegas, D., Piñol, J., Viegas, M., Ogaya, R., 2001. Estimating live fine fuels moisture content using meteorologically-based indices. *International Journal of Wildland Fire* 10, 223–240.

Viegas, D.X., Bovio, G., Ferreira, A., Nosenzo, A., Sol, B., 1999. Comparative study of various methods of fire danger evaluation in southern europe. *International Journal of wildland fire* 9, 235–246.

Vilar, L., Camia, A., San-Miguel-Ayanz, J., Martín, M.P., 2016. Modeling temporal changes in human-caused wildfires in mediterranean europe based on land use-land cover interfaces. *Forest Ecology and Management* 378, 68–78.

Viney, N.R., 1991a. A review of fine fuel moisture modelling. *International Journal of Wildland Fire* 1, 215–234.

Viney, N.R., 1991b. A Review of Fine Fuel Moisture Modelling. *International Journal of Wildland Fire* 1, 215–234. URL: <https://www.publish.csiro.au/wf/wf9910215>, doi:10.1071/wf9910215. publisher: CSIRO PUBLISHING.

Vinodkumar, V., Dharssi, I., Yebra, M., Fox-Hughes, P., 2021. Continental-scale prediction of live fuel moisture content using soil moisture information. *Agricultural and Forest Meteorology* 307, 108503. URL: <https://www.sciencedirect.com/science/article/pii/S0168192321001866>, doi:10.1016/j.agrformet.2021.108503.

Viswanathan, S., Anand Kumar, M., Soman, K., 2019. A sequence-based machine comprehension modeling using lstm and gru, in: *Emerging Research in Electronics, Computer Science and Technology: Proceedings of International Conference, ICERECT 2018*, Springer, pp. 47–55.

Vitolo, C., Di Giuseppe, F., Barnard, C., Coughlan, R., San-Miguel-Ayanz, J., Libertà, G., Krzeminski, B., 2020. ERA5-based global meteorological wildfire danger maps. *Scientific Data* 7, 216. URL: <https://www.nature.com/articles/s41597-020-0554-z>, doi:10.1038/s41597-020-0554-z. publisher: Nature Publishing Group.

Wagner, C.V., 1993. Prediction of crown fire behavior in two stands of jack pine. *Canadian Journal of Forest Research* 23, 442–449.

Walker, X.J., Rogers, B.M., Veraverbeke, S., Johnstone, J.F., Baltzer, J.L., Barrett, K., Bourgeau-Chavez, L., Day, N., de Groot, W., Dieleman, C., et al., 2020. Fuel availability not fire weather controls boreal wildfire severity and carbon emissions. *Nature Climate Change* 10, 1130–1136.

Wang, L., Quan, X., He, B., Yebra, M., Xing, M., Liu, X., 2019. Assessment of the dual polarimetric sentinel-1a data for forest fuel moisture content estimation. *Remote Sensing* 11, 1568.

Wang, Q., Ihme, M., Gazen, C., Chen, Y.F., Anderson, J., 2024. Firebench: A high-fidelity ensemble simulation framework for exploring wildfire behavior and data-driven modeling. *arXiv preprint arXiv:2406.08589* .

Wang, S.S.C., Qian, Y., Leung, L.R., Zhang, Y., 2021. Identifying Key Drivers of Wildfires in the Contiguous US Using Machine Learning and Game Theory Interpretation. *Earth's Future* 9, e2020EF001910. URL: <https://onlinelibrary.wiley.com/doi/abs/10.1029/2020EF001910>, doi:10.1029/2020EF001910. _eprint: <https://onlinelibrary.wiley.com/doi/pdf/10.1029/2020EF001910>.

Wang, W., Quan, X., 2023. Estimation of live fuel moisture content from multiple sources of remotely sensed data. *IEEE Geoscience and Remote Sensing Letters* .

Wang, Y., Xi, X., Wang, C., Yang, X., Wang, P., Nie, S., Du, M., 2022. A novel method based on kernel density for estimating crown base height using uav-borne lidar data. *IEEE Geoscience and Remote Sensing Letters* 19, 1–5. doi:10.1109/LGRS.2022.3171316.

Wing, B.M., Ritchie, M.W., Boston, K., Cohen, W.B., Gitelman, A., Olsen, M.J., 2012. Prediction of understory vegetation cover with airborne lidar in an interior ponderosa pine forest. *Remote Sensing of Environment* 124, 730–741.

Xie, J., Qi, T., Hu, W., Huang, H., Chen, B., Zhang, J., 2022a. Retrieval of live fuel moisture content based on multi-source remote sensing data and ensemble deep learning model. *Remote Sensing* 14, 4378.

Xie, L., Zhang, R., Zhan, J., Li, S., Shama, A., Zhan, R., Wang, T., Lv, J., Bao, X., Wu, R., 2022b. Wildfire risk assessment in liangshan prefecture, china based on an integration machine learning algorithm. *Remote Sensing* 14, 4592.

Xu, C., Xie, Y., Vazquez, D.A.Z., Yao, R., Qiu, F., 2023. Spatio-temporal wildfire prediction using multi-modal data. *IEEE Journal on Selected Areas in Information Theory* 4, 302–313.

Xu, R., Yang, S., Wang, Y., Cai, Y., Du, B., Chen, H., 2024. Visual mamba: A survey and new outlooks. URL: <https://arxiv.org/abs/2404.18861>, arXiv:2404.18861.

Xu, W., Wooster, M.J., 2023. Sentinel-3 slstr active fire (af) detection and frp daytime product-algorithm description and global intercomparison to modis, viirs and landsat af data. *Science of Remote Sensing* 7, 100087.

Yahia, O., Ghabi, M., Karoui, M.S., 2023. The Prediction of Regional Wildfire Risk Using High-Resolution Remotely Sensed Soil Moisture Content Estimation, Case Study: Sidi Douma Forest, Saida, Algeria, in: IGARSS 2023 - 2023 IEEE International Geoscience and Remote Sensing Symposium, pp. 3387–3390. URL: <https://ieeexplore.ieee.org/abstract/document/10281986>, doi:10.1109/IGARSS52108.2023.10281986. iSSN: 2153-7003.

Yang, C.E., Fu, J.S., Liu, Y., Dong, X., Liu, Y., 2022. Projections of future wildfires impacts on air pollutants and air toxics in a changing climate over the western United States. *Environmental Pollution* 304, 119213. URL: <https://www.sciencedirect.com/science/article/pii/S0269749122004274>, doi:10.1016/j.envpol.2022.119213.

Yang, J., He, H.S., Gustafson, E.J., 2004. A hierarchical fire frequency model to simulate temporal patterns of fire regimes in landis. *Ecological Modelling* 180, 119–133.

Yebra, M., Chuvieco, E., Riano, D., 2008. Estimation of live fuel moisture content from modis images for fire risk assessment. *Agricultural and forest meteorology* 148, 523–536.

Yebra, M., Dennison, P.E., Chuvieco, E., Riaño, D., Zylstra, P., Hunt Jr, E.R., Danson, F.M., Qi, Y., Jurdao, S., 2013a. A global review of remote sensing of live fuel moisture content for fire danger assessment: Moving towards operational products. *Remote Sensing of Environment* 136, 455–468.

Yebra, M., Dennison, P.E., Chuvieco, E., Riaño, D., Zylstra, P., Hunt, E.R., Danson, F.M., Qi, Y., Jurdao, S., 2013b. A global review of remote sensing of live fuel moisture content for fire danger assessment: Moving towards operational products. *Remote Sensing of Environment* 136, 455–468. URL: <https://www.sciencedirect.com/science/article/pii/S0034425713001831>, doi:10.1016/j.rse.2013.05.029.

Ying, L., Cheng, H., Shen, Z., Guan, P., Luo, C., Peng, X., 2021. Relative humidity and agricultural activities dominate wildfire ignitions in yunnan, southwest china: Patterns, thresholds, and implications. *Agricultural and Forest Meteorology* 307, 108540.

Ying, L., Shen, Z., Yang, M., Piao, S., 2019. Wildfire detection probability of modis fire products under the constraint of environmental factors: A study based on confirmed ground wildfire records. *Remote Sensing* 11, 3031.

Yoon, H.J., Voulgaris, P., 2022. Multi-time predictions of wildfire grid map using remote sensing local data, in: 2022 IEEE International Conference on Knowledge Graph (ICKG), pp. 365–372. doi:10.1109/ICKG55886.2022.00053.

You, X., Zheng, Z., Yang, K., Yu, L., Liu, J., Chen, J., Lu, X., Guo, S., 2023. A pso-cnn-based deep learning model for predicting forest fire risk on a national scale. *Forests* 15, 86.

Zacharakis, I., Tsihrintzis, V.A., 2023a. Environmental forest fire danger rating systems and indices around the globe: a review. *Land* 12, 194.

Zacharakis, I., Tsihrintzis, V.A., 2023b. Integrated wildfire danger models and factors: A review. *Science of The Total Environment* 899, 165704. URL: <https://linkinghub.elsevier.com/retrieve/pii/S0048969723043279>, doi:10.1016/j.scitotenv.2023.165704.

Zarzycki, K., Ławryńczuk, M., 2022. Advanced predictive control for gru and lstm networks. *Information Sciences* 616, 229–254.

Zerveas, G., Jayaraman, S., Patel, D., Bhamidipaty, A., Eickhoff, C., 2021. A Transformer-based Framework for Multivariate Time Series Representation Learning, in: Proceedings of the 27th ACM SIGKDD Conference on Knowledge Discovery & Data Mining, Association for Computing Machinery, New York, NY, USA. pp. 2114–2124. URL: <https://dl.acm.org/doi/10.1145/3447548.3467401>, doi:10.1145/3447548.3467401.

Zhang, C., Pan, X., Li, H., Gardiner, A., Sargent, I., Hare, J., Atkinson, P.M., 2018. A hybrid MLP-CNN classifier for very fine resolution remotely sensed image classification. *ISPRS Journal of Photogrammetry and Remote Sensing* 140, 133–144. URL: <https://www.sciencedirect.com/science/article/pii/S0924271617300254>, doi:10.1016/j.isprsjprs.2017.07.014.

Zhang, G., Wang, M., Liu, K., 2019. Forest Fire Susceptibility Modeling Using a Convolutional Neural Network for Yunnan Province of China. *International Journal of Disaster Risk Science* 10, 386–403. URL: <https://doi.org/10.1007/s13753-019-00233-1>, doi:10.1007/s13753-019-00233-1.

Zhang, G., Wang, M., Liu, K., 2021. Deep neural networks for global wildfire susceptibility modelling. *Ecological Indicators* 127, 107735. URL: <https://www.sciencedirect.com/science/article/pii/S1470160X21004003>, doi:10.1016/j.ecolind.2021.107735.

Zhang, G., Wang, M., Liu, K., 2022. Dynamic prediction of global monthly burned area with hybrid deep neural networks. *Ecological Applications* 32, e2610.

Zhang, G., Wang, M., Yang, B., Liu, K., 2024a. Current and future patterns of global wildfire based on deep neural networks. *Earth's Future* 12, e2023EF004088.

Zhang, W., Cai, M., Zhang, T., Zhuang, Y., Mao, X., 2024b. Earthgpt: A universal multimodal large language model for multisensor image comprehension in remote sensing domain. *IEEE Transactions on Geoscience and Remote Sensing* 62, 1–20. doi:10.1109/TGRS.2024.3409624.

Zhao, F., Liu, Y., 2021. Important meteorological predictors for long-range wildfires in China. *Forest Ecology and Management* 499, 119638. URL: <https://www.sciencedirect.com/science/article/pii/S0378112721007283>, doi:10.1016/j.foreco.2021.119638.

Zhao, S., Prapas, I., Karasante, I., Xiong, Z., Papoutsis, I., Camps-Valls, G., Zhu, X.X., 2024. Causal graph neural networks for wildfire danger prediction. URL: <https://arxiv.org/abs/2403.08414>, arXiv:2403.08414.

Zhu, L., Webb, G.I., Yebra, M., Scortechini, G., Miller, L., Petitjean, F., 2021. Live fuel moisture content estimation from MODIS: A deep learning approach. *ISPRS Journal of Photogrammetry and Remote Sensing* 179, 81–91. URL: <https://www.sciencedirect.com/science/article/pii/S0924271621001957>, doi:10.1016/j.isprsjprs.2021.07.010.

ZORMPAS, K., VASILAKOS, C., ATHANASIS, N., SOULAKELLIS, N., KALABOKIDIS, K., 2017. Dead fuel moisture content estimation using remote sensing. *European Journal of Geography* 8.

Zubkova, M., Lötter, M., Bronkhorst, F., Giglio, L., 2024. Assessment of the effectiveness of coarse resolution fire products in monitoring long-term changes in fire regime within protected areas in south africa. *International Journal of Applied Earth Observation and Geoinformation* 132, 104064.